SOLID-STATE KU-BAND POWER AMPLIFIER

B.D. Geller
Westinghouse Defense and Electronic Systems Center
Systems Development Division
Baltimore, Maryland 21203

February 10, 1975

Final Report for Period August 1971 - August 1974

Prepared For

National Aeronautics and Space Administration
GODDARD SPACE FLIGHT CENTER
Greenbelt, Maryland 20771

TECHNICAL REPORT STANDARD TITLE PAGE

1. Report No. 74-1068	2. Government Accession No.	3. Recipient's Catalog No.
4. Title and Subtitle: Solid-State Ku-Band Power Amplifier		5. Report Date 2/10/75
		6. Performing Organization Code
7. Author(s) B.D. Geller		8. Performing Organization Report No.
9. Performing Organization Name and Address: Westinghouse Defense and Electronic Systems Center, Systems Development Division, Baltimore, Maryland 21203		10. Work Unit No.
		11. Contract or Grant No. NAS5-20291
12. Sponsoring Agency Name and Address: National Aeronautics and Space Administration, Goddard Space Flight Center, Greenbelt, Md. 20771, Technical Officer: W.E. Hughes, Code 811		13. Type of Report and Period Covered: Final, August 1971 - August 1974
		14. Sponsoring Agency Code
15. Supplementary Notes		

16. Abstract

The design of a 5-watt Ku-Band Solid-State Power Amplifier is described.

Section 2 presents a survey of IMPATT diodes and negative resistance amplifiers.

Section 3 discusses the first phase of the amplifier effort, in which a single diode reflection amplifier delivering 0.5 watt at 15 GHz with 10-dB gain over a 1-GHz band was developed. During this phase, an attempt was made to combine 20 diodes in a radial combiner. The attempt was unsuccessful due to poor understanding of multimode combiners and spurious coupling effects between elemental amplifiers.

Sections 4,5, and 6 describe the design of a dominant mode resonant combiner, discuss the characterization of the IMPATT diodes, and give results on the complete amplifier. The amplifier consists of 12 GaAs diodes, combined in two TM_{010} cavities which are subsequently combined by a circuit utilizing a "magic tee" hybrid. Results are also given on the thermal and "graceful failure" characteristics of the unit.

17. Key Words (Selected by Author(s))	18. Distribution Statement		
19. Security Classif. (of this report) Unclassified	20. Security Classif. (of this page) Unclassified	21. No. of Pages	22. Price*

* For sale by the Clearinghouse for Federal Scientific and Technical Information, Springfield, Virginia 22151.

TABLE OF CONTENTS

	Page
1. INTRODUCTION	1-1
2. CHARACTERISTICS OF IMPATT DIODES	2-1
2.1 Device Physics	2-1
2.2 Circuit Considerations	2-7
3. RADIAL COMBINER AMPLIFIER	3-1
3.1 Diode Characterization	3-1
3.2 Single-Diode Amplifier	3-5
3.3 Radial Combiner	3-18
3.4 Analysis and Recommendations	3-26
4. RESONANT COMBINER	4-1
4.1 Combiner Analysis	4-1
4.2 Inter-Element Coupling	4-12
5. DIODE CHARACTERIZATION	5-1
5.1 Package Characterization	5-1
5.2 Characterization of Packaged Diode	5-7
6. ELEMENTAL AND MULTI-DIODE AMPLIFIER	6-1
7. CONCLUSIONS AND RECOMMENDATIONS	7-1
Appendix A. Derivation of Gain-Bandwidth Relationship for a Negative Resistance Amplifier	A-1
Appendix B. Amplifier Test Procedure	B-1
Appendix C. Spurious Oscillations in IMPATT Devices (G. I. Haddad)	C-1
Appendix D. Bibliography	D-1

LIST OF ILLUSTRATIONS

Figure		Page
2-1	Typical P^+NN^+ Avalanche Diode Doping Profile and Corresponding Electric Field Distribution	2-3
2-2	Variation of IMPATT Mode Admittance with Frequency	2-5
2-3	Negative Admittance as Function of Signal Level	2-6
2-4	Variation of Packaged Diode Impedance with Frequency, Bias, and Power Level	2-6
2-5	Output Characteristics of a High Power IMPATT Oscillator	2-8
3-1	Raytheon GaAs IMPATT Diode, Bias Current = 0.160A	3-3
3-2	Hughes Si Diode, Bias Current = 0.148A	3-4
3-3	Single Diode Amplifier Assembly	3-6
3-4	Comparison of Impedance Behavior of Single Quarter Wavelength Filter and 7-Section Low Pass Filter	3-8
3-5	Adjustable Circuit Configuration	3-9
3-6	Mechanical Configuration of Adjustable Circuit	3-9
3-7	Smith Chart Representation of Capacitive Transformation Design	3-10
3-8	SDA Gain for Four Diodes	3-12
3-9	Test Circuit for Measuring Gain of SDA	3-13
3-10	Adjustable Circuit Configuration	3-15
3-11	SDA Gain vs P_{in} at 14.9, 15.0, 15.1 GHz. Diode #29, I = 145 mA	3-16
3-12	Effect of Bias Filter Position on Gain	3-17
3-13	Radial Transmission Line Quantities	3-20
3-14	Total Characteristic Impedance vs. Radius (F = 15.0 GHz)	3-21
3-15	Impedance of Radial Power Combiner at Elemental Amplifier Radius	3-23
3-16	RADCOM With Twenty Elemental Amplifiers	3-25

Figure		Page
4-1	Resonant Combiner	4-2
4-2	Cavity Return Loss with Elemental Amplifier Holes Empty (10 dB/div., 6 to 18 GHz)	4-4
4-3	VSWR at Resonance for Various Insertions of Probe	4-6
4-4	Equivalent Circuit of Cavity (Valid Only in the Neighborhood of the Resonant Frequency) Loaded by the Generator Impedance	4-8
4-5	Equivalent Circuit of Six Diode Amplifier	4-9
4-6	Six Diode Combiner Internal Configuration	4-10
4-7	Illustration of Technique Used to Determine Even- and -Odd Mode Impedances	4-14
5-1	Schematic of Diode Package	5-1
5-2	Diode Package Lumped - Equivalent Circuit	5-4
5-3	Cross Section of Diode Test Fixture Connected to Slotted Line	5-6
5-4	Equivalent Circuits of (A) Open-Circuited Diode Package, and (B) Short-Circuited Diode Package	5-8
5-5	Test Circuit Used for Impedance Measurements	5-9
5-6	Comparison of Measured and Fitted Shorted Package Impedance Locus	5-10
5-7	Smith Chart Plot of ($-Z_{diode}$) vs. Frequency and Input RF Power Level (Z_o = 50 Ω)	5-12
5-8	Y_{in} vs. R_L at Diode Negative Conductance Terminals	5-13
5-9	Diode Conductance and Susceptance vs. RF Voltage	5-15
5-10	Computed Gain and Power Added vs. P_{in} for G_{circ} = 0.010, B_{circ} = 0.027	5-16
6-1	Elemental Amplifier Equivalent Circuit Using Mismatched Termination	6-3
6-2	Computed Impedance Locus of Circuit of Figure 6-1	6-4
6-3	Gain Reduction Due to Parametric Oscillation (2 dB/div., 14.5 to 15.5 GHz)	6-5
6-4	Elemental Amplifier Circuit Using Matched Termination	6-9
6-5	Loaded Q for λ/2 Resonator	6-10

Figure		Page
6-6	Final Center Conductor Assembly	6-12
6-7	Single - Diode Amplifier in Cavity. Gain vs. Frequency as Function of Input Power. Diode #G24. (5 dB/div., 14.5 to 15.5 GHz) (Sheet 1 of 2)	6-14
6-7	Single - Diode Amplifier in Cavity. Gain vs. Frequency as Function of Input Power. Diode #G24. (5 dB/div., 14.5 to 15.5 GHz) (Sheet 2 of 2)	6-15
6-8	Three - Diode Amplifier in Cavity. Gain vs. Frequency as Function of Input Power. Diodes #G24, E3, E4. (5 dB/div., 14.5 to 15.5 GHz) (Sheet 1 of 2)	6-17
6-8	Three - Diode Amplifier in Cavity. Gain vs. Frequency as Function of Input Power. Diodes #G24, E3, E4. (5 dB/div., 14.5 to 15.5 GHz) (Sheet 2 of 2)	6-18
6-9	Pass - Band Characteristics of (a) Combiner #1 and (b) Combiner #2. (5 dB/div., 14.5 to 15.5 GHz)	6-19
6-10	Pass - Band Characteristic of 12 - Diode Amplifier (5 dB/div., 14.5 to 15.5 GHz)	6-20
6-11	Twelve - Diode Amplifier Breadboard, Including Cooling Fans	6-21
6-12	Twelve - Diode Amplifier Intermodulation Distortion ($\Delta f = 12$ MHz, $f = 15.0$ GHz, Driver Third Order IMP's = 24 dB)	6-22
6-13	Amplifier Characteristics for Various "Failure" Configurations (5 dB/div., 14.5 to 15.5 GHz) (Sheet 1 of 3)	6-24
6-13	Amplifier Characteristics for Various "Failure" Configurations (5 dB/div., 14.5 to 15.5 GHz) (Sheet 2 of 3)	6-25
6-13	Amplifier Characteristics for Various "Failure" Configurations (5 dB/div., 14.5 to 15.5 GHz) (Sheet 3 of 3)	6-26
6-14	Amplifier Gain Variation as A Function of Temperature (0.4 dB/div., markers at 14.91 and 15.01 GHz) (Sheet 1 of 3)	6-28
6-14	Amplifier Gain Variation as A Function of Temperature (0.4 dB/div., markers at 14.91 and 15.01 GHz) (Sheet 2 of 3)	6-29
6-14	Amplifier Gain Variation as A Function of Temperature (0.4 dB/div., markers at 14.91 and 15.01 GHz) (Sheet 3 of 3)	6-30

TABLE OF SYMBOLS AND ABBREVIATIONS

ω_a	avalanche frequency (radian)
C_p	package capacitance
L_p	package inductance
Γ	voltage reflection coefficient
SDA	Single Diode Amplifier
λ	wavelength
μ	permeability
ϵ	permittivity
η	characteristic impedance of free space
$H_j^{(k)}$	j'th order Hankel function of the k'th kind
N_j	j'th order Neumann function
J_j	j'th order Bessel function
η_c	circuit efficiency

1. INTRODUCTION

The work to be described here covers the second and final phase of NASA contract No. NAS5-20291. During the first phase, a single-diode reflection amplifier was developed using silicon diodes. The diode was capable of delivering approximately 0.5 watt at 15 GHz with 10-dB gain over a 1-GHz band. During this phase an attempt was made to combine 20 such elemental amplifiers in a single radial transmission line combiner. The attempt was unsuccessful in the sense that efficient power combining with all 20 diodes was never achieved. However, it was successful in pointing out many of the poorly understood areas which must be brought under control if such an effort were to succeed. These areas are:

a. Spurious modes in a multi-mode combining structure.

b. Coupling between individual elemental amplifiers and the combiner as well as between each other.

c. Proper design for unconditional stability under all drive conditions.

The present design either avoids or incorporates a greater understanding of these problem areas.

The goal of the work to be described in this report is the development of a stable Ku-band solid-state power amplifier with the following specifications:

PARAMETER		SPECIFICATION	
		FINAL	ORIGINAL
1.	Center Frequency	15.0 GHz	
2.	1-dB Bandwidth	100 MHz	
3.	Ripple within Pass Band	± 0.2 dB	
4.	Power Output at Full Gain	5 watts	10 watts
5.	dc Power Input Maximum	150 watts	
6.	Gain at Maximum Output Power Level	4 dB	7 dB
7.	Maximum Noise Figure at Full Gain	30 dB	
8.	Maximum Volume	0.25 ft^3	
9.	Maximum Weight	2.8 lb	2.5 lb
10.	Maximum Input/Output VSWR	1.2:1	
11.	Input and Output Connectors	UG-419/U	
12.	Intermodulation Products	2 tone test, Δf = 10 MHz: 10 dB down from each of 2 tones at output, design goal.	
13.	dc Power Input	Supply as accessary.	
14.	Operating Temperature Range	-25° C/+ 50° C	-30° C/+ 50° C

In order to achieve the required output power a total of 12 IMPATT diodes are used with 6 diodes coupled through each of two resonant cavities. The outputs of each of the two cavities are subsequently combined through the use of a waveguide "magic-tee" hybrid.

The diodes used were manufactured by the Microstate Division, Raytheon, Waltham, Massachusetts. They are GaAs devices with a Read-type doping profile. As oscillators, they are capable of delivering about 1 watt with an efficiency (dc to RF) of 10 to 17 percent.

A good background on the problem of power combining of IMPATT diodes may be obtained from the papers by Rucker, Kurokawa, Kenyon, and Harp et. al. listed in the bibliography[1-5]. The papers by Harp are especially noteworthy in

reference to the work to be reported since his approach is very similar to the one taken here.

Section 2 presents a survey of IMPATT diodes and negative resistance amplifiers.

Section 3 describes the 20-diode radial combiner effort and presents some of the problems encountered.

Section 4 describes the design and characterization of the resonant combiner.

Section 5 discusses the characterization of the packaged IMPATT diodes that were used in the program, including the synthesis of a lumped equivalent circuit for the diode package.

Section 6 describes the design of the elemental amplifier and contains results of tests on the multi-diode amplifier.

Section 7 contains conclusions and recommendations for further work.

2. CHARACTERISTICS OF IMPATT DIODES

2.1 DEVICE PHYSICS

In 1954 W. S. Shockley[6] proposed a mechanism for the negative resistance effect in an avalanching P-N junction. It was not until 1958, however, that W. J. Read[7] showed that a certain type of P-N junction device (P^+NIN^+) should exhibit a negative resistance at microwave frequencies. Read's device allowed for a narrow N region in which carrier multiplication would occur, and a wider I region in which the injected carriers would drift until collected at the N^+ layer. Negative resistance arises in this structure due to the combined effects of the avalanche process, which introduces phase shift between the voltage and current, and the drift (transit) process, which introduces another phase shift. The combination of these processes results in an overall phase shift which appears as a negative resistance at the output terminals.

In 1966, T. Misawa[8] published an analysis of the case in which the avalanche multiplication process occurred throughout the region between cathode and anode. He assumed that electrons and holes travel at the same saturated velocity through the whole depletion region and that they have the same ionization rates. Misawa's equations show that in a uniformly avalanching region small disturbances tend to grow as they travel in either direction, so that a confined plasma of avalanching holes and electrons would exhibit amplification properties in the absence of a separate drift region.

One major difference between the Read and Misawa models is that the Read model predicts the existence of a specific frequency, known as the avalanche frequency, below which the diode does not exhibit negative resistance. The Misawa model does not predict the existence of a lower frequency bound on the negative resistance.

The Read and Misawa models are, of course, idealized in the sense that there are no physically realizable structures which would be purely one or the other. On the contrary, all actual IMPATT devices have some of the characteristics of each model. For instance, avalanche regions can be made small compared to drift regions, but not negligibly so.

The structures used most commonly in the fabrication of IMPATT devices are P^+NN^+, GaAs Schottky barrier, P^+PNN^+ (double drift) and a modified Read structure. Figure 2-1 illustrates the doping profile and corresponding electric field variation across the P^+NN^+ diode under reverse avalanche conditions.

As the field intensity in the region of the P^+- N junction increases, a free electron or hole entering the region has a correspondingly increased probability of ionizing a hole-electron pair and contributing to the avalanche process. As the number of ionized carriers in the region increases, the crest of the electric field distribution will move towards the N^+ region carrying in its wake an electron plasma (the holes generated in the avalanche region have, during this time, drifted into the P^+ region and for all intents have dropped out of the transit process). If the field intensity in the drift zone is kept above a certain critical value (approximately 2×10^4 V/cm for silicon), the carriers will drift at a constant saturated velocity until they are collected at the N^+ junction, when the process is repeated. The

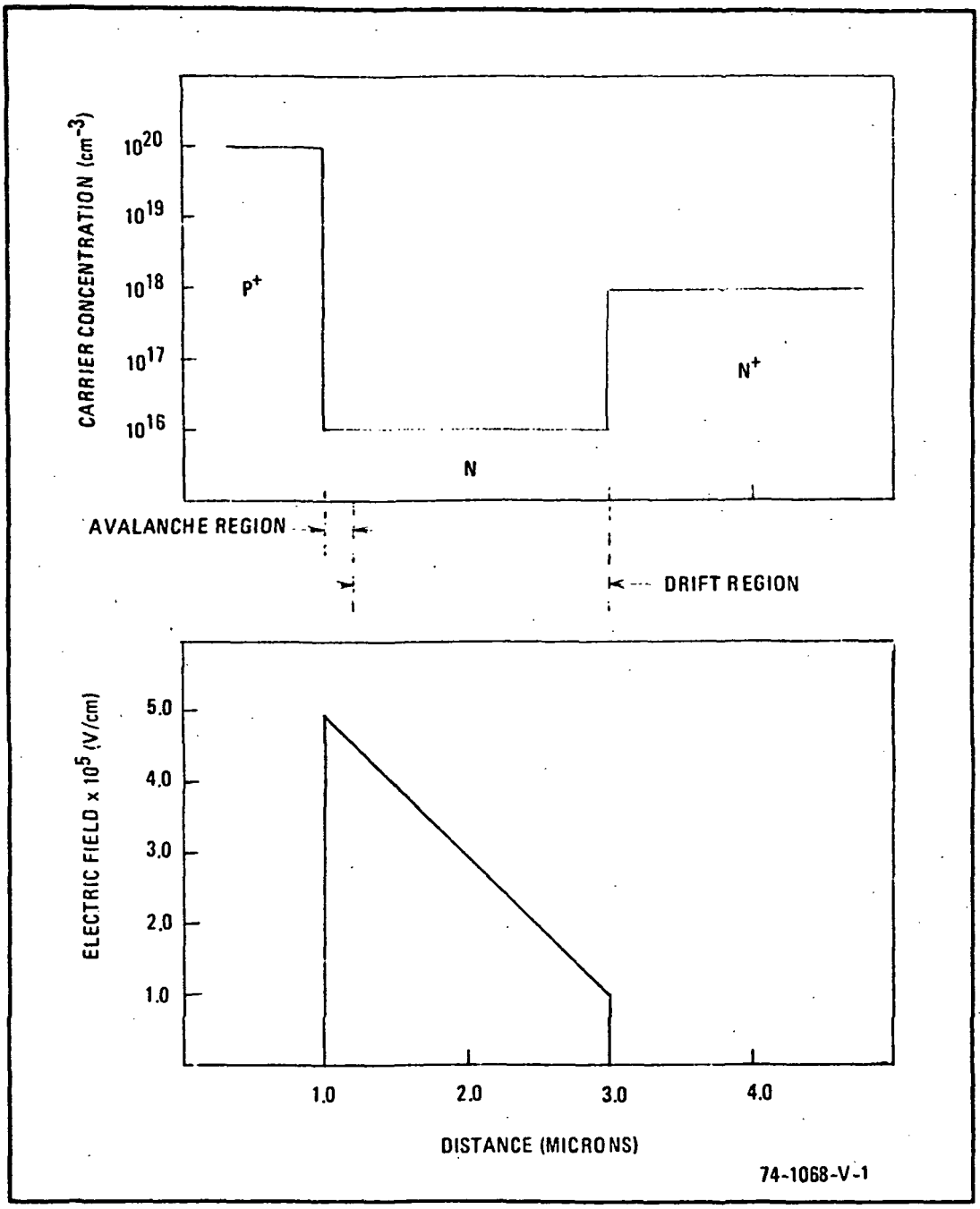

Figure 2-1. Typical P^+NN^+ Avalanche Diode Doping Profile and Corresponding Electric Field Distribution

negative resistance arises out of the combination of the avalanche and drift processes, as discussed earlier.

From an equivalent circuit point of view, the diode admittance can be represented as a parallel combination of a conductance, G_D, and a susceptance, B_D. Figure 2-2 illustrates the variation of the small-signal admittance of a typical X-band diode with frequency at high bias current.[9] Assuming that the diode reactance can be effectively tuned out over a narrow operating band, we must now consider the effect of signal level on the negative conductance of the diode. Figure 2-3 illustrates this effect at various operating frequencies relative to the small signal avalanche frequency.[10] In the mode of operation where the operating frequency is above ω_a, $|-G_D|$ is a monotonically decreasing function of signal level. In this mode, unconditionally stable amplification can be achieved as long as the load conductance, G_{LA}, is greater in magnitude than the small signal negative conductance G_{DO}. For operation at or below ω_a, the diode exhibits very low negative conductance at low signal levels and, furthermore, has a susceptance which varies rapidly with frequency. These combined effects tend to result in a very nonlinear gain characteristic as a function of signal level.

Figure 2-4 shows the impedance variation of a packaged diode as a function of frequency, signal level, and bias current.[10] The small signal avalanche frequency of the diode was approximately 6.9 GHz at 120 mA of bias current. Several significant effects can be noted. First, as the frequency of operation is lowered towards ω_a, the diode reactance increases substantially with varying signal level. Second, the effect of increasing signal level is, to a large extent, the same as the effect of decreasing

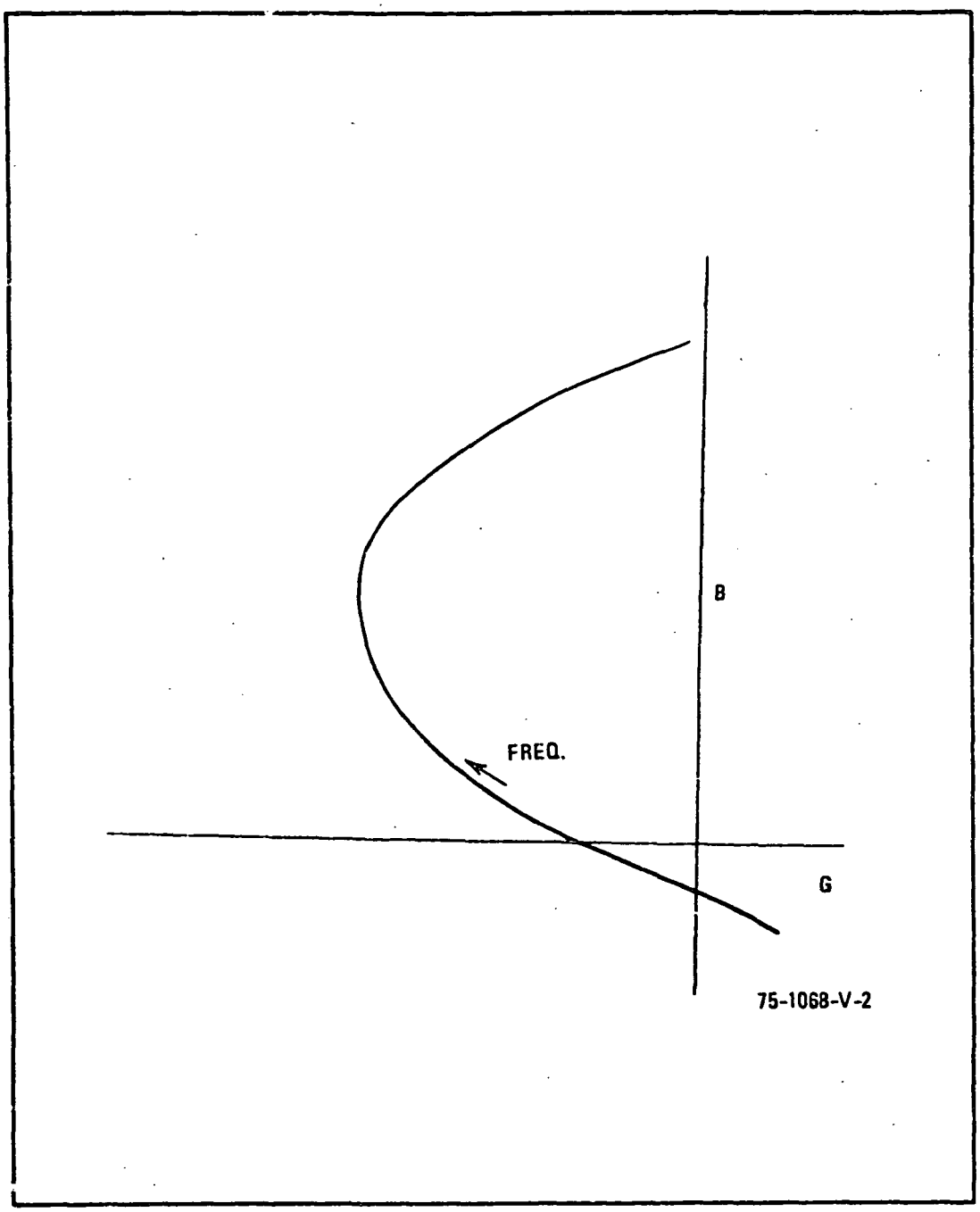

Figure 2-2. Variation of IMPATT Mode Admittance with Frequency

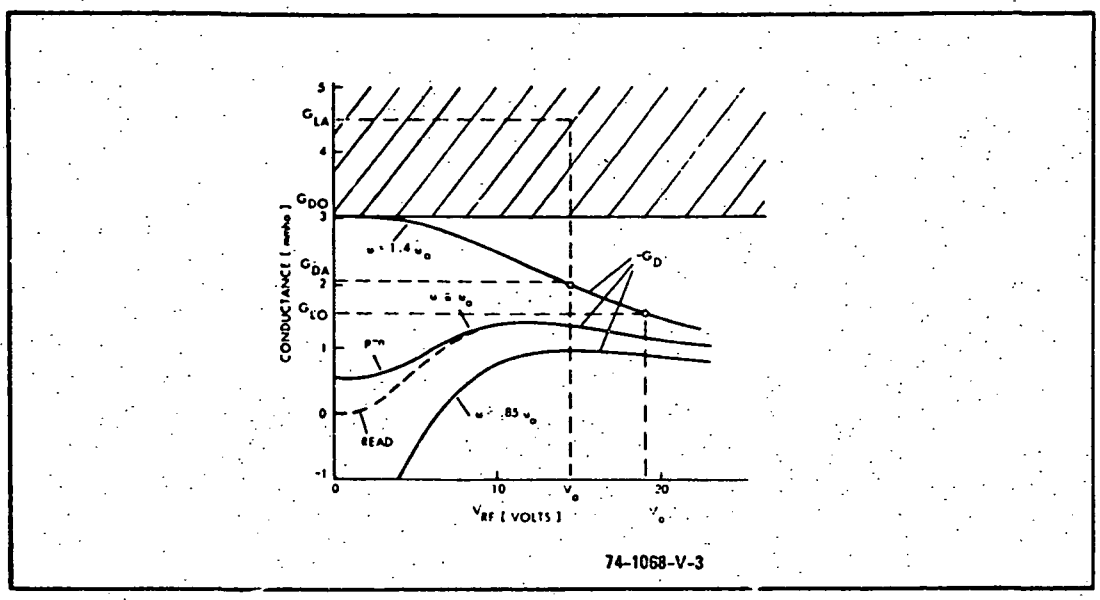

Figure 2-3. Negative Admittance As Function of Signal Level

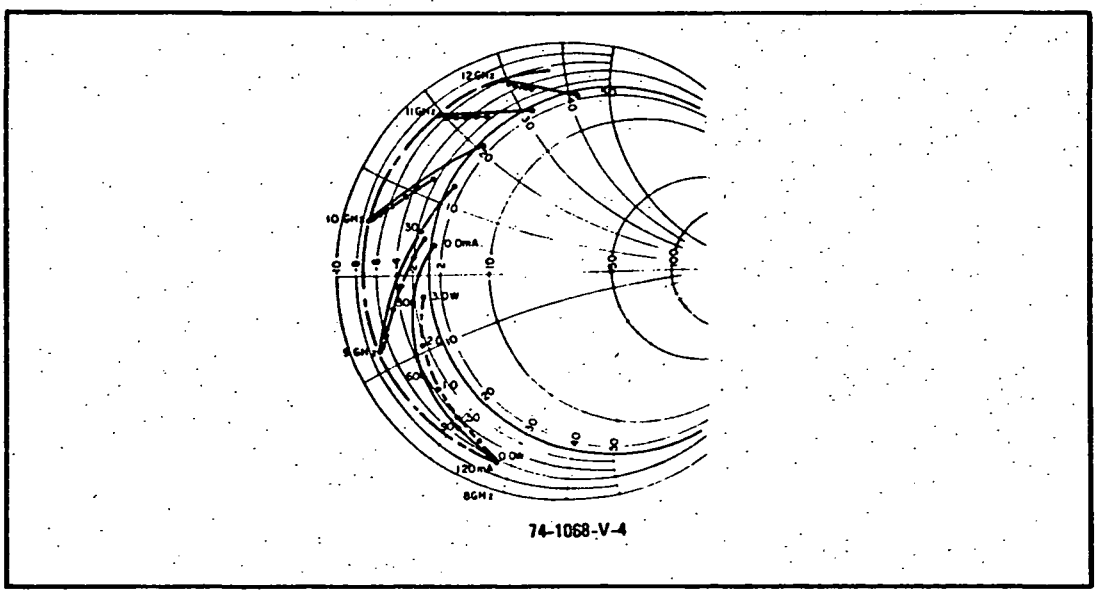

Figure 2-4. Variation of Packaged Diode Impedance With Frequency, Bias, and Power Level

bias current. The decrease in bias current lowers the avalanche frequency and thus lowers the magnitude of the negative conductance. The reduction of $|-G_D|$ causes the saturation phenomenon at high signal levels. Figure 2-5 illustrates the output characteristic of a 1 watt oscillator including the observed leveling in efficiency as the oscillator approaches saturation.

2.2 CIRCUIT CONSIDERATIONS

The discussion this far has been somewhat simplified since several significant points have been omitted for the sake of clarity. Probably the most important of these is the effect of the termination of harmonic and subharmonic frequencies. This effect can be readily demonstrated in the behavior of high power oscillators, where tuning of the second harmonic impedance has been observed to change the output power by as much as 10 dB. Although this effect is also present in amplifiers, it is not quite as pronounced.

Of far more importance in amplifier applications is the termination in the vicinity of the subharmonic.[11] The equivalent circuit of an avalanche diode consists of a negative conductance, a junction capacitance and an inductance due to carrier multiplication and drift. The junction capacitance may be considered to be essentially linear, that is, independent of signal amplitude. The inductance, however, is nonlinear since ionization rates and drift velocities will vary strongly with field intensity under large signal conditions. The presence of the nonlinear inductive susceptance, therefore, can give rise to a parametric negative resistance since the presence of a large RF signal across the diode will act as a pump. If the diode is not properly stabilized in the vicinity of half the signal frequency, oscillation will occur and this oscillation will detract from the power delivering capability at the signal frequency.

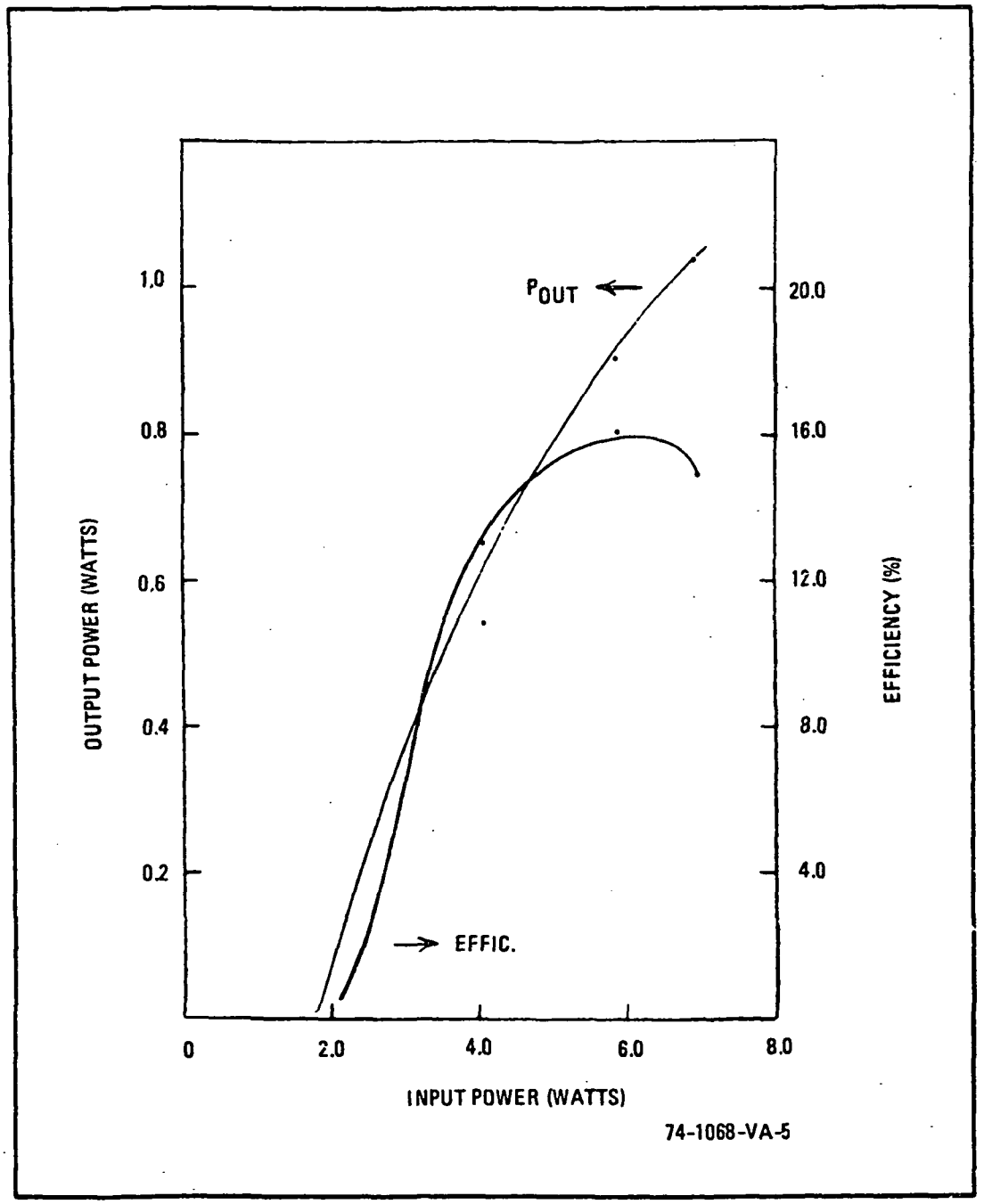

Figure 2-5. Output Characteristics of a High Power IMPATT Oscillator

Until recently this problem has not been widely reported in the literature, perhaps because of the lack of commercial availability of high efficiency (10 - 20 percent) diodes. With recent availability of such high efficiency devices, however, the problem has become quite serious since the primary mechanism for increased efficiency has been the reduction of the diode (positive) series resistance. This reduction of series resistance makes greater demands on the circuit designer since diode stabilization must now occur primarily due to proper external (to the diode package) circuit loading.

The problem facing the circuit designer is therefore one of presenting a low impedance to the diode in the vicinity of half the signal frequency in order that the build-up of a large "idler" voltage is prevented [12, 15]. This criterion must, of course, be satisfied simultaneously with the criteria required at the signal ("pump") frequency for proper operation as an amplifier.

Oscillations of a different type are also often encountered in IMPATT devices. These oscillations are generally confined in frequency to the dc to 20-MHz range and are caused by the rectification effect caused by the nonlinear avalanche process[13]. A simple explanation of the process is as follows. An increase of dc current increases the RF negative conductance, which causes an increase in RF voltage in order to satisfy the conjugate-match circuit constraint. The increase in RF voltage, however, causes a decrease in dc voltage due to the rectification effect of the avalanche process. The incremental increase in dc current with an incremental decrease in dc voltage therefore gives rise to a negative resistance. In certain circumstances (primarily when the bias circuit presents a transmission zero at these frequencies) these oscillations

can build up to a level sufficient for destruction of the diode. The bias circuit, therefore, must present a resistive termination to the diode of sufficient magnitude to prevent the build-up of oscillation. This can often be accomplished by a suitably chosen parallel L-R circuit which has a transmission pole at dc in order to allow essentially lossless biasing of the diode.

Other major considerations in the design of circuits employing IMPATT devices are biasing and heat sinking. The use of a constant current bias source is required since small fluctuations in the bias current can have significant effects on the diode impedance. With regard to heat sinking, it has been demonstrated that thermal resistance is a major cause of the drop-off efficiency of IMPATT devices operating at high RF power levels. The thermal resistance can be minimized by techniques such as the plating of an integral heat sink on the junction side of the $P^+ - N - N^+$ diode or by the use of a Schottky barrier diode, in which the source of heat, that is, the avalanche region, is not separated from the heat sink by a high thermal resistance region such as in the $P^+ - N - N^+$ structure.

3. RADIAL COMBINER AMPLIFIER

At the conclusion of Phase I (December 1971) of the present contract, a final report was submitted which described a proposed amplifier configuration in which a radial combiner, operating in the TM_{030} mode, combined the powers of 20 IMPATT diodes. The design goal at that time was a reflection amplifier capable of delivering 10 watts with 10-dB gain over a 100-MHz, 1-dB band centered at 15.0 GHz.

The design effort was divided into three consecutive areas. These were:

a. Diode Characterization

b. Construction of a Single-Diode Amplifier

c. Construction of the 20-Diode Amplifier

3.1 DIODE CHARACTERIZATION

Both silicon diodes and GaAs diodes were tested. The package parasitics and typical dc operating parameters are tabulated below:

Diode	C_p (pf)	L_p (nH)	V	I (mA) (typical)
Si	0.25	0.12	62	148
GaAs	0.25	0.12	55	180

Microwave measurements were made of the negative resistance and reactance of these diodes over the 13 - to 17 - GHz band for various signal voltages across the diode. The measurements were carried out using a precision 50-ohm coaxial slotted line terminated with a diode mount constructed by modifying a 7 - mm APC7 short circuit to accept a threaded diode package. The mount was air cooled. A wide band, 3 - dB coaxial pad was placed in the

slotted line input to prevent oscillations, which otherwise were found to occur in certain conditions. A computer program was written to compute the diode impedance $R_D + jX_D$ using the relations

$$\frac{R_D}{R_o} = \frac{S}{S^2 \cos^2 \theta + \sin^2 \theta} \qquad (3\text{-}1)$$

$$\frac{X_D}{R_o} = \frac{(1 - S^2) \sin \theta \cdot \cos \theta}{S^2 \cos^2 \theta + \sin^2 \theta} \qquad (3\text{-}2)$$

describing the dependence of the normalized diode series equivalent impedance $R_D + jX_D$ in terms of the standing wave ratios and the position of minimum given by the electrical length referred to the short plane, θ . R_o is the characteristic impedance of the transmission line.

Knowledge of incident power, P_{inc}, and standing wave ratio or reflection coefficient was also used to compute the total RF voltage across the diode V_{TOT}, using the relations

$$V_{TOT} = V_{inc} + V_{refl} = V_{inc} (1 + \Gamma) \qquad (3\text{-}3)$$

and

$$V_{inc} = \sqrt{2 P_{inc} R_o} \qquad (3\text{-}4)$$

Impedance data versus frequency and $|V_{TOT}|$ for both types of diodes are shown in Figures 3-1 and 3-2, where for convenience we use the rectangular complex plane. Note that there is considerable increase in reactance and the expected reduction in negative resistance as the signal level increases. Later we will see that this phenomenon was used to stabilize a single-diode negative resistance amplifier.

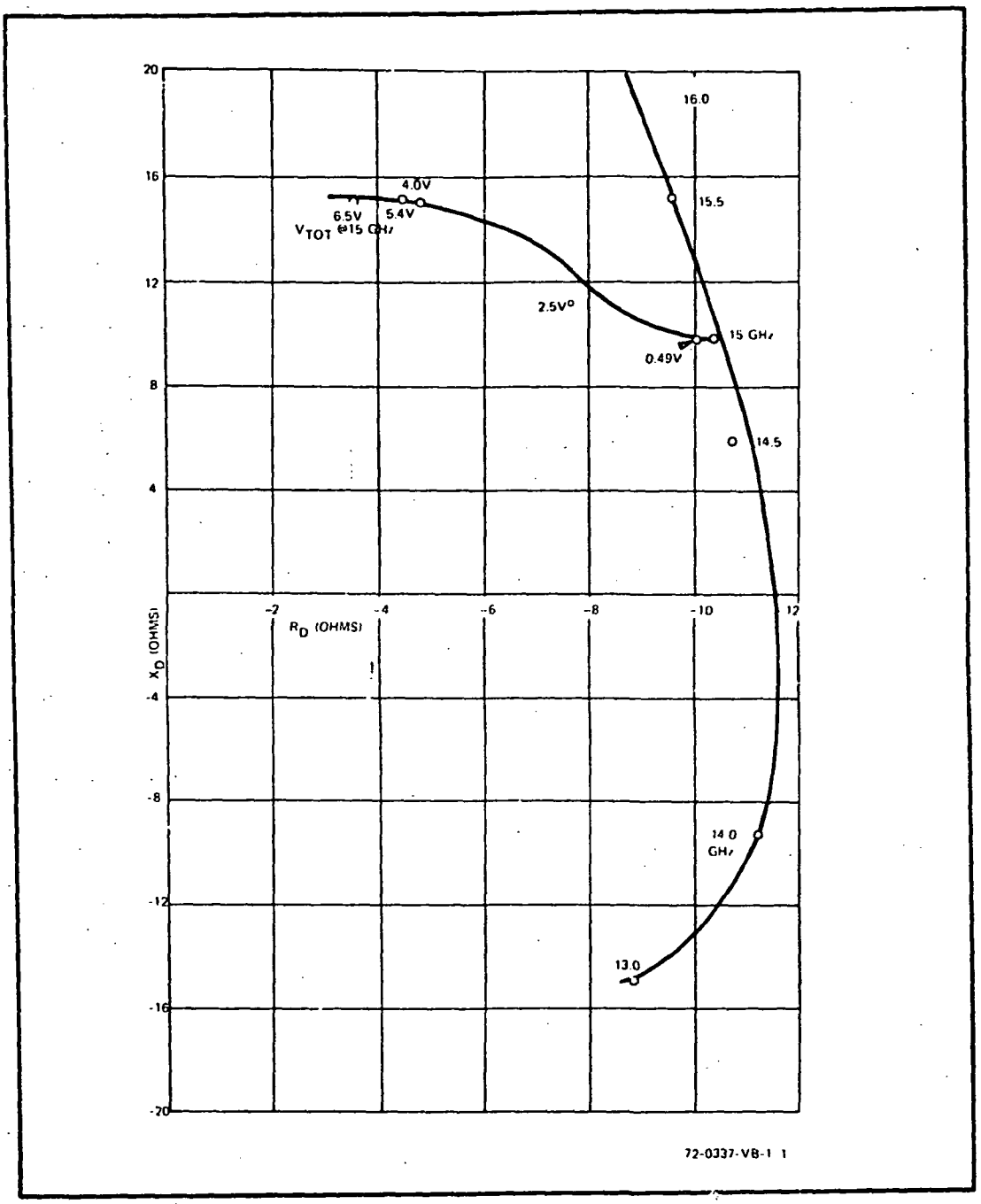

Figure 3-1. Raytheon GaAs IMPATT Diode, Bias Current = 0.160A

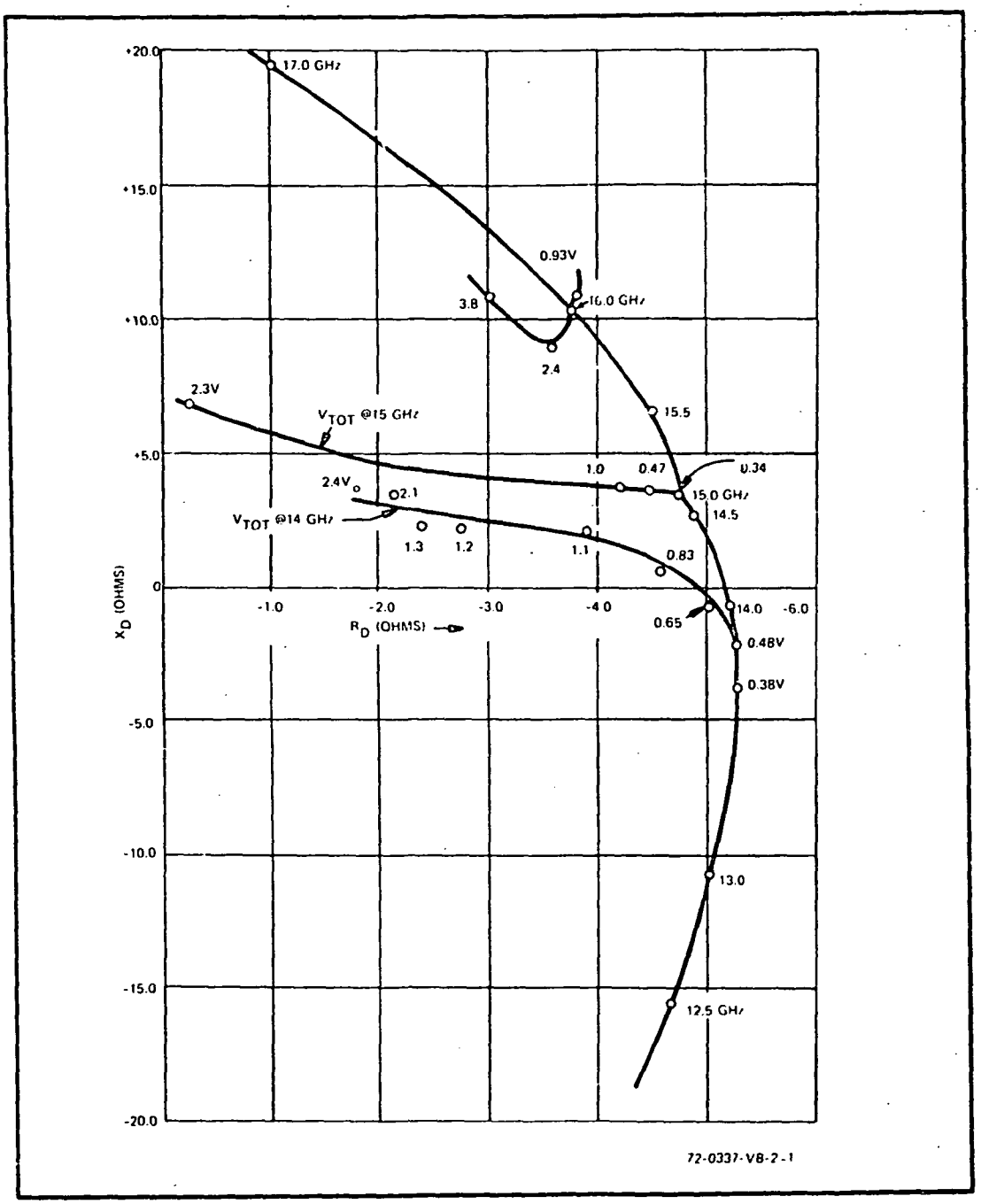

Figure 3-2. Hughes Si Diode, Bias Current = 0.148A

Summarizing these tests, the GaAs diodes clearly exhibited larger negative resistance components by about a factor of two with about the same reactance-frequency slope. On the other hand, experience with these diodes indicated that the silicon diodes were considerably more rugged. One Si diode has had in the order of 100 hours of operation at or near rated current operation into a wide variety of load impedances. Of three GaAs diodes, two had failed at a below rated bias current and the other had the bias lead open up. It was decided, therefore, to use the Si diodes in later development.

3.2 SINGLE-DIODE AMPLIFIER

The purpose of the SDA was to establish the proper impedance matching conditions for the individual elemental amplifiers which were to be combined later in the radial combiner. In order to accomplish this, the mount was designed to simulate a pie-shaped segment of the radial combiner by a length of reduced height waveguide whose characteristic impedance equaled the desired per-diode impedance (50 ohms). On one end of the reduced guide section is a tunable short and at the other end is a 4-section stepped waveguide impedance transformer designed to have a minimum ripple response from 10 to 20 GHz. Centered in the reduced height section is a 0.234 inch diameter hole penetrating both broad walls of the guide to accommodate the bias filter on one side, and the diode stud and matching transformer. Figure 3-3 shows a photograph of the unit.

Results of amplifier tests in the SDA using five and seven section stabilization/bias filters indicated that the circuit was very sensitive to the position of the sliding short and could easily break into oscillation.

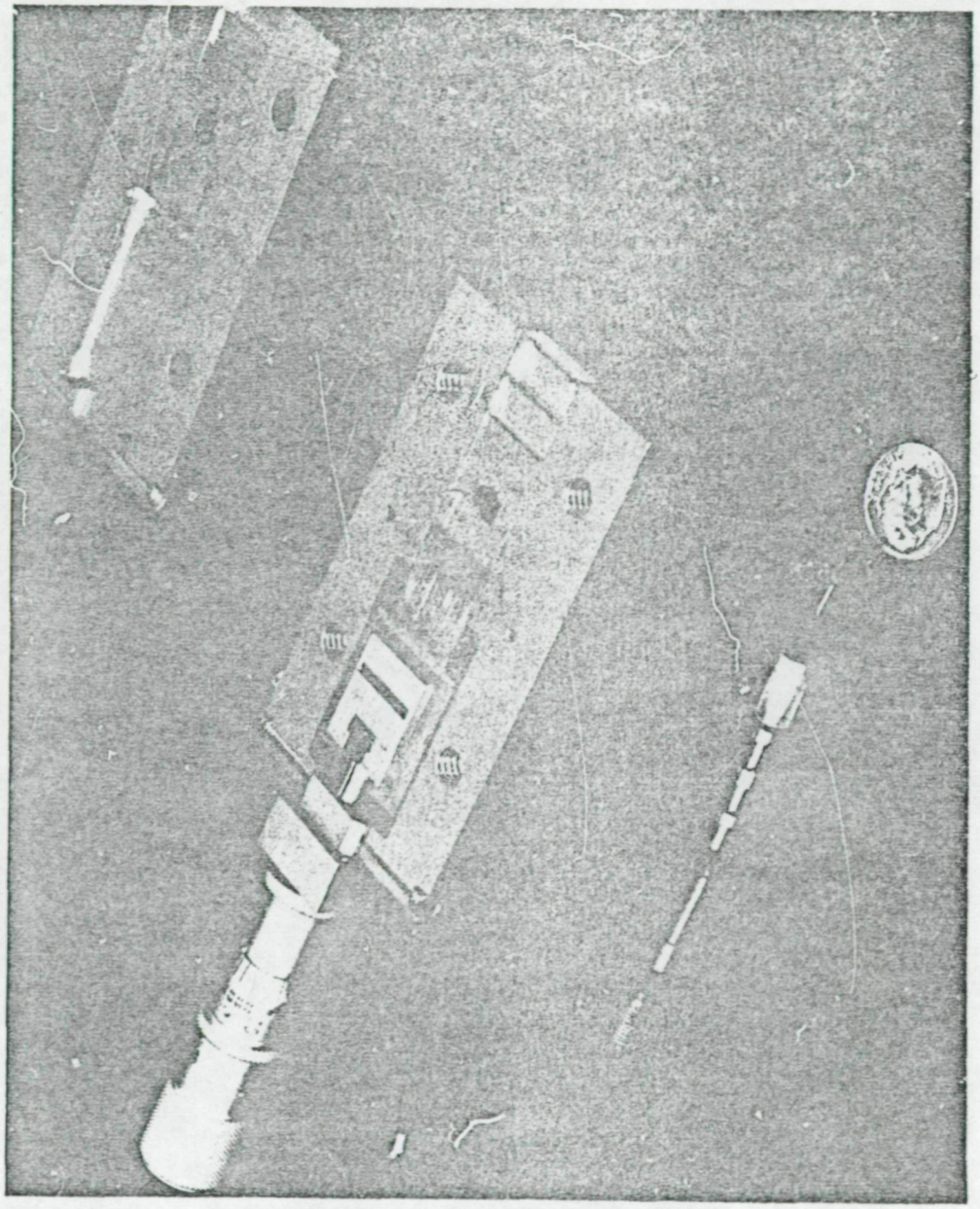

Figure 3-3.

Figure 3-3. Single Diode Amplifier Assembly

This resulted in a re-evaluation of several aspects of the SDA and primarily of the bias filter. The original philosophy behind the design of a multi-section filter was that the circuit had to be loaded below the band of desired amplification in order to suppress possible oscillation due to the high negative resistance of the diode in that region. After reconsideration, however, it was concluded that the problem of stabilization at lower frequencies was not as severe as was originally thought. Furthermore, the introduction of a circuit element with a multipole impedance characteristic was considered undesirable since it would tend to complicate the analysis of the circuit and could possibly tend to enhance the chances of oscillation at the frequencies at which the poles exist. Figure 3-4 shows a comparison of the impedance characteristics of a seven section low pass filter and that of a single quarter-wave low impedance filter section.

At this point it was decided to modify the proposed design to incorporate some degree of mechanical tuning on an active diode. Figure 3-5 shows the idea conceived. The circuit consists of a transformer of short electrical length shunted with a mechanically variable capacitance and a slidable trim capacitor approximately one-half wavelength away from the transformer. For the purpose of the following discussion, the transformer is represented as a lumped shunt capacitance C_{SH}. This is mechanically represented in Figure 3-6; a Smith chart representation of the impedance is shown in Figure 3-7.

The impedance transformation is accomplished as follows. The chart is normalized to 50-ohms and a circle representing a 10-dB reflection gain locus is drawn. It should be noted here that all computations on the chart are

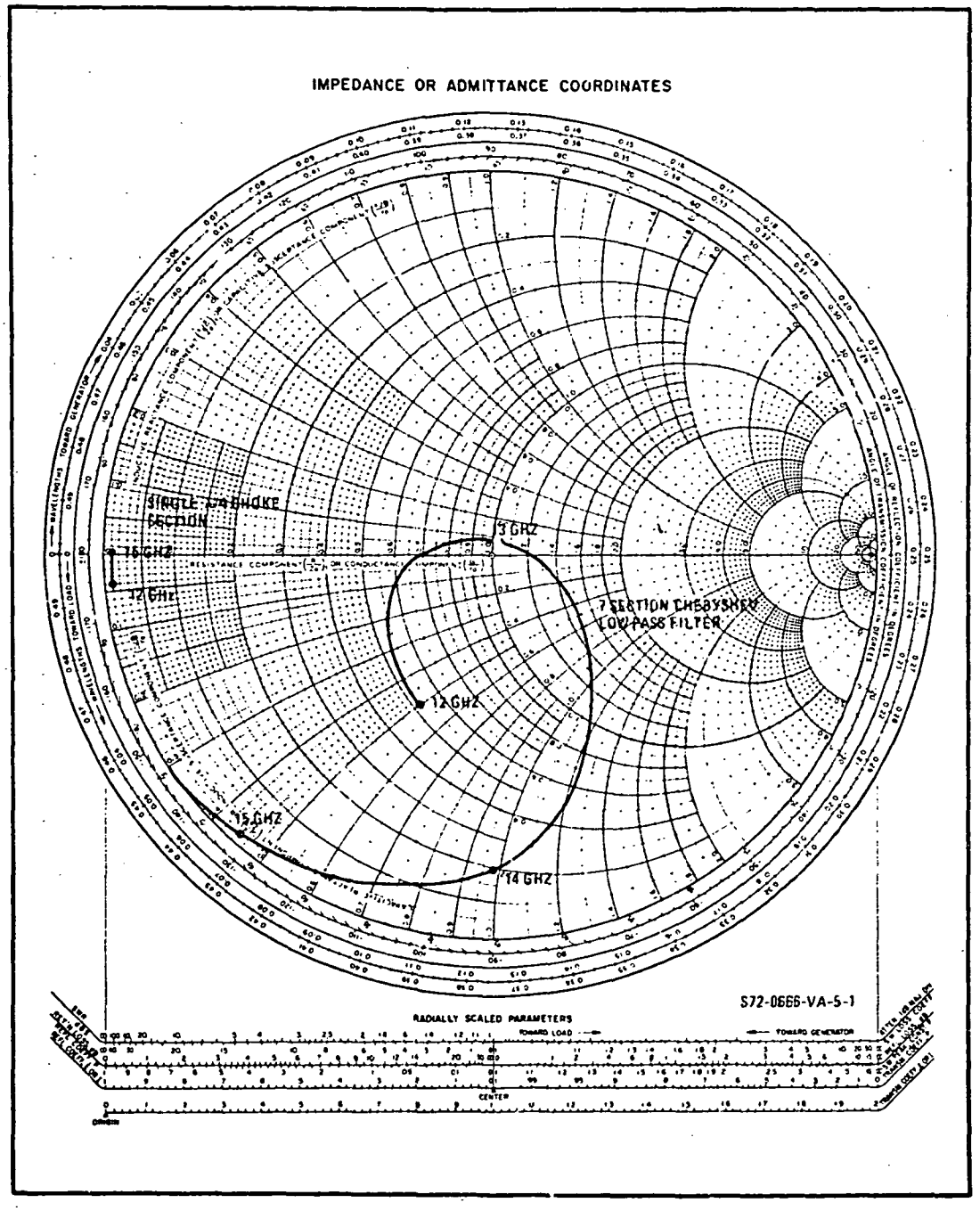

Figure 3-4. Comparison of Impedance Behavior of Single Quarter Wavelength Filter and 7-Section Low Pass Filter

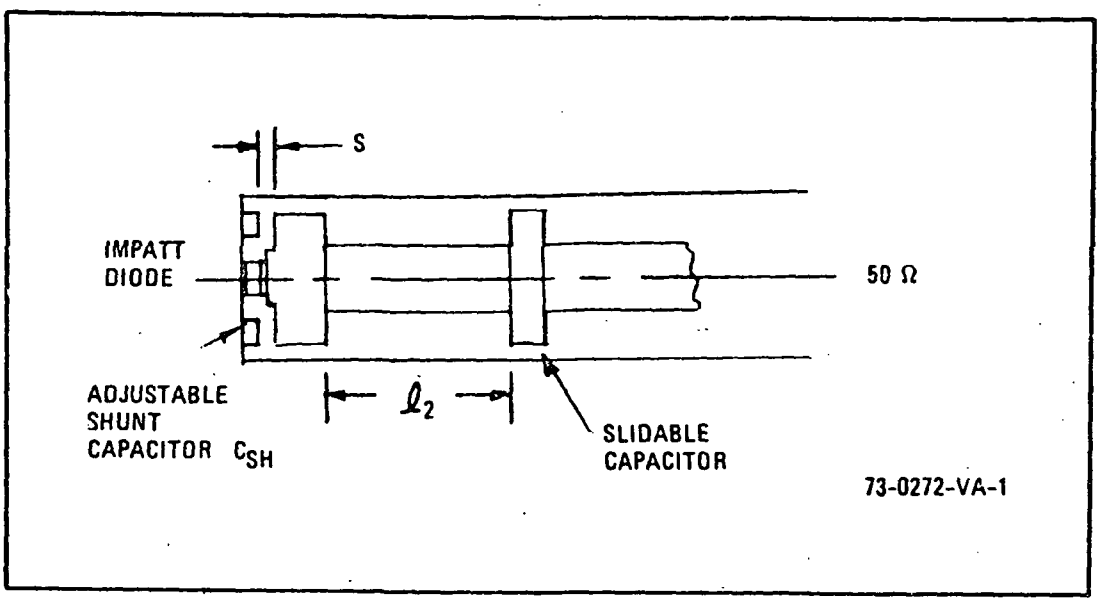

Figure 3-5. Adjustable Circuit Configuration

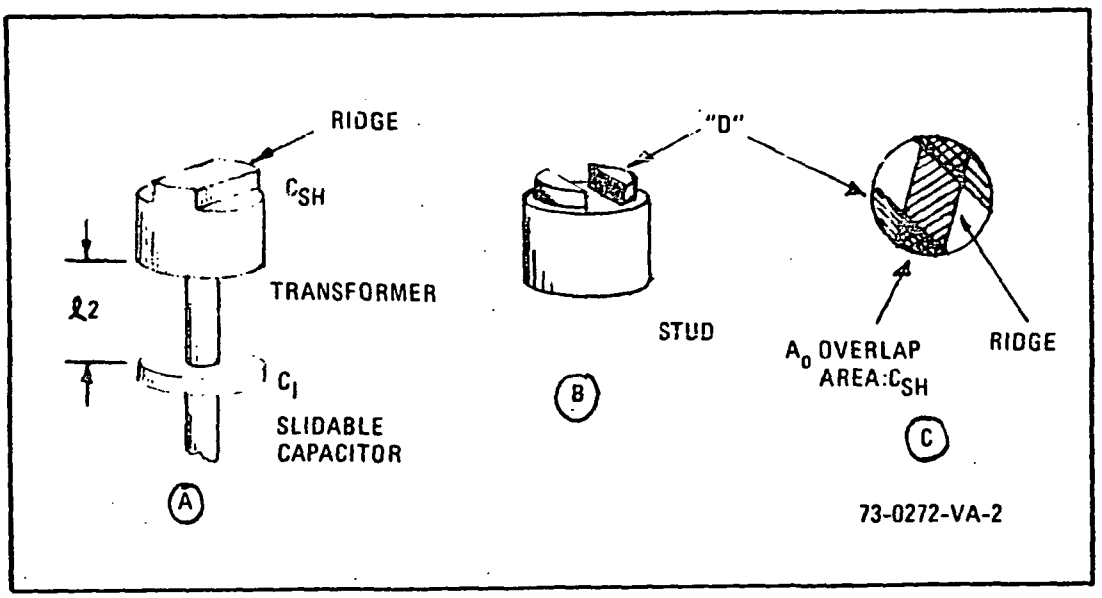

Figure 3-6. Mechanical Configuration of Adjustable Circuit

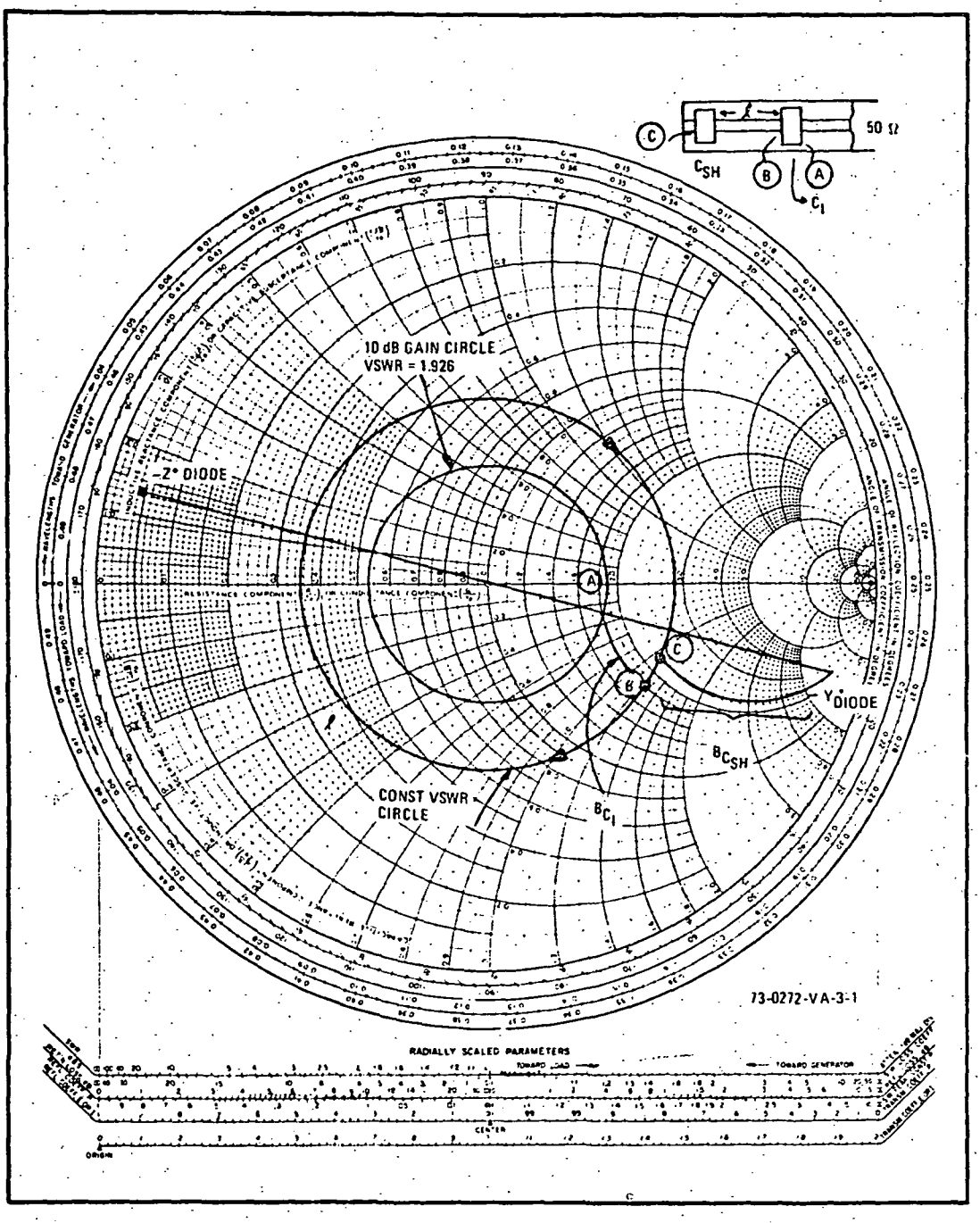

Figure 3-7. Smith Chart Representation of Capacitive Transformation Design

carried out with impedances and admittances having positive real parts. It can be shown that a given return loss under these circumstances implies reflection gain of the same magnitude under negative resistance circumstances.

The chart is entered at the point marked $-Z^*$, representing the diode impedance with the sign of the real part changed. Since we will be adding shunt positive susceptances we transform $-Z^*$ to $-Y^*$. Adding the susceptance represented by C_{SH}, we move along a constant conductance circle to a point C. We now move along a constant VSWR circle towards the generator. This represents the effect of the length ℓ_2 of 50-ohm transmission line. Arriving at point B (representing, here, an electrical length of just over $\lambda/2$), we add the second susceptance, represented by C_1, and move along another constant conductance circle until we intersect the previously determined 10-dB gain circle at point A.

Testing such a circuit in the SDA with four randomly selected diodes indicated that a wideband 10-dB gain curve with 0.5-watt output centered near 15 GHz was possible with little or no adjustment of the length ℓ_2 between C_{SH} and C_1, but did require individual tuning of the magnitude of C_{SH} by rotation of the asymmetrical stud, and by adjusting the position of the sliding waveguide short. This short position turned out to be somewhat less than $\lambda/2$ from the center line of the plug. Figure 3-8 shows typical gain vs frequency curves as displayed on an Alfred Model 8000/7051 analyzer.

The experimental setup used in most of these tests comprised a reflectometer circuit as shown in Figure 3-9. For fixed frequency measurements, power meters were used. For swept displays, the Alfred network analyzer was used. Calibration was made by replacing the SDA with a short circuit.

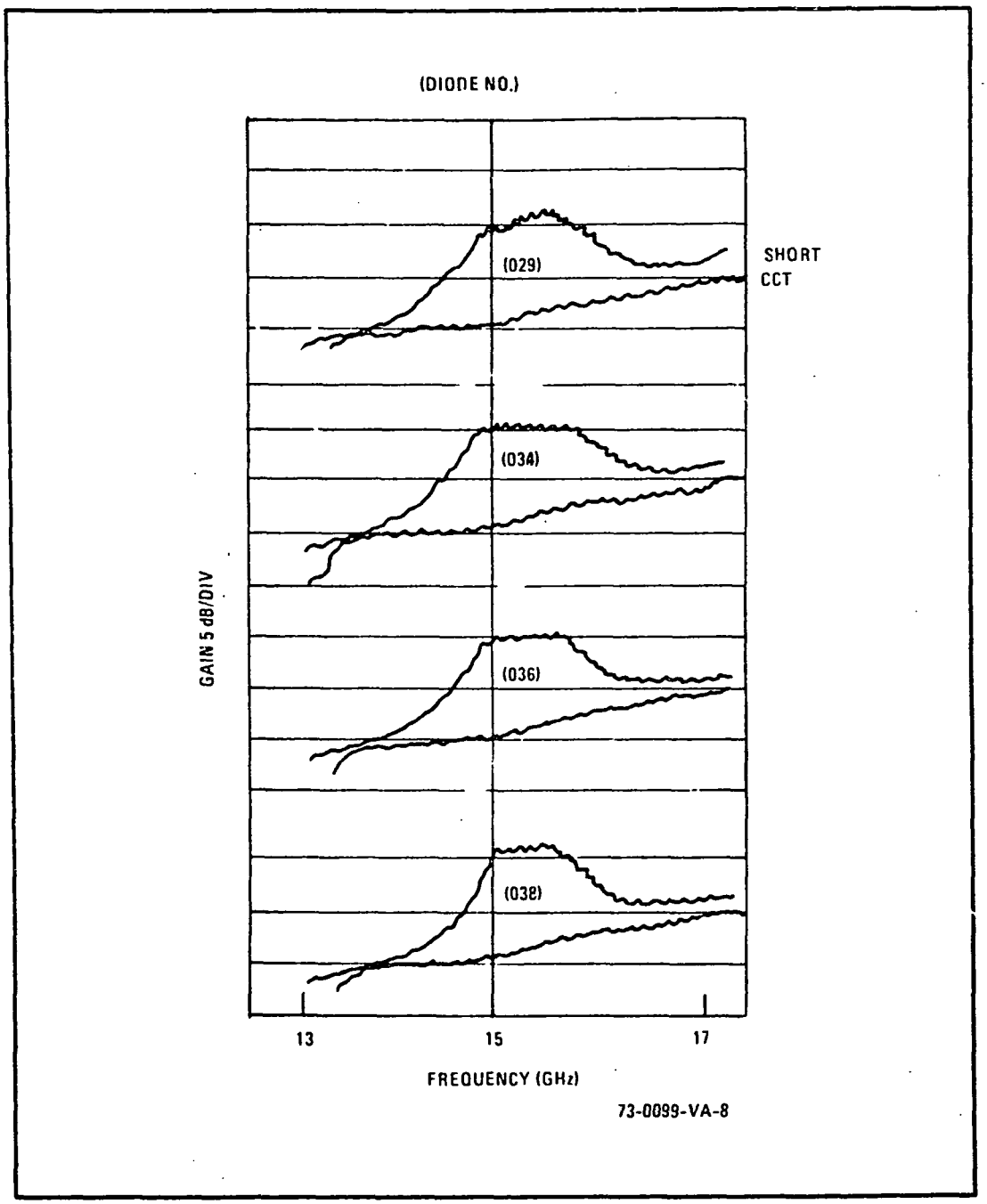

Figure 3-8. SDA Gain for Four Diodes

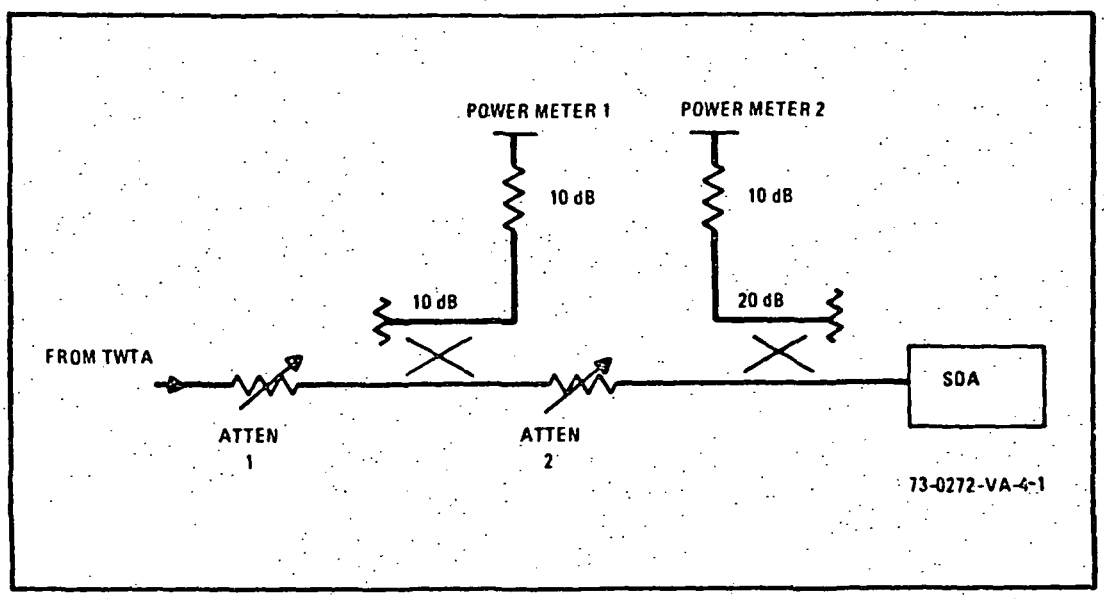

Figure 3-9. Test Circuit for Measuring Gain of SDA

The circuit configuration used is shown in Figure 3-10. Adjustments that could be made were ℓ_1 and ℓ_2. The axial positions of the bias filter and slidable capacitor and rotation angle θ of C_{SH}, as shown in Figure 3-10, were experimentally determined to give the gain curves shown in Table 3-1. Table 3-1 shows the typical GAIN vs P_{IN} data for the three frequencies 14.9, 15.0, 15.1 GHz which bracket the specified band. The data is plotted in Figure 3-11. These results were achieved with ℓ_1 and ℓ_2 values as on Figure 3-10. Notice that gain expansion occurs due to the effect of intentional reactive detuning.

The effect of moving the bias filter spacing ℓ_1, all other parameters held constant as in Figure 3-10, is shown in Figure 3-12. An increase of this spacing causes a smaller shunt capacitance to appear across the narrow height waveguide-to-coaxial-line transition within the SDA. This in turn tends to raise the center frequency of the amplifier.

TABLE 3-1 - TYPICAL GAIN vs INPUT POWER DATA FOR THREE FREQUENCIES

P_{IN} (mw)	GAIN (dB)		
	14.9 GHz	15.0 GHz	15.1 GHz
100	8.2	8.5	8.2
50	9.9	10.4	10.9
25	11.8	12.5	12.5
12.5	12.3	14.9	14.6
6.25	9.9	12.3	16.8
3.12	9.4	10.5	18.8
1.56	9.6	10.3	17.1
0.78	9.8	10.0	15.1
DIODE No. 29, I_{BIAS} = 145 mA			

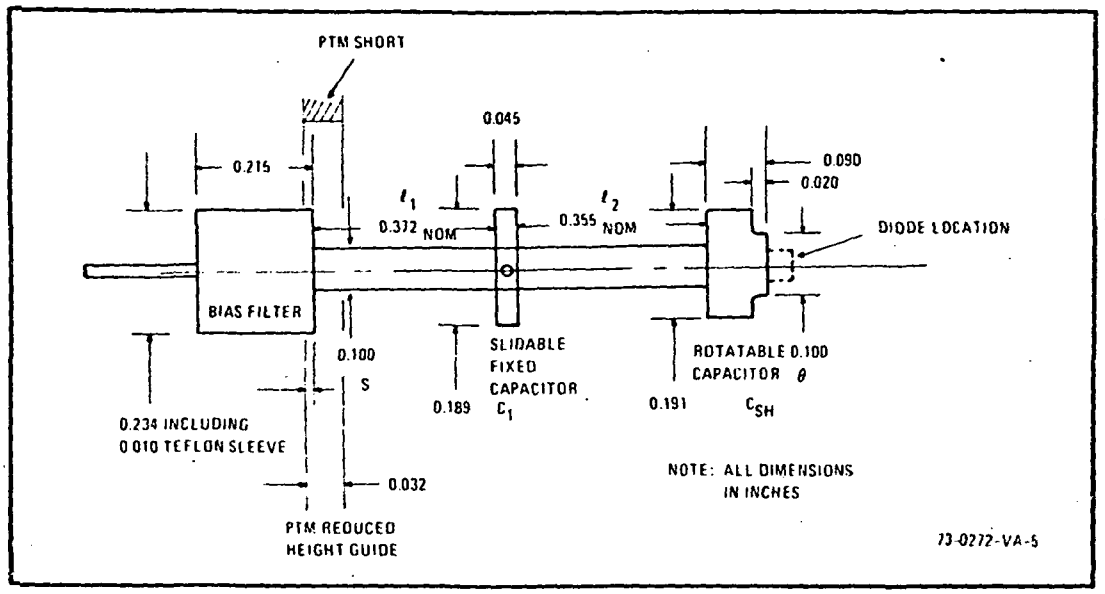

Figure 3-10. Adjustable Circuit Configuration

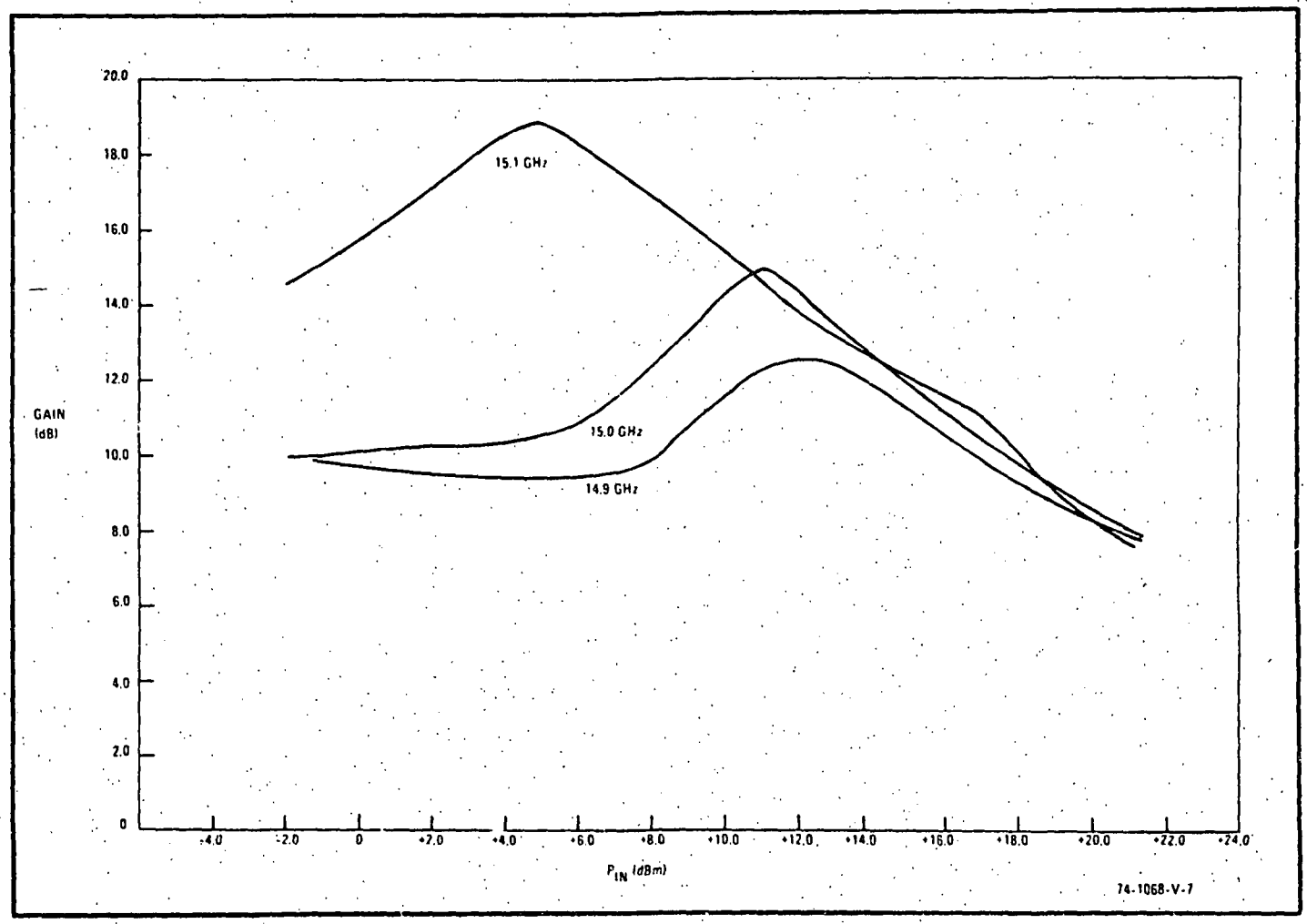

Figure 3-11. SDA Gain vs P_{in} at 14.9 15.0, 15.1 GHz. Diode #29, I = 145 mA

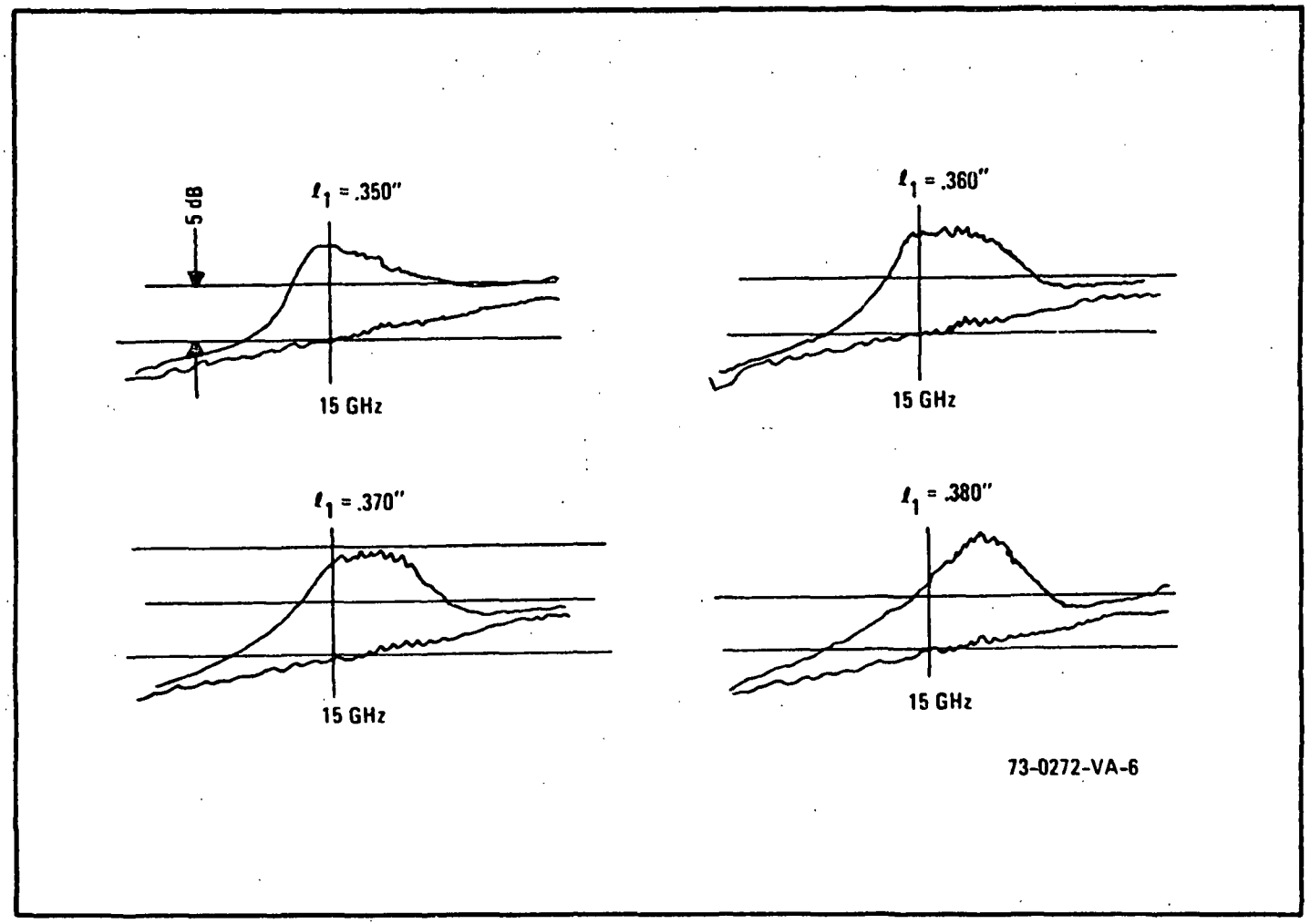

Figure 3-12. Effect of Bias Filter Position on Gain

3.3 RADIAL COMBINER

The choice of a radial transmission line as the power combining element in a multiple diode amplifier was based on the following:

a. All diodes are subjected to the same incident power.

b. All diodes are of the same type.

c. All elemental amplifier circuits are identical.

d. Virtually unlimited expansion potential in terms of the number of diodes used.

The equations governing the field variation in the radial line combiner, assuming no azimuthal or axial field variation, are, setting $k = \frac{2\pi}{\lambda}$,

$$E_z = A H_o^{(1)}(kr) + B H_o^{(2)}(kr) \tag{3-5}$$

$$H_\phi = \frac{1}{j\omega\mu}\frac{\partial E_z}{\partial r} = \frac{j}{\eta}\left[A H_1^{(1)}(kr) + B H_1^{(2)}(kr)\right] \tag{3-6}$$

where $\eta = 377$ ohm.

These can be further expressed in terms of radial angle functions which for large argument approach the ordinary trigonometric functions; viz,

$$\theta(X) \triangleq \tan\left[\frac{N_o(X)}{J_o(X)}\right] \tag{3-7}$$

$$\psi(X) \triangleq \tan^{-1}\left[\frac{J_1(X)}{-N_1(X)}\right] \tag{3-8}$$

The field variation then becomes

$$E_z = G_o(kr)\left[A\ e^{j\theta(kr)} + B\ e^{-j\theta(kr)}\right] \tag{3-9}$$

$$H_\phi = \frac{G_o(kr)}{Z_o(kr)}\left[A\ e^{j\psi(kr)} - B\ e^{-j\psi(kr)}\right] \tag{3-10}$$

$$\text{where } G_o(kr) \overset{\Delta}{=} \sqrt{J_o^{\,2}(kr) + N_o^{\,2}(kr)} \tag{3-11}$$

$$\text{and } Z_o(kr) \overset{\Delta}{=} \eta\sqrt{\frac{J_o^{\,2}(kr) + N_o^{\,2}(kr)}{J_1^{\,2}(kr) + N_1^{\,2}(kr)}} \tag{3-12}$$

$Z_o(kr)$ can be thought of as a radially varying characteristic wave impedance of the line. It is independent of the cavity height. These functions are plotted for the range of kr values of interest in Figure 3-13. Another function of interest can be called the total characteristic impedance and is given by

$$Z_{o_{TOT}}(kr) = Z_o(kr)\left(\frac{D}{2\pi r}\right) \tag{3-13}$$

where D is the height of the combiner.

This total characteristic impedance (Figure 3-14) is in terms of total potential across the cavity and current rather than a point function wave impedance. $Z_{o_{TOT}}$ has a pole at the origin.

Looking inward toward an assumed 50-ohm load in the coaxial output line, one can compute the real and imaginary part of the impedance, as seen by a given elemental amplifier. This will be given in general by

$$Z = \frac{D}{2\pi r}\left[H(kr)\right] \tag{3-14}$$

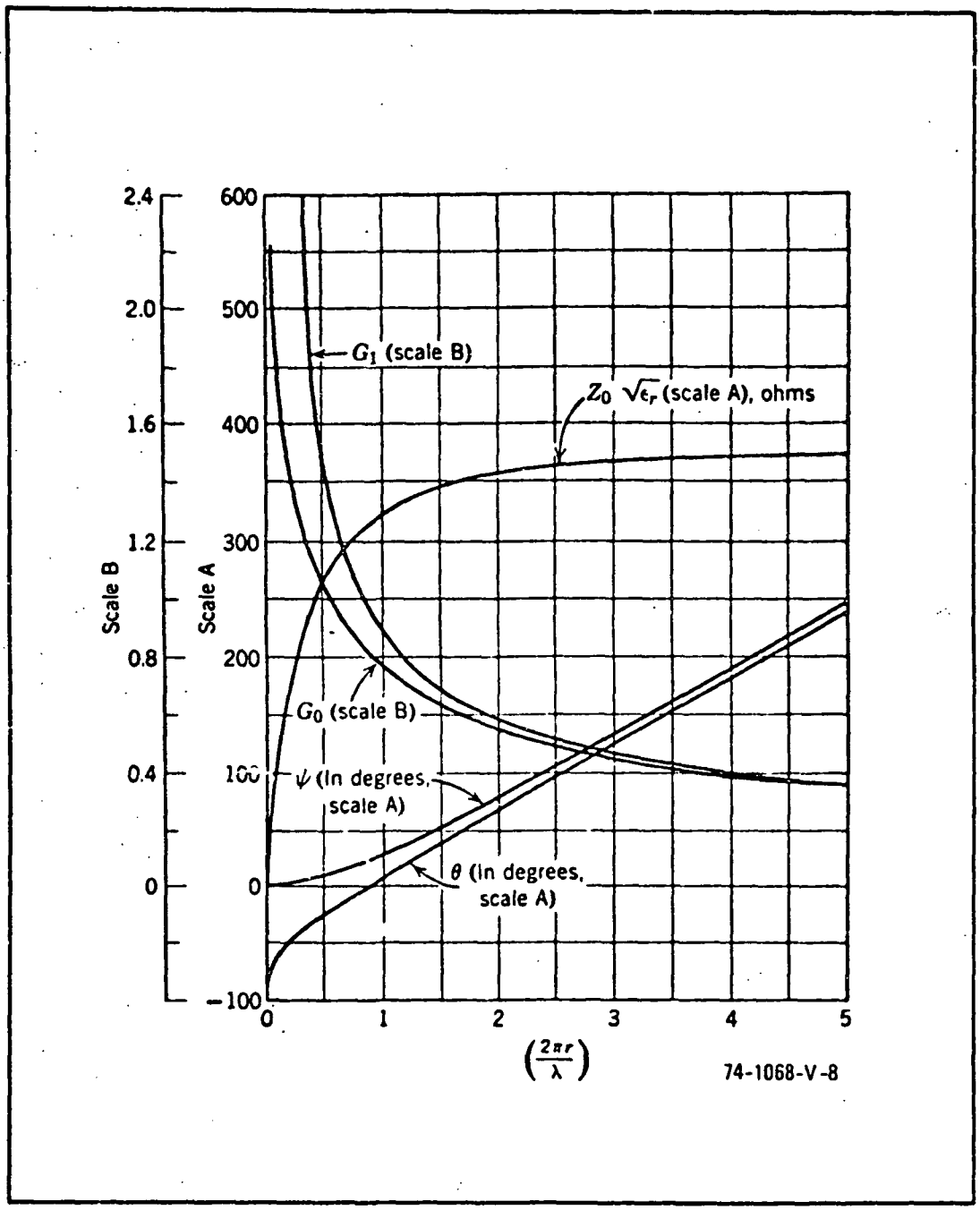

Figure 3-13. Radial Transmission Line Quantities

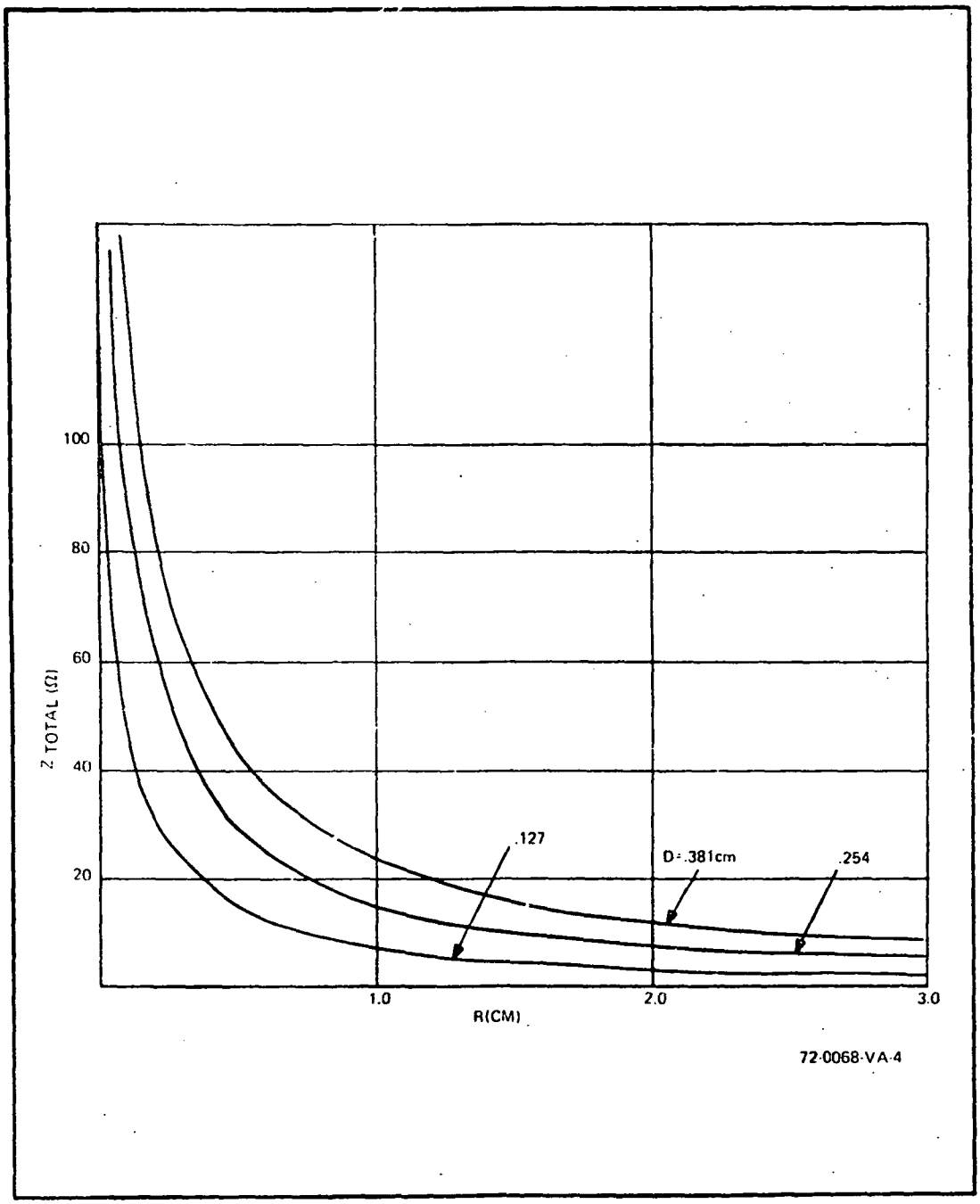

Figure 3-14. Total Characteristic Impedance vs Radius (F = 15.0 GHz)

where

$$H(kr) = \frac{Z_L \cos\left[\theta(r)-\psi(r_{load})\right] + jZ_o \sin\left[\theta(r)-\theta(r_{load})\right]}{Z_{OL} \cos\left[\psi(r)-\theta(r_{load})\right] + jZ_L \sin\left[\psi(r)-\psi(r_{load})\right]} \qquad (3\text{-}15)$$

where $Z_{OL} = Z_0\,(kr_{load})$, r_{load} is the equivalent radial coordinate of the 50 ohm load, and $Z_L = 50 \times \frac{2\pi r_{load}}{D}$, the wave impedance equivalent of the 50 ohm load at $r = r_{load}$.

For a cavity height D of 0.254 cm, load impedance of 50 ohms, $r_{diode} = 2.25$ cm and center frequency of 15 GHz, the impedance looking toward the load is plotted versus r_{load} in Figure 3-15 with frequency as a parameter. It can be seen that we have a region of relatively constant real impedance of about 50 ohms with a zero of reactance. It is important to recognize that this is the impedance looking toward the load per diode and is given by multiplying (k) by $N_d = 20$, the number of diodes. This arises from the fact that the 20 diodes are arranged in parallel, such that the overall impedance seen by them all is 1/20 of that seen by any given one.

Thus, we can set a point in the radial line at which the individual elemental amplifiers see a real impedance in the neighborhood of 50 ohms. The radial line length from the diode ring out to the short should in this case be a quarter wave long.

At the radii of output, diode and short, kr is large enough such that $Z_o(kr)$, $\theta(kr)$, and $\phi(kr)$ approach their corresponding values in free space or in a parallel plane guide.

As was stated earlier, the preceding equations are valid only for the radially propagating modes, that is TM_{omo}. (It is assumed here that the

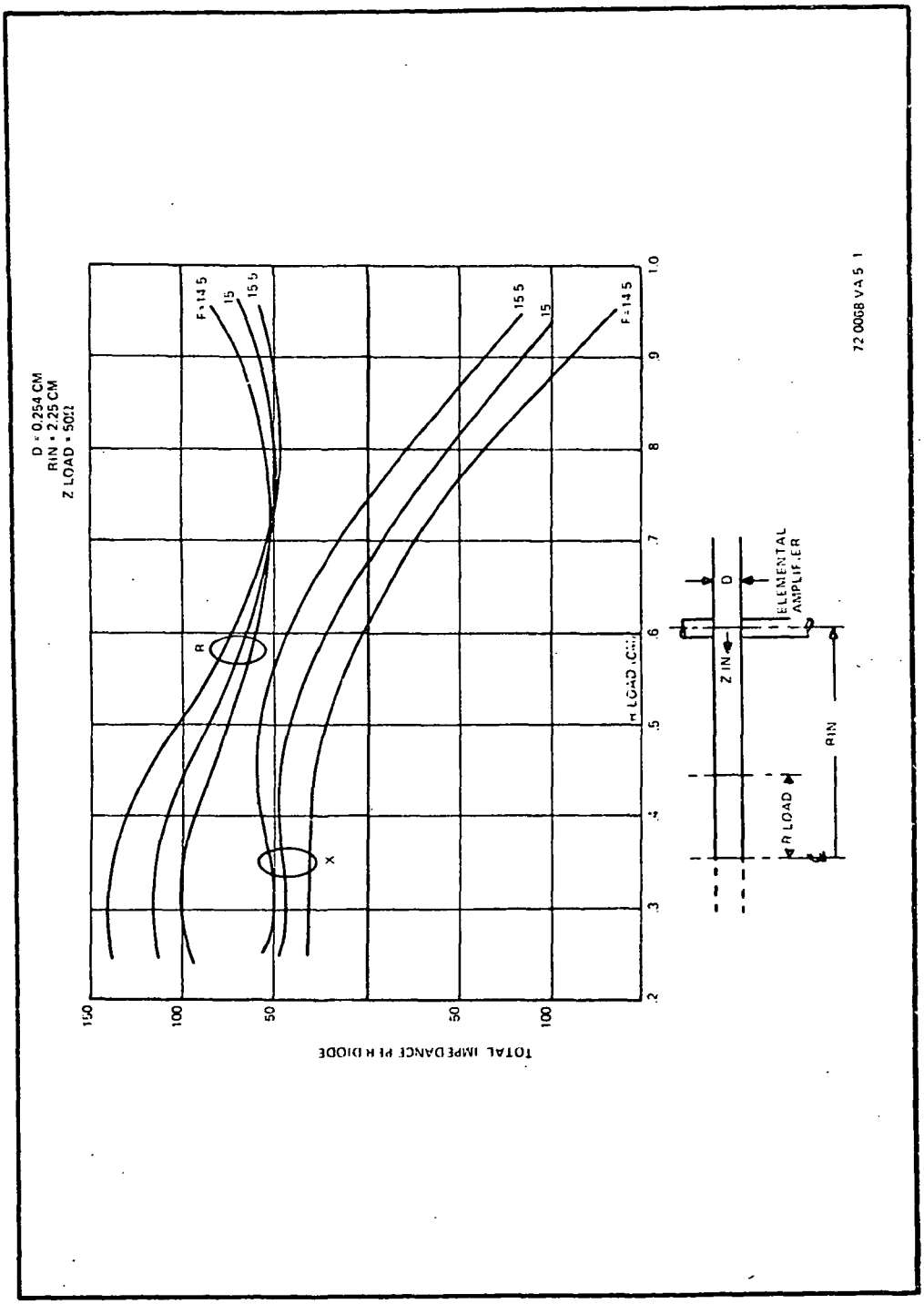

Figure 3-15. Impedance of Radial Power Combiner at Elemental Amplifier Radius

combiner height is small enough so that there is no field variation in that direction.) The other possible modes have azimuthal components of current which can be damped by radial lossy slots in the top and/or bottom plates. These slots will not affect the TM_{omo} class of modes. Stabilization of the amplifier with respect to the TM_{010} and TM_{020} modes is accomplished within the individual elemental amplifiers due to the combined effects of the load resistance and the roll-off of negative resistance at lower frequencies. Figure 3-16 is a photograph of the entire combiner showing the radial slots and the elemental amplifier structure.

Testing of the complete amplifier revealed multiple frequency oscillations. It was also observed that some of the apparent frequencies were intermodulation products. The threshold current for oscillations was approximately 55 mA, indicating that a large impedance mismatch existed. Attempts at stabilization through the variation of elemental amplifier circuit parameters as well as combiner parameters were both unsuccessful.

Some of the techniques which were attempted with the aim of stabilizing the amplifier were:

a. Modification of the input coax/radial transition to form a 50-ohm conical transmission line section.

b. Introduction of tuning screws into the top plate of the radial line and into the side wall.

c. Introduction of lossy material into both the radial line and the elemental amplifiers.

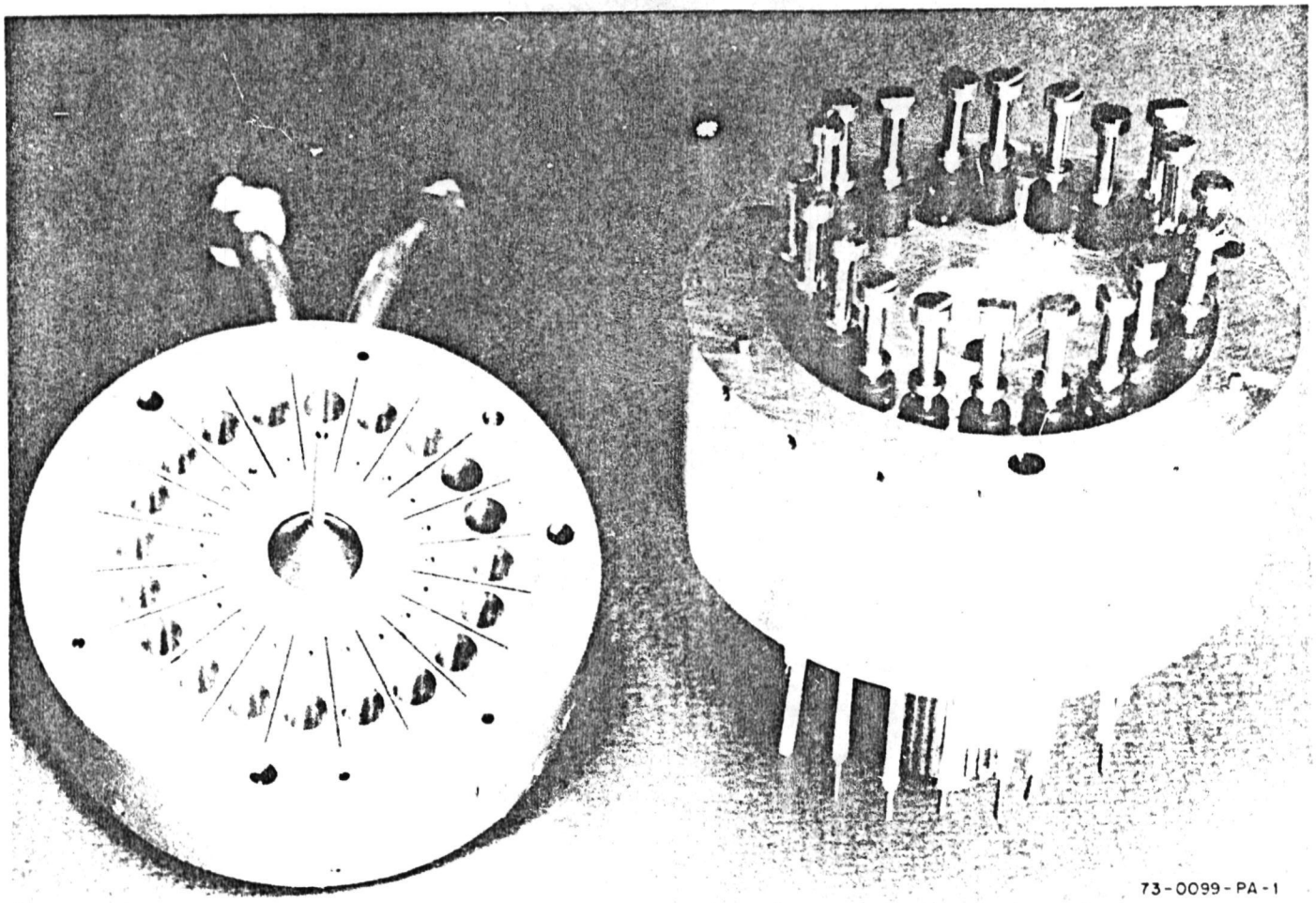

Figure 3-16. RADCOM With Twenty Elemental Amplifiers

3.4 ANALYSIS AND RECOMMENDATIONS

In retrospect, the failure of the radial combiner approach was due to the lack of understanding of several areas, the most significant of which was the radial combiner itself.

In theory, at least, it is possible to find a load radius and a diode radius at which, for example, a 50-ohm load is transformed to a 50-ohm input impedance. This characteristic, however, will be band-limited in nature, meaning that extreme care must be taken in controlling the out-of-band characteristic. Furthermore, from a practical point of view, it is very difficult to define the effective load radius and simultaneously impose a given load impedance at that radius.

The radial combiner, by definition, is a low Q_L circuit, as opposed to a resonant combiner which is a relatively high Q_L circuit. This implies that if the elemental amplifiers are not sufficiently isolated from each other in all possible modes other than the desired radially propagating, symmetric mode, spurious oscillations at different frequencies can occur. This possibility requires the use of some form of selective mode suppression such as radial lossy slots. It appears now that one of the problems in the present design was that the slots which were used did not load sufficiently the undesired modes.

A basic question now arises. Which of the two components, combiner or elemental amplifier, should be the primary frequency and bandwidth determining element? It appears that by the nature of the components the most effective approach would be to construct a broadband elemental amplifier and couple it to a narrow band power combiner. This arrangement lessens the requirement on

having identical elemental amplifiers since their exact bandwidth is not a critical parameter as long as it is sufficiently broad. Furthermore, it allows frequency tuning by the variations of one parameter (combiner resonance) rather than 20. Some degree of tuning would still be desirable on the elemental amplifier level, but its effect on the overall amplifier would not be as great as in the high Q_L case.

In summary, it is recommended that in future designs of higher order mode combiners the resonant combiner approach be given the most serious consideration. Using effective mode suppression, this configuration appears to be far superior to the low Q radial combiner in ease of characterization and in the design of the elemental amplifiers.

4. RESONANT COMBINER

The resonant combiner is the primary frequency and bandwidth determining element in the amplifier. It also, as the name implies, acts as a power combining network. Figure 4-1 illustrates the combiner geometry. The combiner operates in the TM_{010} mode, the dominant mode for a cylindrical cavity. The field configuration in this mode has no variation in the axial or azimuthal direction. Coupling into and out of the cavity is accomplished by a coaxial line whose center conductor protrudes into the cavity at the center. The cavity is tuned by a centrally located dielectric rod which enters the cavity from the wall opposite the coupling probe.

The elemental amplifiers are made up of coaxial lines in which the IMPATT diodes and their impedance transforming networks are embedded. As the center conductor passes through the region in which the cavity intersects the elemental amplifier some energy is coupled, primarily through the circular magnetic fields, into the cavity.

4.1 COMBINER ANALYSIS

The field components in the uperturbed cavity are given by

$$E_z = E_o J_o(kr) \tag{4-1}$$

$$H_\phi = \frac{jE_o}{\eta} J_1(kr) \tag{4-2}$$

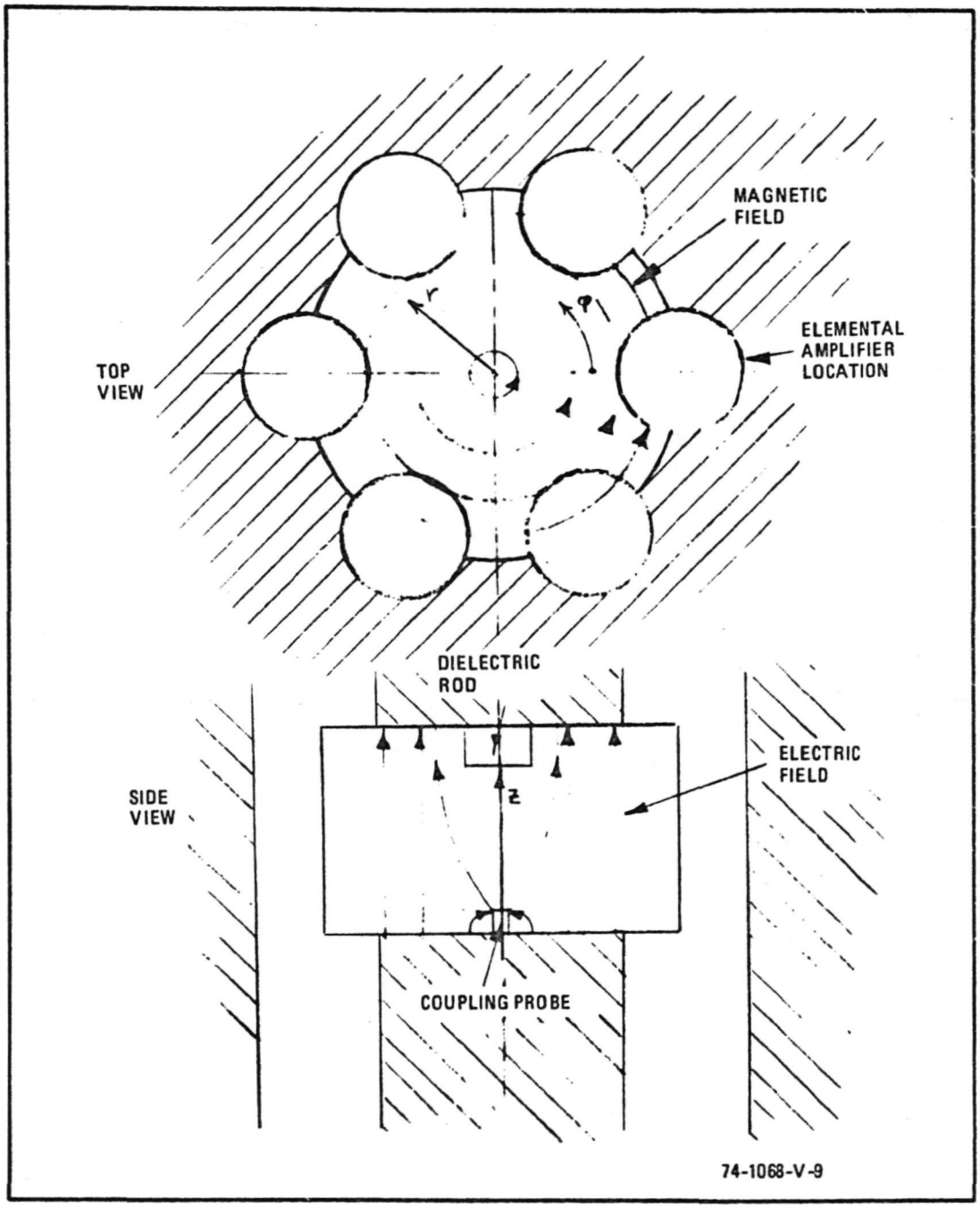

Figure 4-1. Resonant Combiner

where J_o and J_1 are the zero and first-order Bessel functions and $\eta = \sqrt{\mu/\epsilon}$. The first zero of the zero-order Bessel function represents the fundamental resonance of the cavity. That is, if the cavity radius is given by

$$r_o = \frac{P_{o1}}{k} = \frac{2.405}{k} \qquad (4\text{-}3)$$

where P_{o1} is the first zero of J_o, the resonant wavelength is given by

$$\lambda = \frac{2\pi}{k} = 2.61\ r_o. \qquad (4\text{-}4)$$

At 15 GHz, $\lambda_o = 2$ cm, and therefore $r_o + 0.766$ cm or 0.302 inches. From a practical point of view, however, it would be desirable to set the cavity resonance to a frequency somewhat over the desired operating frequency in order to allow some flexibility in tuning around the nominal operating point.

The cavity geometry being used, however, has a non-cylindrical form due to the intersections with elemental amplifier coaxial sections. These perturbations on the purely cylindrical model affect both the resonant frequency and the unloaded Q, tending to reduce both. The introduction of perturbations also introduces the possibility of spurious resonances at frequencies other than the desired frequency. To check for this possibility, the return loss at the input-output cavity port was measured versus frequency with the fundamental resonance adjusted to 15 GHz. The elemental amplifier holes were empty i.e. the central conductors of the coaxial section, the loads and diodes were removed. This is illustrated in Figure 4-2. The large spike is the return loss at 15 GHz. The other is switching transient in the sweep circuit.

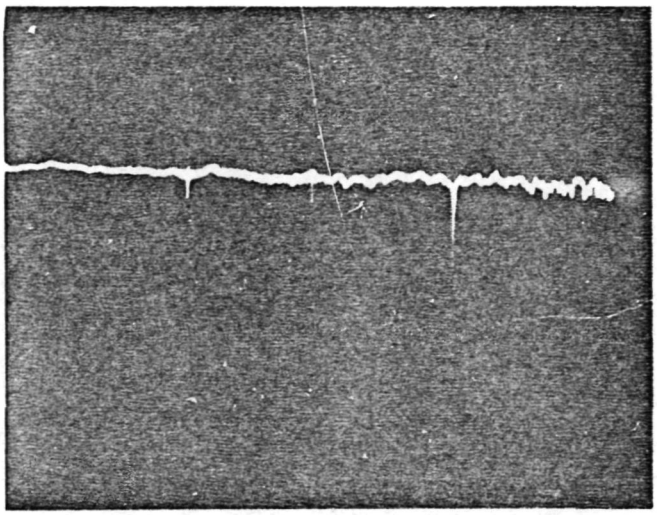

74-1068-PA-10

Figure 4-2. Cavity Return Loss With Elemental Amplifier Holes Empty (10 dB/div., 6 to 18 GHz)

The unloaded Q, Q_o, will determine the efficiency of the resonator as a power combiner. For an unperturbed cylindrical cavity, Q_o for the fundamental resonant mode is given by[14]

$$Q_o = \frac{\eta}{R_s} \quad \frac{P_{o1}}{2\,(r_o/h + 1)} \tag{4-5}$$

where h is the cavity height and R_s is the surface resistivity. For the present cavity, r_o = 0.283 inches, h = 0.311 inches, and R_s = 0.038 ohm. Therefore, Q_o = 6241. Measurements, however, indicate a Q_o of 1000, reflecting losses in the empty coaxial sections, the dielectric tuning rod, and the probe coupling structure.

Since the cavity is the primary frequency and bandwidth determining element in the amplifier, it must be adjusted (through adjustment of the coupling probe) to the required loaded Q. Figure 4-3 illustrates the VSWR variation with probe insertion at the central port. The region to the left of the minimum corresponds to the undercoupled condition, in which more power is dissipated in the internal cavity losses than in the load. For efficient operation, then, the cavity must be adjusted to the proper <u>over-coupled</u> condition. The required Q_L for a given gain and bandwidth is given by

$$Q_L = \frac{2}{(1 + \sqrt{G})\,b} \tag{4-6}$$

where G is the power gain ratio and b is the fractional 3 dB-bandwidth. Assuming 7-dB gain and a 200-MHz, 3-dB bandwidth at 15 GHz, the required Q_L becomes 46.3.

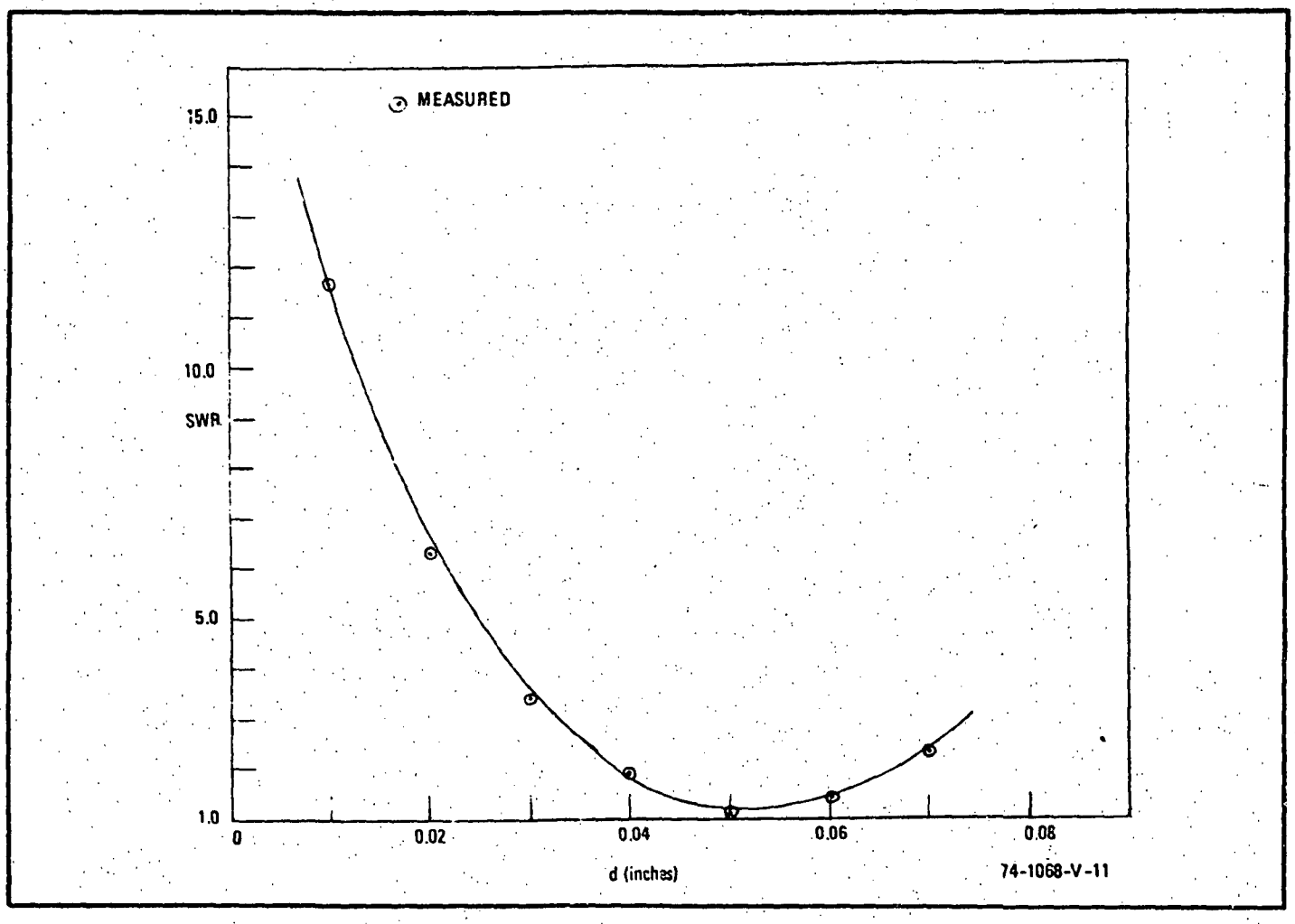

Figure 4-3. VSWR at Resonance For Various Insertions of Probe

Referring to Figure 4-4 which represents the equivalent circuit of the cavity loaded by the generator impedance, we can write

$$Q_L = \frac{n_1^2 R_L R_c}{R_c + n_1^2 R_L} \cdot \frac{1}{\omega_o L_c} \tag{4-7}$$

$$Q_o = \frac{R_c}{\omega_o L_c} \tag{4-8}$$

therefore,

$$Q_L = \frac{n_1^2 R_L}{R_c + n_1^2 R_L} Q_o \tag{4-9}$$

$$= \frac{1}{\left(R_c / n_1^2 R_L\right) + 1} Q_o$$

Rearranging we get

$$\frac{R_c}{n_1^2 R_L} = \rho_o = \frac{Q_o}{Q_L} - 1 \tag{4-10}$$

where ρ_o is the VSWR at resonance. Equation 4-10 gives us, therefore, a criterion for the adjustment of Q_L.

Figure 4-5 illustrates the equivalent circuit of the entire six-diode amplifier. In the figure, $-R'_D$ represents the transformed diode negative resistance, R_s is the stabilization resistance (to be discussed later), and n_2 is the equivalent turns ratio of the coupling network between each elemental amplifier and the resonant cavity. Figure 4-6 shows a cross section of the actual amplifier.

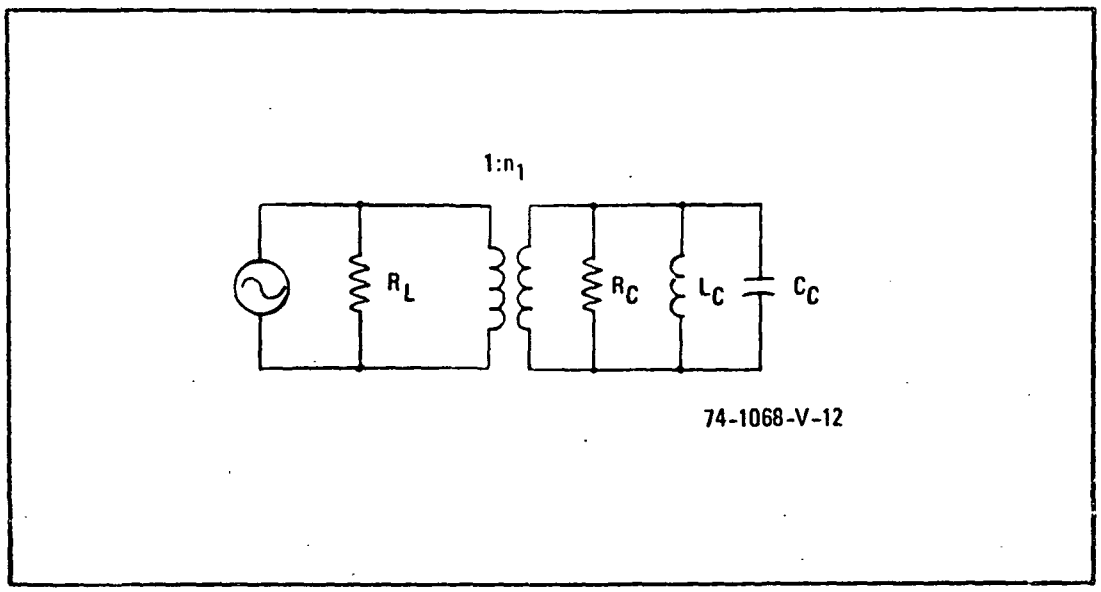

Figure 4-4. Equivalent Circuit of Cavity (Valid Only in the Neighborhood of the Resonant Frequency) Loaded By the Generator Impedance

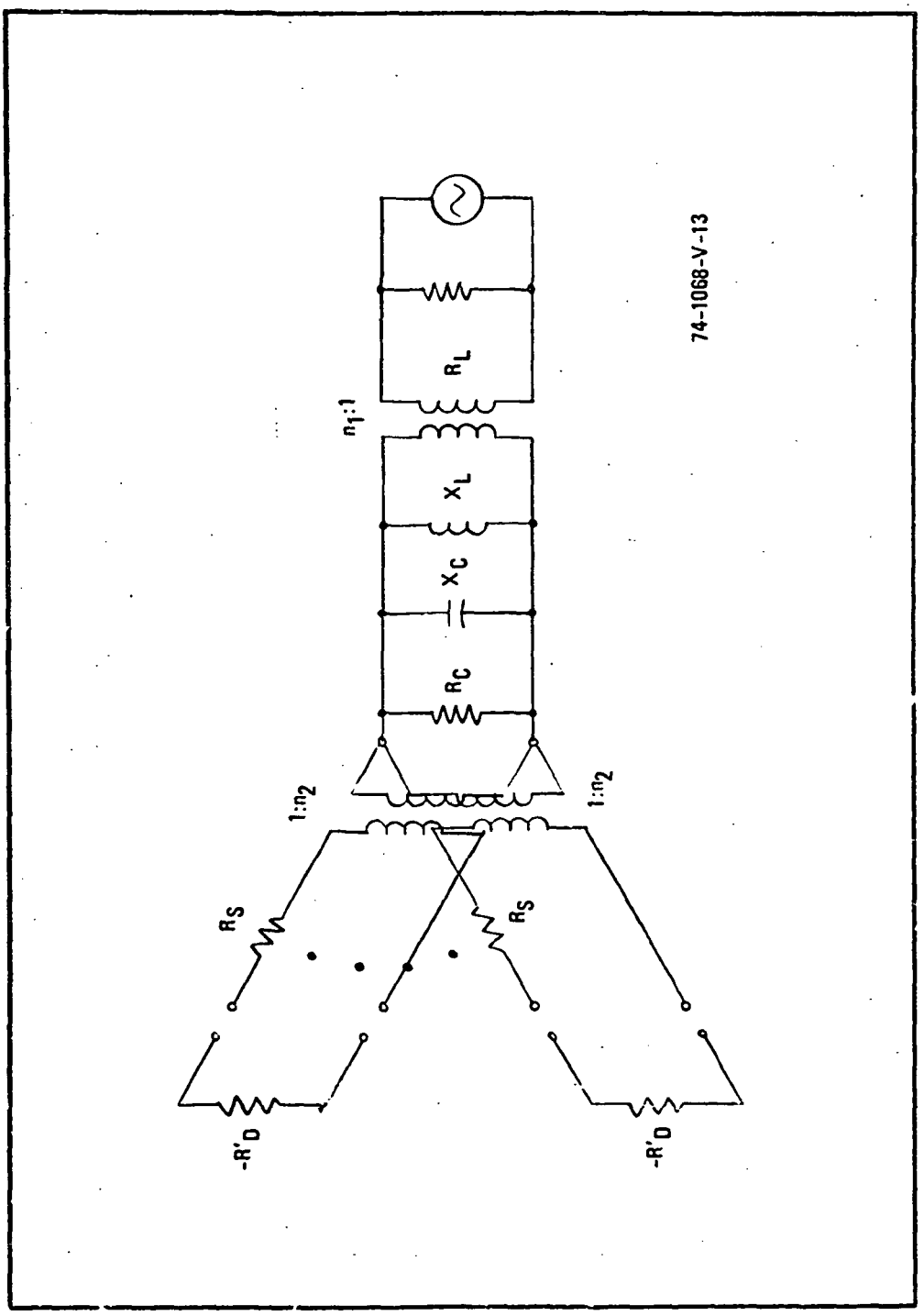

Figure 4-5. Equivalent Circuit of Six Diode Amplifier

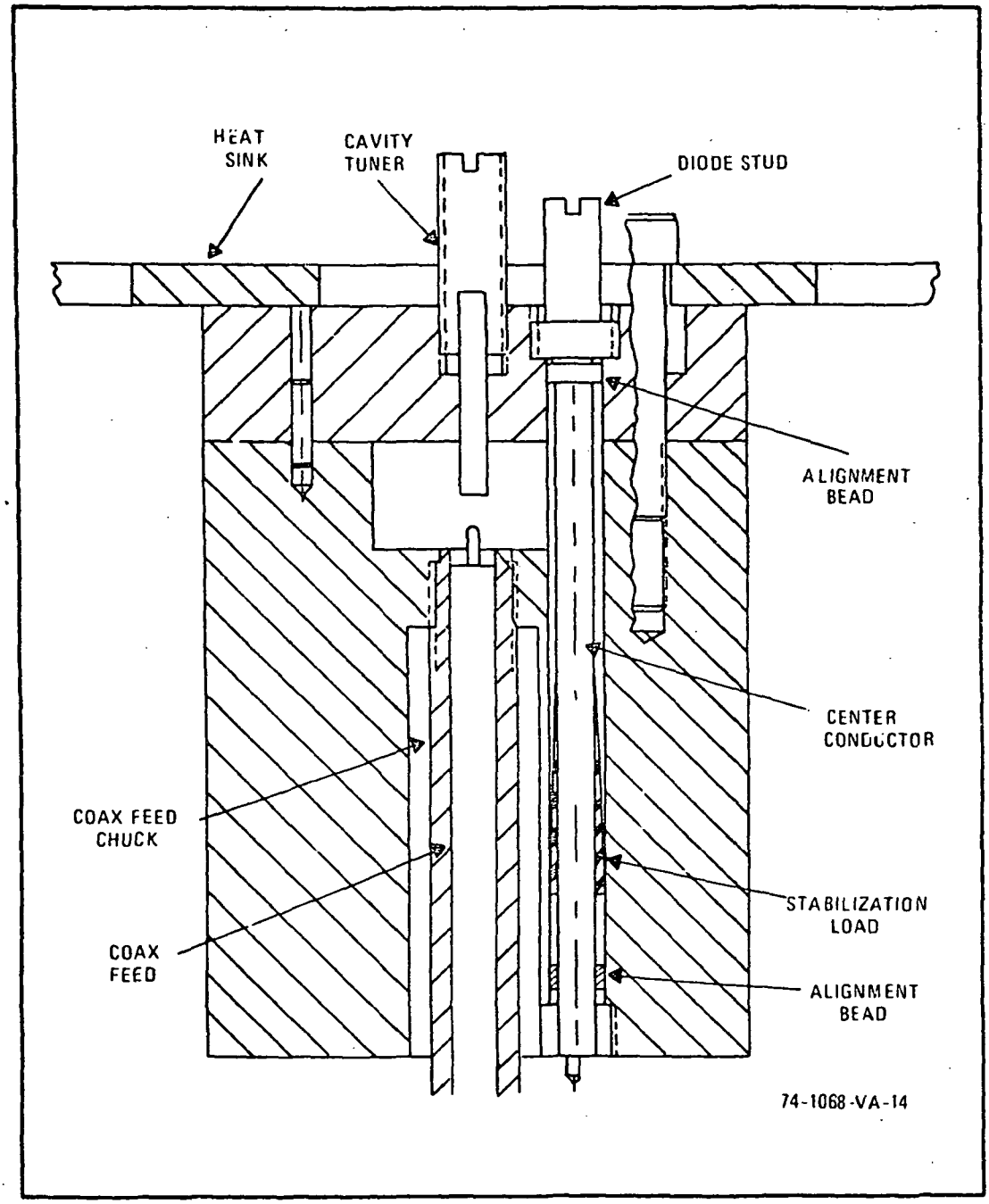

Figure 4-6. Six Diode Combiner Internal Configuration

4.2 INTER-ELEMENT COUPLING

A major problem in all multi-element active circuits is the effect of spurious coupling between the active elements. The coupling problem can be divided into two possible cases. One case is the situation in which the cavity is resonant in the desired mode and at the desired frequency. In this case, all the diodes are tightly coupled to the positive load impedance through the cavity, implying that they are also tightly coupled to each other. This condition is, in fact, required in order that the composite structure act as a single unit. The second case corresponds to the situation where a signal is present at a frequency other than the cavity resonant frequency. In this case, there are two mechanisms which will tend to stabilize the system. One mechanism is the presence of the stabilization load in each elemental amplifier and the band-limited nature of the coaxial transformer, which can be considered as making the elemental amplifier stable in the operating band and more stable outside the operating band. In other words, the negative conductance of the elemental amplifier is at a maximum at the operating frequency. The other mechanism is due to the nature of the fields in the cavity when the cavity is detuned. Since the cavity will not support a resonance under these conditions, coupling will occur only through evanescent fields present in the region where the elemental amplifier center conductor passes through the cavity. The solution of the boundary value problem in this structure would be very complicated and time-consuming and therefore a qualitative approach will be taken here. One direct observation is that the magnitude of the physical discontinuity will determine the magnitude and rate of decay of the evanescent fields present in the vicinity of the discontinuity. The evanescent fields can be represented as voltages on a short length of

lossy transmission line. A rapid decay rate would therefore correspond to a highly lossy line connecting the elemental amplifiers. The structure will be stable, therefore, if the equivalent loss resistance is greater than the negative resistance presented by the elemental amplifiers.

If we now consider only adjacent-element coupling, we can analyze the similar problem of TEM directional coupler. Jones and Bolljahn[16] derive an equation for the coupled voltage of the form

$$V_2 = V \frac{jk \sin \theta}{\sqrt{1 - k^2} \cos \theta + j \sin \theta} \qquad (4\text{-}11)$$

where θ is the electrical length of the coupling regions at a given frequency; where k is the mid-band coupling parameter ($\theta = \pi/2$) and is defined by

$$k = \frac{Z_{oe} - Z_{oo}}{Z_{oe} + Z_{oo}} \quad . \qquad (4\text{-}12)$$

The parameters Z_{oe} and Z_{oo} are, respectively, the even- and odd-mode characteristic impedances of the coupled structure. Z_{oe} is the impedance between the conductors when both conductors are at the same potential while Z_{oo} is the impedance when the two conductors are at opposite potentials. The same result can be arrived at by considering the electrostatic case, that is

$$Z_{oe} \longrightarrow 1/C_{oe}$$

$$Z_{oo} \longrightarrow 1/C_{oo} \qquad (4\text{-}13)$$

where C_{oe} and C_{oo} are capacitances defined as above. The expression for k in this case becomes

$$k = \frac{C_{oo} - C_{oe}}{C_{oo} + C_{oe}} \cdot \qquad (4\text{-}14)$$

(See the paper by Getsinger[17] for a discussion of the electrostatic analog.)

Using the impedance formulation we can therefore construct a two dimensional resistive analog (with the same boundary conditions) where the measured resistances will be the analogs of impedances per unit length (or 1/C per unit length).

To implement this, a scaled version of two adjacent elemental amplifier coaxial lines was deposited on resistive paper using silver paint. The coupling parameter was then calculated from measured values of even- and odd-mode resistances, as schematically illustrated in Figure 4-7. The results indicated that the coupling would be greater than 30 dB down, which should be sufficient to prevent spurious oscillations even under small-signal, high-gain conditions.

Once we have defined the required loaded Q, Q_L, of the cavity, we have also uniquely defined the impedance presented by the cavity to the elemental amplifier (for a given transformation ratio n_2) at resonance. In the original design of the overall amplifier it was assumed that a large ratio could be achieved between R_C/n_2^2 and Z_o, the characteristic impedance of the coaxial line passing through the cavity, thus allowing termination of the line in $R_S = Z_o$, and maintaining a high circuit efficiency. Testing of the final version of the cavity indicated, however, that R_C/n_2^2 was a relatively constant function of Z_o

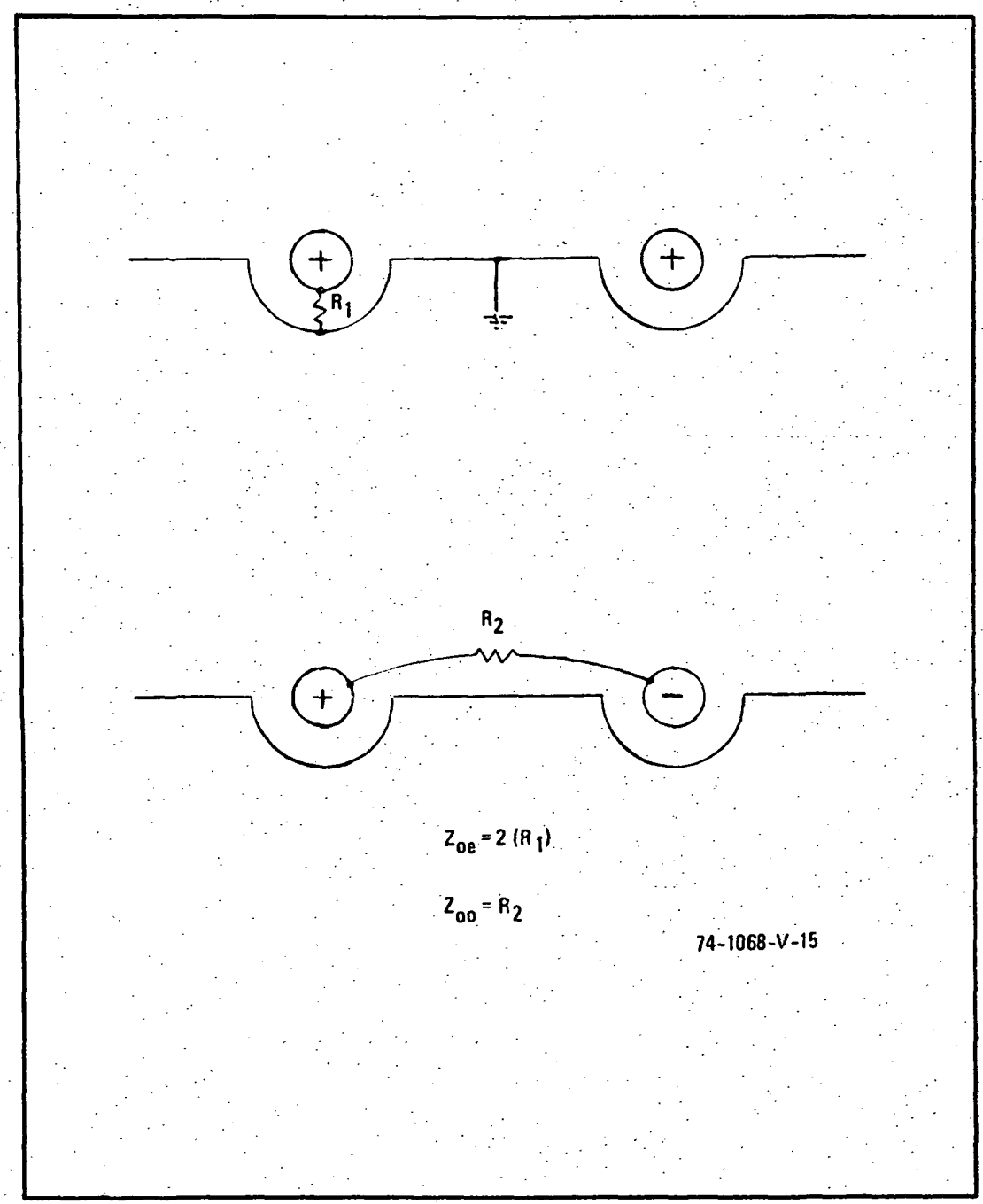

Figure 4-7. Illustration of Technique Used to Determine Even-and-Odd Mode Impedances

and, in fact, was approximately $3 Z_o$. These tests were carried out with three transmission lines of $Z_o = 15\ \Omega$, $50\ \Omega$, and $90\ \Omega$, each terminated with $R_S = Z_o$. At this point three possible choices were considered.

a. Redesign the cavity in order to decrease n_2 by approximately a factor of 2.

b. Maintain the cavity design but terminate the line in $R_S \approx Z_o/3$.

c. Terminate the line in $R_S = Z_o$ and thereby concede a loss in efficiency.

It was decided that redesign of the cavity would be both expensive and time-consuming. Furthermore, there was uncertainty that the redesign would yield the required increase in coupling (decrease in n_2) and simultaneously maintain the 30-dB isolation between adjacent elemental amplifiers. The latter two possibilities appeared worthy of exploration. Section 6 will discuss the investigation of these alternatives.

5. DIODE CHARACTERIZATION

In most IMPATT circuit designs the diode is the basic limiting component in the circuit. This is especially true if, as in this case, the diodes are purchased commercially. The circuit designer is often at the mercy of the manufacturer when it comes to the fundamental design of the semiconductor element as well as in the selection of a suitable diode package from a limited range of types. Assuming that the circuit designer has chosen the diode and package wisely the first step is to measure the impedance of the packaged diode over the range of frequencies and RF power levels at which the diode exhibits negative resistance. These measurements are of fundamental importance since the elemental amplifier circuit design will be based on them. The procedure which was used in this program is outlined below:

a. Derivation of a lumped-element equivalent circuit for the diode package in the circuit in which it will be tested and, possibly a modified version of the equivalent circuit for the circuit in which it will finally be used.

b. Measurements to determine the actual values of the elements in the package equivalent circuit(s).

c. Measurements of impedance versus frequency and RF power level for the packaged diode.

5.1 PACKAGE CHARACTERIZATION

Figure 5-1 illustrates the package used and gives its physical dimensions. The package is made up of four basic components.

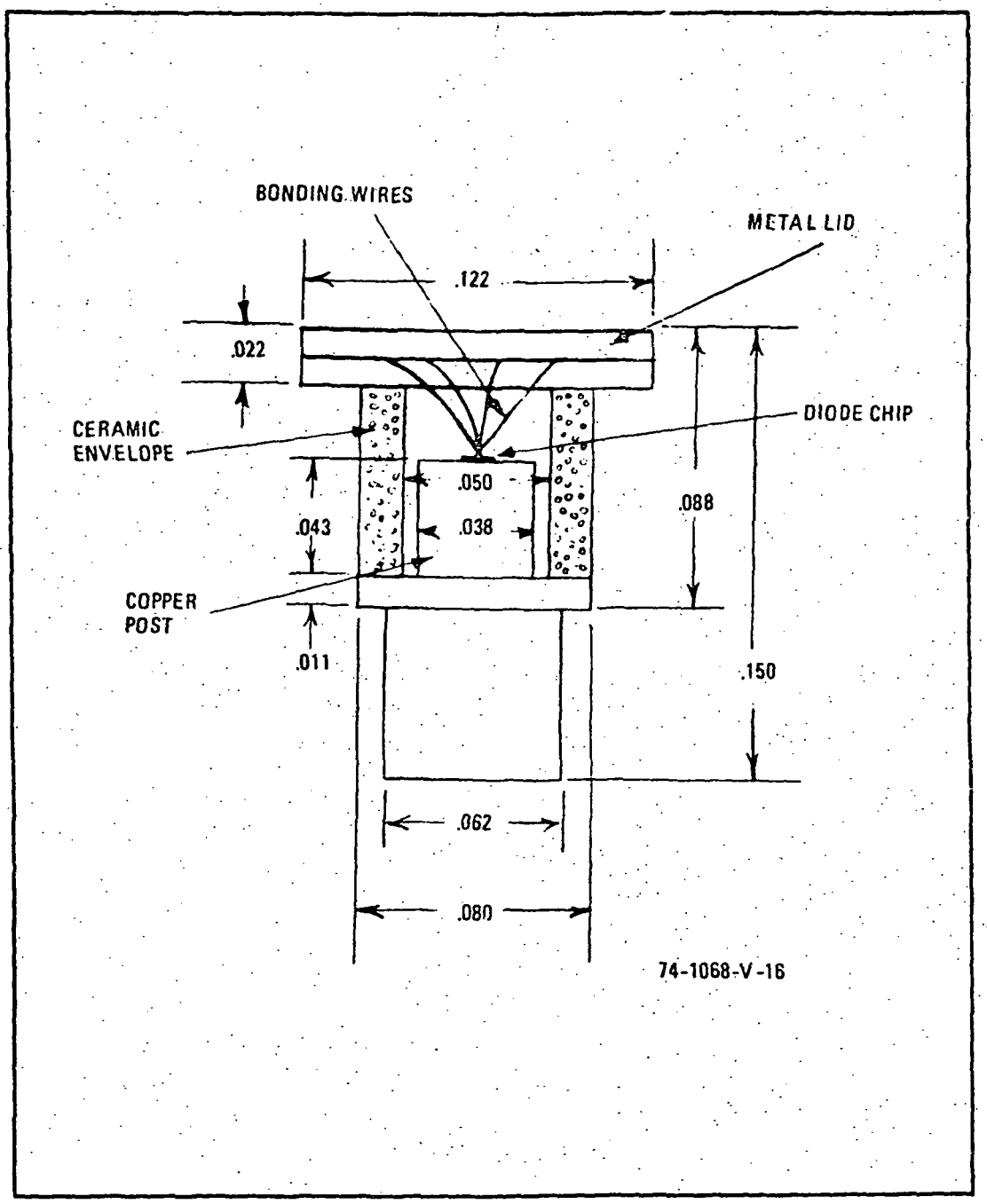

Figure 5-1. Schematic of Diode Package

a. A copper post, which serves as a platform on which the diode is mounted and through which the heat generated at the junction is transferred to a heat sink.

b. A ceramic cylindrical envelope which provides insulation between cathode and anode and also provides a hermetic seal.

c. A pair of crossed gold wires (approximately 0.001 inch in diameter) used to contact the semiconductor chip and connected to the top of the package.

d. A soldered metal lid to maintain the hermetic seal and serve as an electrical contact.

It may be helpful at this point to define what the significance of a lumped-element equivalent is when applied to a microwave circuit such as a diode package.[18] First, any lumped-element circuit is an idealization of the actual circuit it represents. It is an idealization in the sense that in all real circuits the electric and magnetic fields vary in magnitude both spatially and temporally. This means, for example, that unique node voltages and loop currents do not exist in a circuit which has physical extent. The lumped-element approximation, therefore, will never be completely accurate. Its accuracy, however, will improve as the physical size of the circuit becomes a small fraction of a wavelength since under those conditions unique node voltages and loop currents may be defined. This also points out the fact that lumped-element equivalents are band limited. A valid equivalent circuit at 1 MHz may not be valid at 1 GHz.

With these ideas in mind, the lumped-equivalent circuit illustrated in Figure 5-2 was derived from the physical structure of the diode package and the coaxial structure into which it was embedded. Note that it was

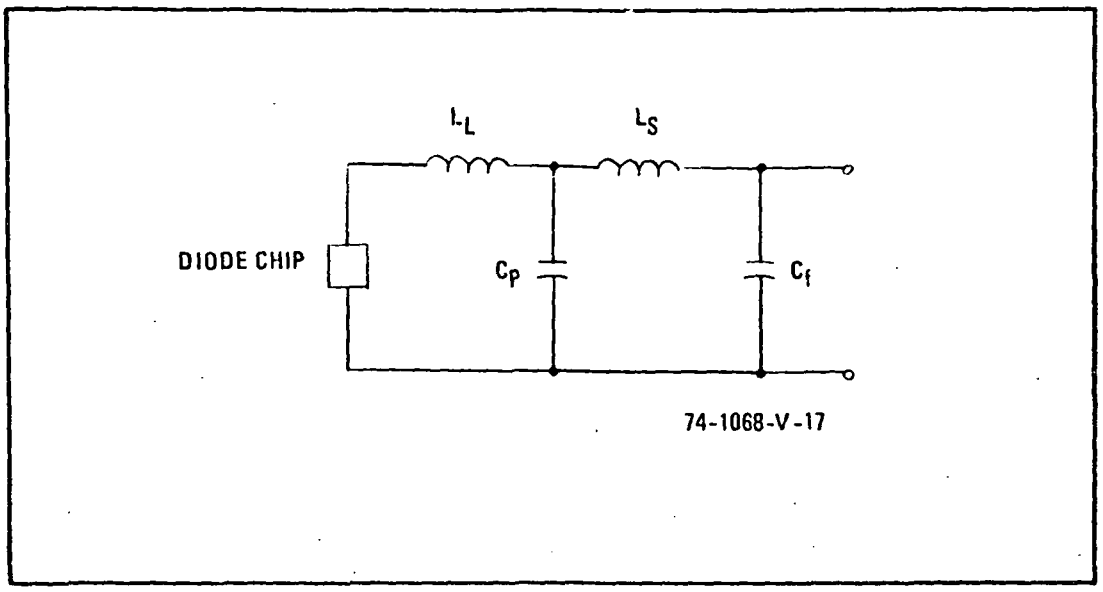

Figure 5-2. Diode Package Lumped - Equivalent Circuit

assumed that the package was lossless. The elements of the circuit are defined as follows:

L_S = stud or post inductance

C_p = capacitance between the post and the package lid

L_L = wire lead inductance

C_f = fringing capacitance between the lid and the coaxial outer conductor.

A test fixture was constructed in order to measure the impedance of the package at several frequencies around 15 GHz. Figure 5-3 illustrates the test fixture when connected to a coaxial slotted line.

These measurements were made on a 7-mm (0.276") diameter slotted line and in order to properly simulate the circuit into which the diode would be placed in the actual elemental amplifier, which would be in a 0.167" diameter coaxial line, a cylindrical hole of that diameter was machined into the test fixture. The depth of the hole was such that the reference plane for the measurements to follow would be at the junction of the package lid and the coaxial center conductor. Making the measurements in this way has the advantages of preserving the required physical structure around the diode package and also of referring the impedance measurements to a reference plane common to both the test fixture and the elemental amplifier. One major difference, however, is the discontinuity in outer diameters at the reference plane and this was accounted for in the lumped equivalent circuit of Figure 5-2 by adding a shunt capacitance, C_{disc}, across C_f.

The measurements on the diode package were done in two steps. In both steps empty diode packages (obtained from the manufacturer) were used. One package merely had a lid mounted on the ceramic cylinder and

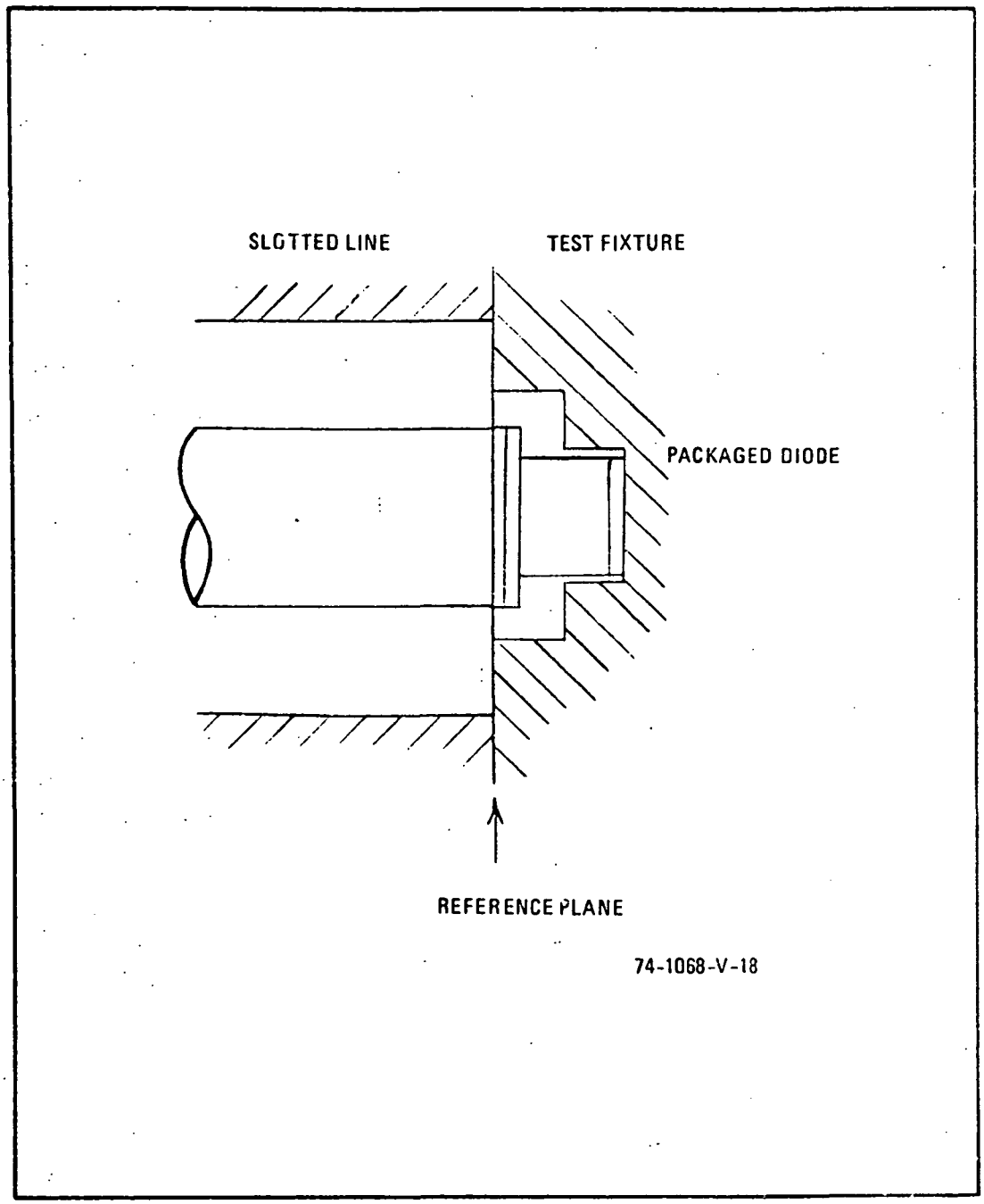

Figure 5-3. Cross Section of Diode Test Fixture Connected to Slotted Line

the other also had the two crossed bonding wires attached between the lid and the copper post on which the chip would have been mounted. The resulting equivalent circuits are illustrated in Figure 5-4. The measurement system used is shown in Figure 5-5.

Impedance measurements were made first on the open circuited package and then on the short-circuited package. Measurements were made at five frequencies; i.e., 13.0, 14.0, 14.5, 15.0, and 15.5 GHz. A computer program was then used to fit, in a least squares sense, element values to the equivalent circuit which would minimize the error between the calculated package input impedance and the measured input impedance. Figure 5-6 gives the fitted element values and a comparison of the calculated and measured input impedance.

It would be of some interest to compare these measured values with those of others for a similar package. Table 5-1 presents published values for C_p and L_s by Getsinger[18] and Monroe[19] along with the values measured here.

TABLE 5-1 - Comparison of Measured Equivalent Circuit Element Values

	This Measurement	Getsinger[18]	Monroe[19]
C_p	0.16 pf	0.14	0.25
L_s	0.37 nH	0.33	0.48

5.2 CHARACTERIZATION OF PACKAGED DIODE

Measurements were made of the actual diode (packaged) impedance versus frequency and input RF power level[20]. A computer program was used to process the raw slotted line data and calculate the corresponding diode impedance, admit -

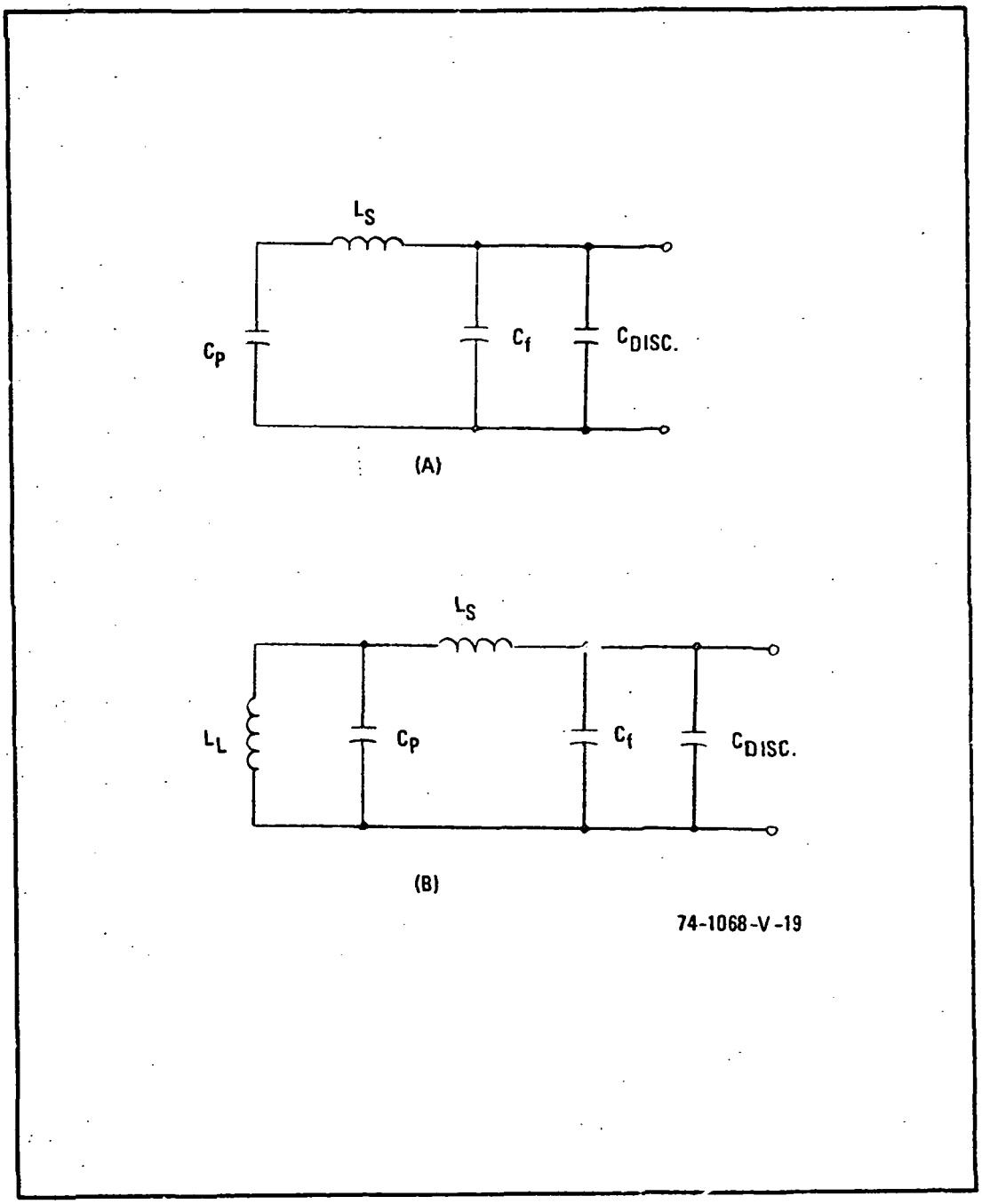

Figure 5-4. Equivalent Circuits of (A) Open-Circuited Diode Package, and (B) Short-Circuited Diode Package

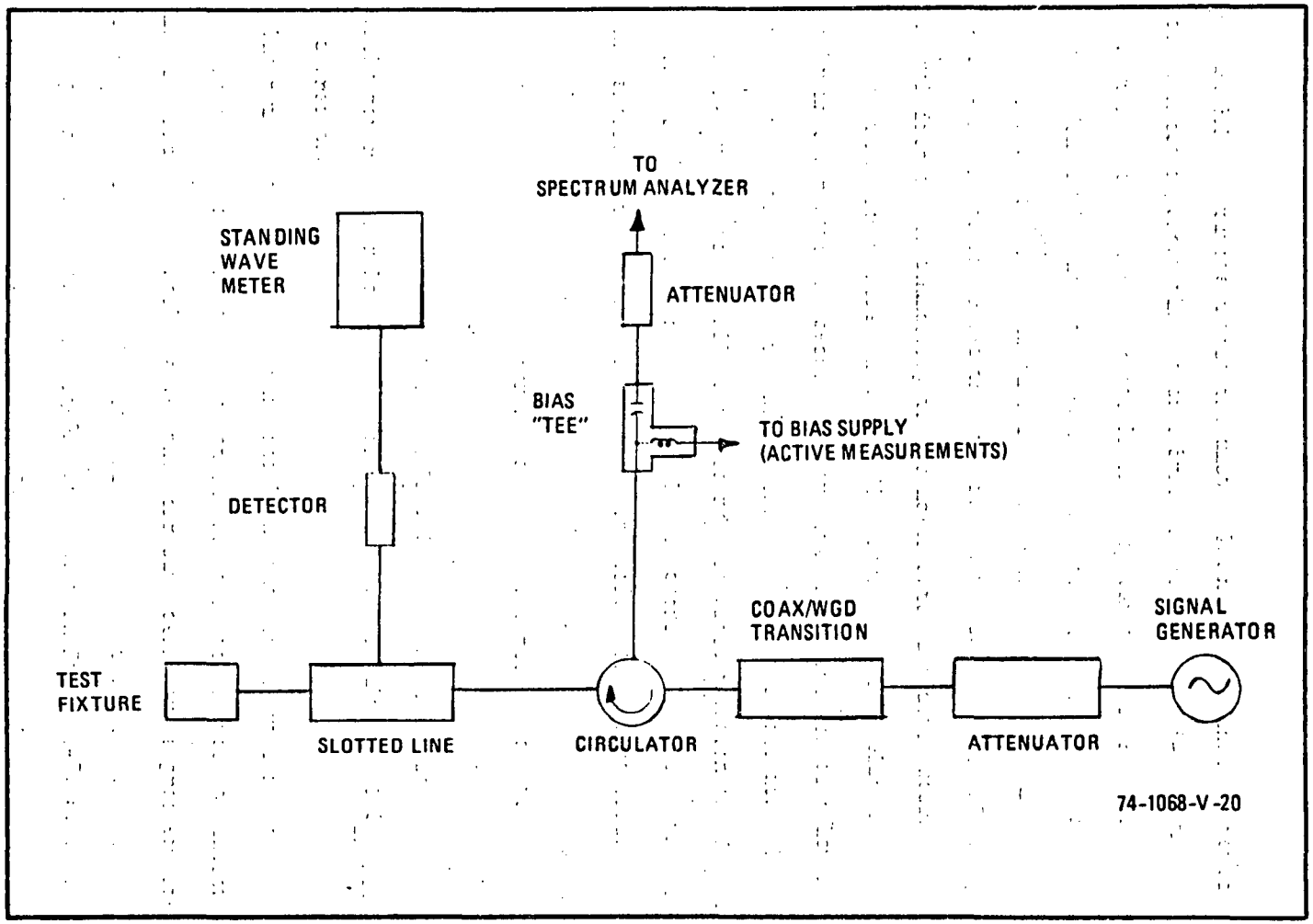

Figure 5-5. Test Circuit Used For Impedance Measurements

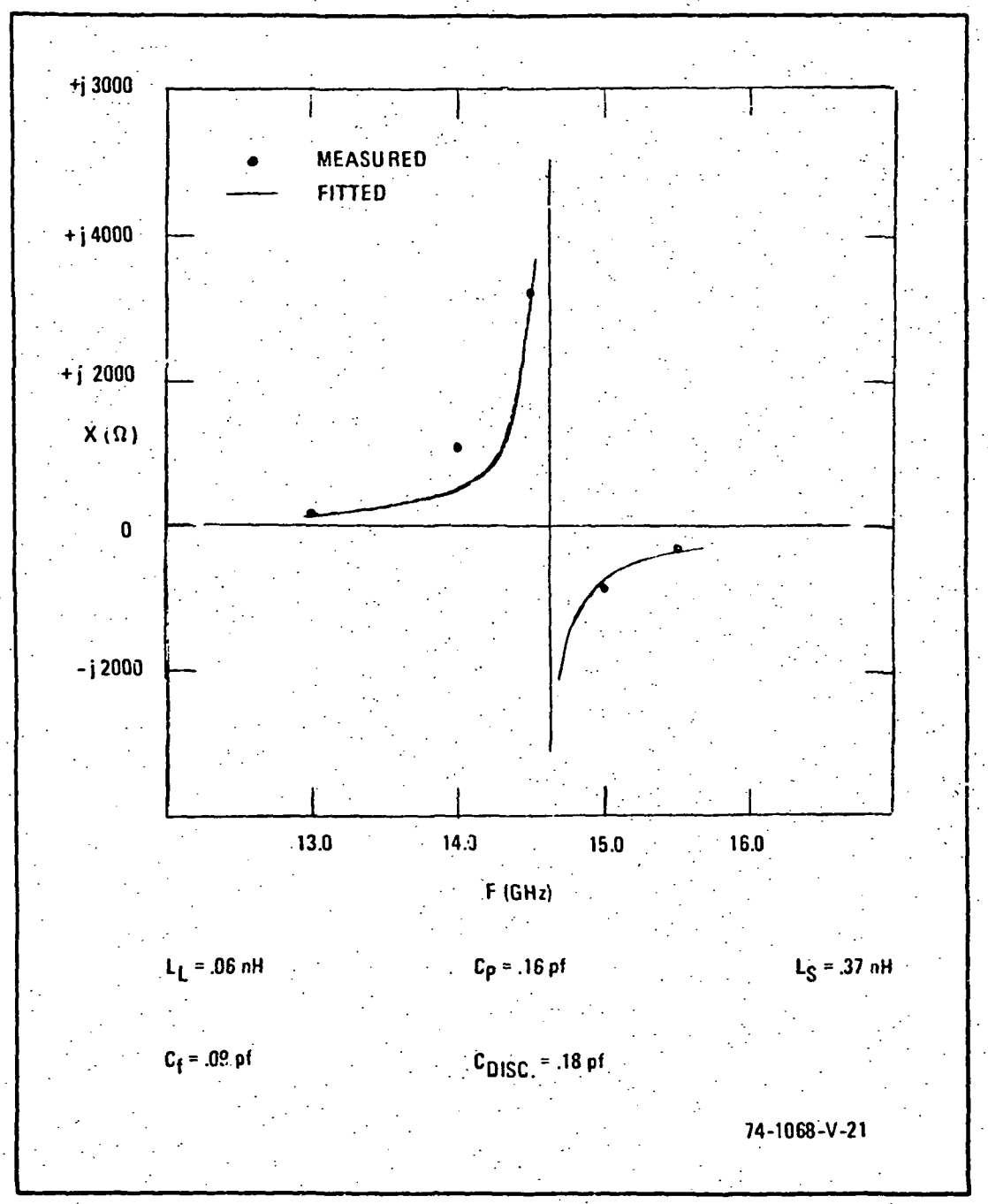

Figure 5-6. Comparison of Measured and Fitted Shorted Package Impedance Locus

tance, and RMS RF voltage across the diode. The negative of the measured diode impedance locus is shown plotted on a Smith Chart in Figure 5-7. During these measurements, subharmonic oscillations appeared at several points at which a relatively high input power was incident on the diode. Subsequent measurements of the circuit input impedance seen by the diode in the 6- to 9-GHz range indicated that the real part was as high as 100 Ω at several frequencies indicating that a lower input impedance would be required at those frequencies if the oscillations were to be eliminated.

Later in the program it became apparent that the criterion of a low load resistance in the vicinity of the subharmonic required modification. It was observed that parametric oscillations occurred for load resistances of 50 ohm and 12 ohm, but were absent for 27 ohm. It was decided, therefore, that an investigation should be undertaken to determine the effect of various circuit resistances on the resistance at the terminals of the equivalent chip negative conductance. The analysis was carried out using the package equivalent circuit discussed earlier. Figure 5-8 is a plot of $1/G_{IN}$ and $1/B_{IN}$ versus R_L at 7.5 GHz. Note that a minimum occurs for $1/G_{IN}$ at $R_L \simeq 27$ ohm. Similar plots were subsequently generated for lower values of L_S, with the result that $1/G_{IN}$ monotonically decreased.

The primary implication of this result is that the elimination of parametric oscillations is dependent on the minimization of package inductance. A minimum inductance would give the circuit designer a greater freedom in choice of load resistances as well as decrease the package Q, thus increasing bandwidth. Using the 15-GHz data shown in Figure 5-7, separate curves for the diode conductance and susceptance were plotted as a function of computed total RF voltage across the diode. These curves were then extrapolated to the point of maximum added power and were fitted with a power

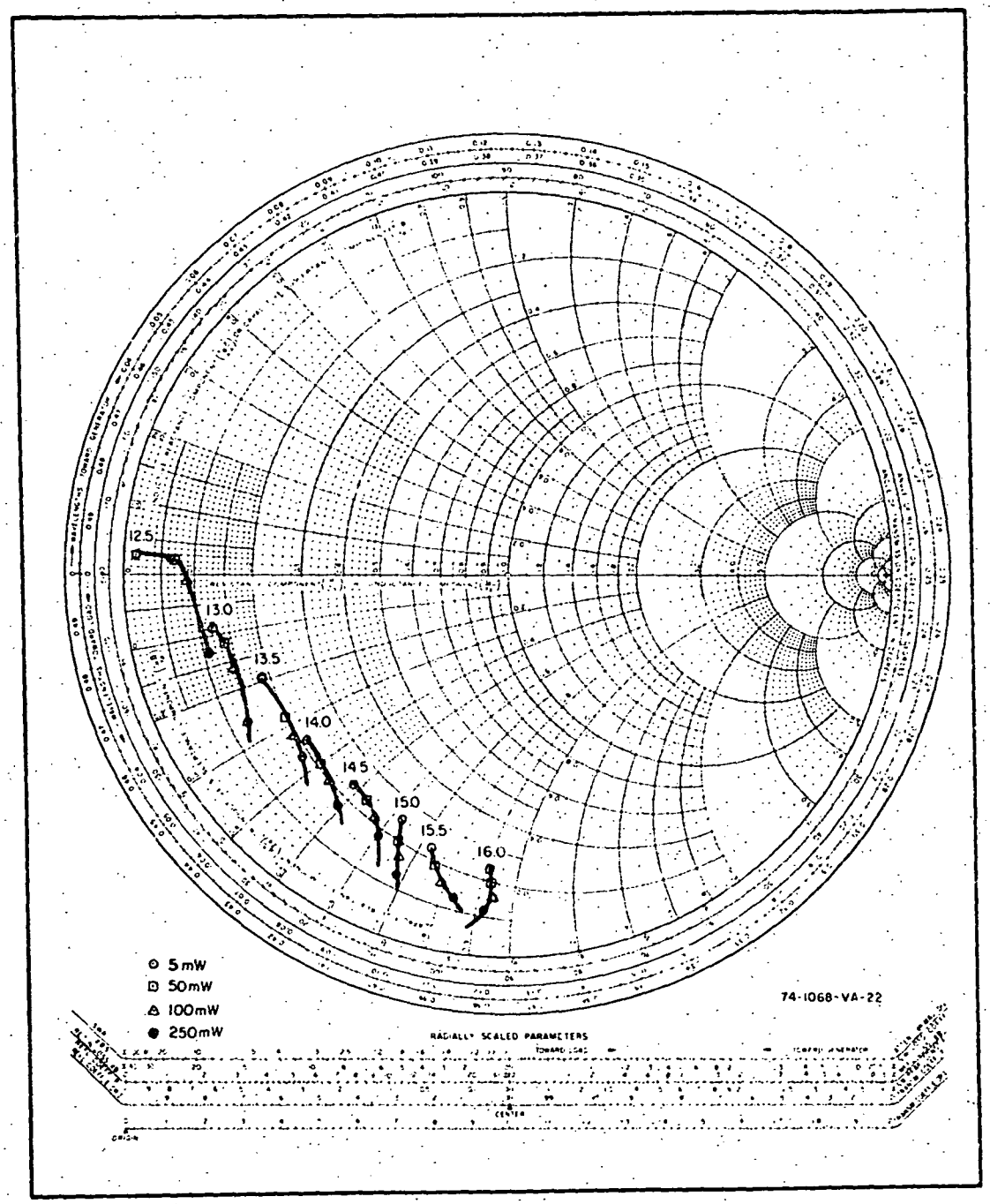

Figure 5-7. Smith Chart Plot of ($-Z_{diode}$) vs. Frequency and Input RF Power Level ($Z_c = 50\,\Omega$)

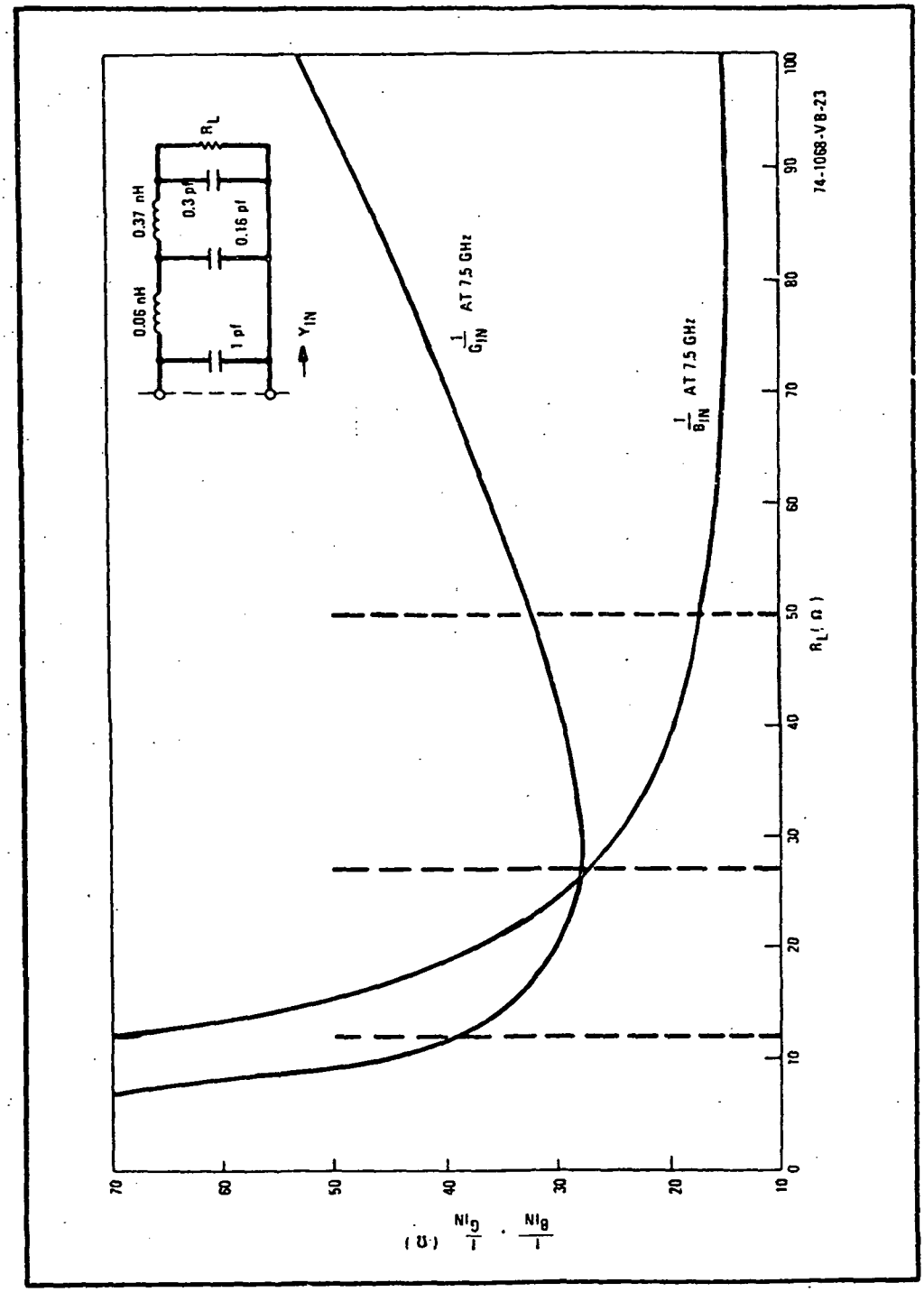

Figure 5-8. Y_{IN} vs R_L at Diode Negative Conductance Terminals

series function. The resulting curves are plotted in Figure 5-9. Using these curves, plots of gain and power added versus input power were generated for various circuit admittances. Figure 5-10 illustrates the computed gain and power added for the case where $G_{CIRC} = 0.010$ and $B_{CIRC} = 0.027$. This is a stable operating point since a conjugate match condition never exists.

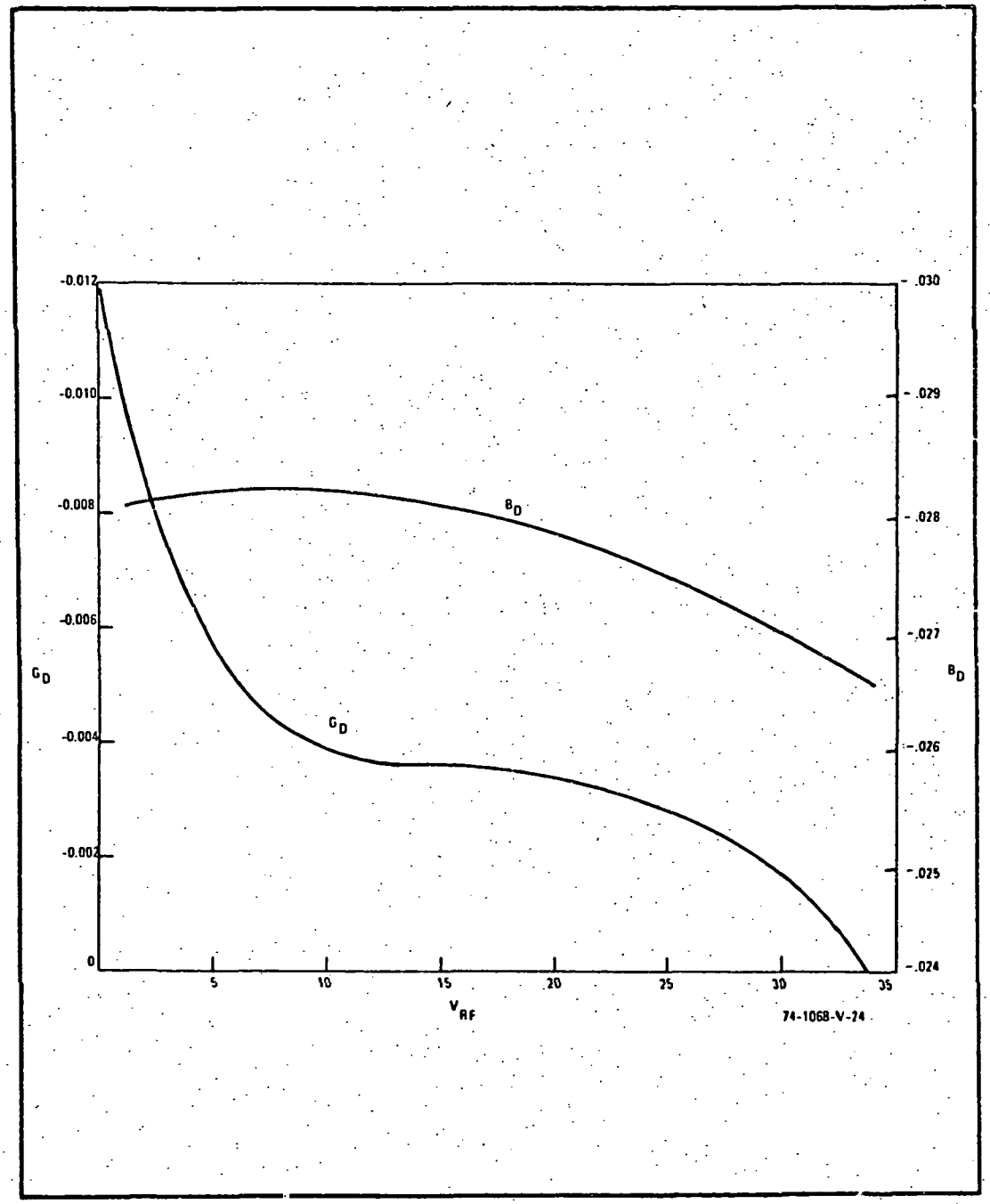

Figure 5-9: Diode Conductance and Susceptance vs. RF Voltage

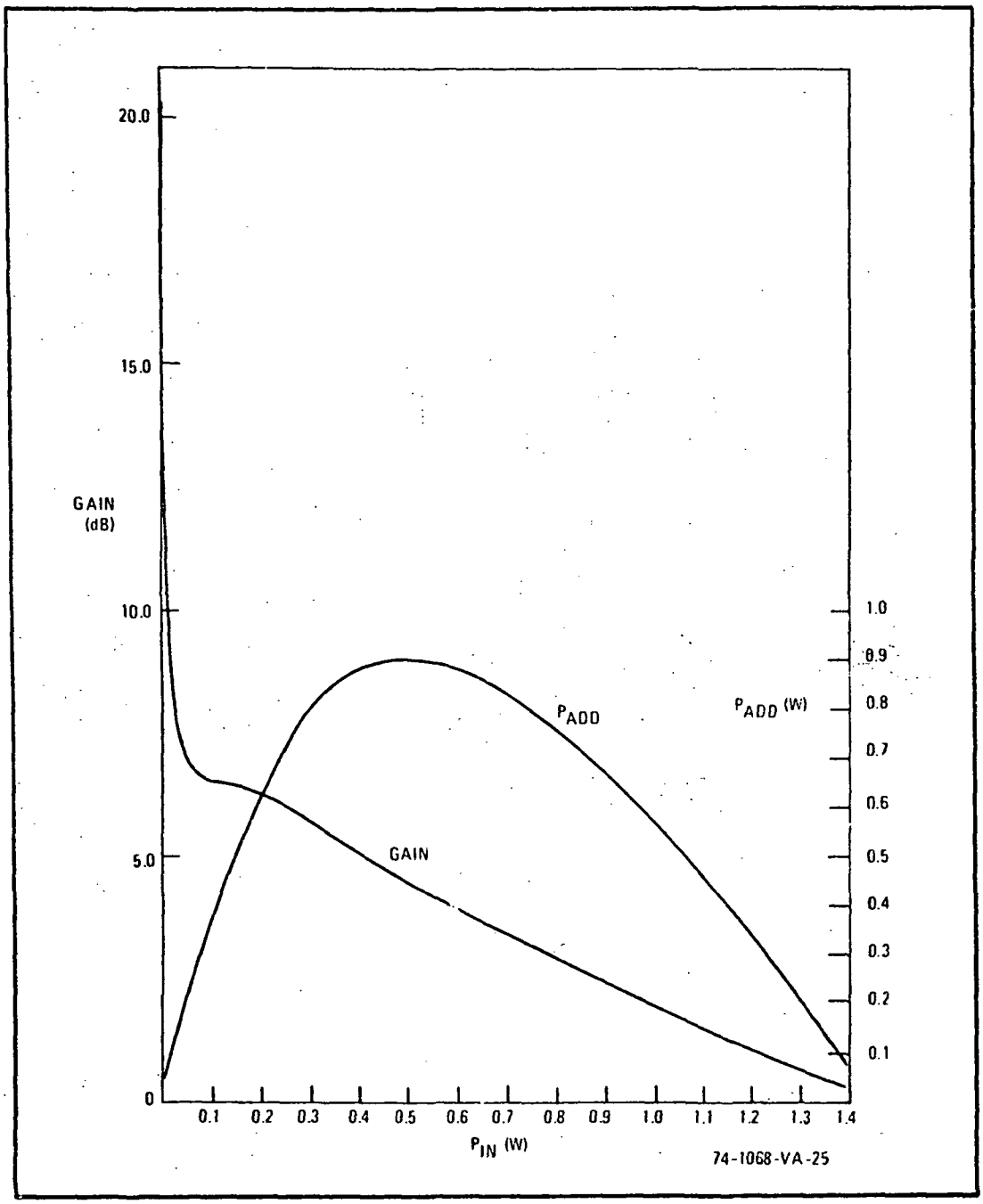

Figure 5-10. Computed Gain and Power Added vs. P_{in} for $G_{circ} = 0.010$, $B_{circ} = 0.027$

6. ELEMENTAL AND MULTI-DIODE AMPLIFIER

The approach to the design of the elemental amplifier was guided by three basic aims. These were:

a. To achieve the required gain and output power at 15 GHz.

b. To achieve a sufficiently low Q structure so that the resonant combiner would be the primary bandwidth and frequency determining component in the network.

c. To achieve unconditional stability at all frequencies outside the frequency band of interest.

These criteria may be restated as follows: The locus of the admittance presented to the diode must be such as to create a high gain situation in the immediate vicinity of 15 GHz and a low (or no) gain situation everywhere else. Furthermore, if the resonant cavity were to be replaced by a purely real resistance of the same magnitude as in the actual circuitry, the resulting elemental amplifier gain should be significantly more broad band (at least by a factor of 2). Although these criteria are somewhat simplified and qualitative, they do summarize the design problem.

Measurements of the coupling characteristics between the elemental amplifier and the cavity (Section 4) indicated that, with the cavity adjusted to the proper Q_L, the impedance presented to the elemental amplifier in series with the internal load resistance was approximately three times the characteristic impedance of the coaxial section. This condition made it undesireable to terminate the coaxial section in its characteristic impedance since approximately 25 percent of the power generated by the diode would be dissipated in the stabilization resistance. An alternative solution was termination of the coaxial line in a load impedance lower

than the characteristic impedance of the line. This technique has the advantage of increasing the circuit efficiency (less power dissipated in the internal load) but has the drawback that the circuit impedance seen from the diode position now becomes more frequency sensitive. It was therefore acknowledged that the impedance may vary considerably with frequency outside the relatively narrow amplifier band, but that this variation would not be a serious problem.

Several possible circuit configurations were evaluated by computer simulation. The circuit which appeared to be most promising is illustrated schematically in Figure 6-1. Figure 6-2 illustrates the computed impedance locus for the same circuit. A prototype impedance transformer was constructed based on the computer simulation and tests were carried out to determine its characteristics.

Stable small signal gain of approximately 15 dB at 15 GHz was obtained using this structure; however, as the input signal power was increased to approach the level at which the diode will operate in the final unit, a severe degradation in gain was observed at the center of the operating band. The degradation was of such a magnitude as to reduce the expected gain of approximately 8 dB to 2 or 3 dB under full RF drive (see Figure 6-3). Investigation into the cause of this effect indicated that a strong signal was present at the subharmonic of the frequency at which maximum gain and output power were expected. The presence of this oscillation caused a reduction of the effective IMPATT mode negative resistance of the diode and thus reduced its amplifying capability. Further investigation into this phenomenon indicated that this was a common problem in IMPATT amplifiers, especially in those where high efficiency diodes are used.[11]

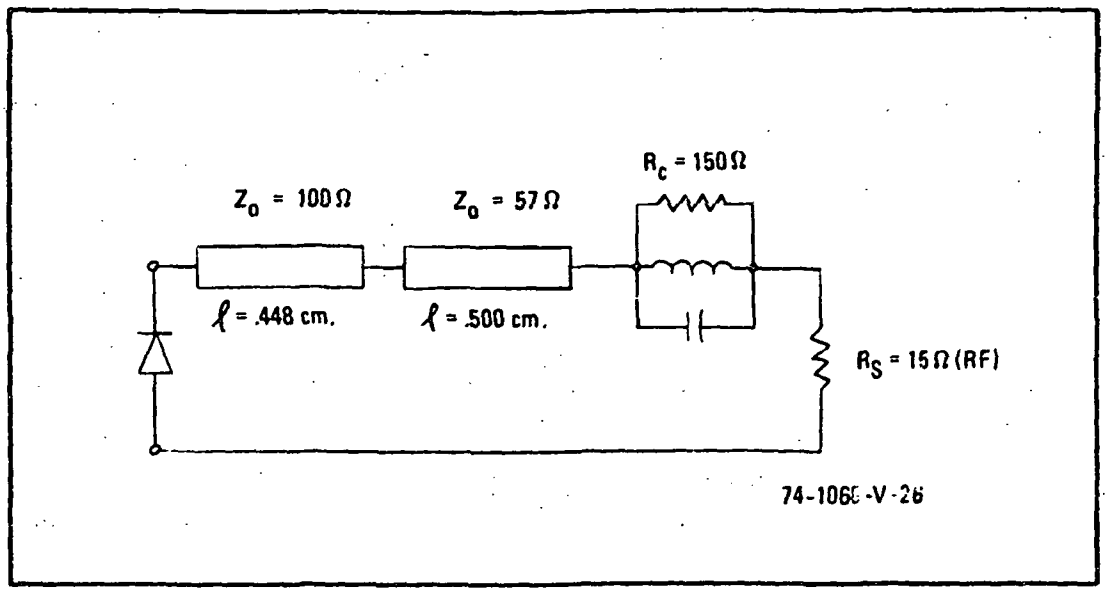

Figure 6-1. Elemental Amplifier Equivalent Circuit Using Mismatched Termination

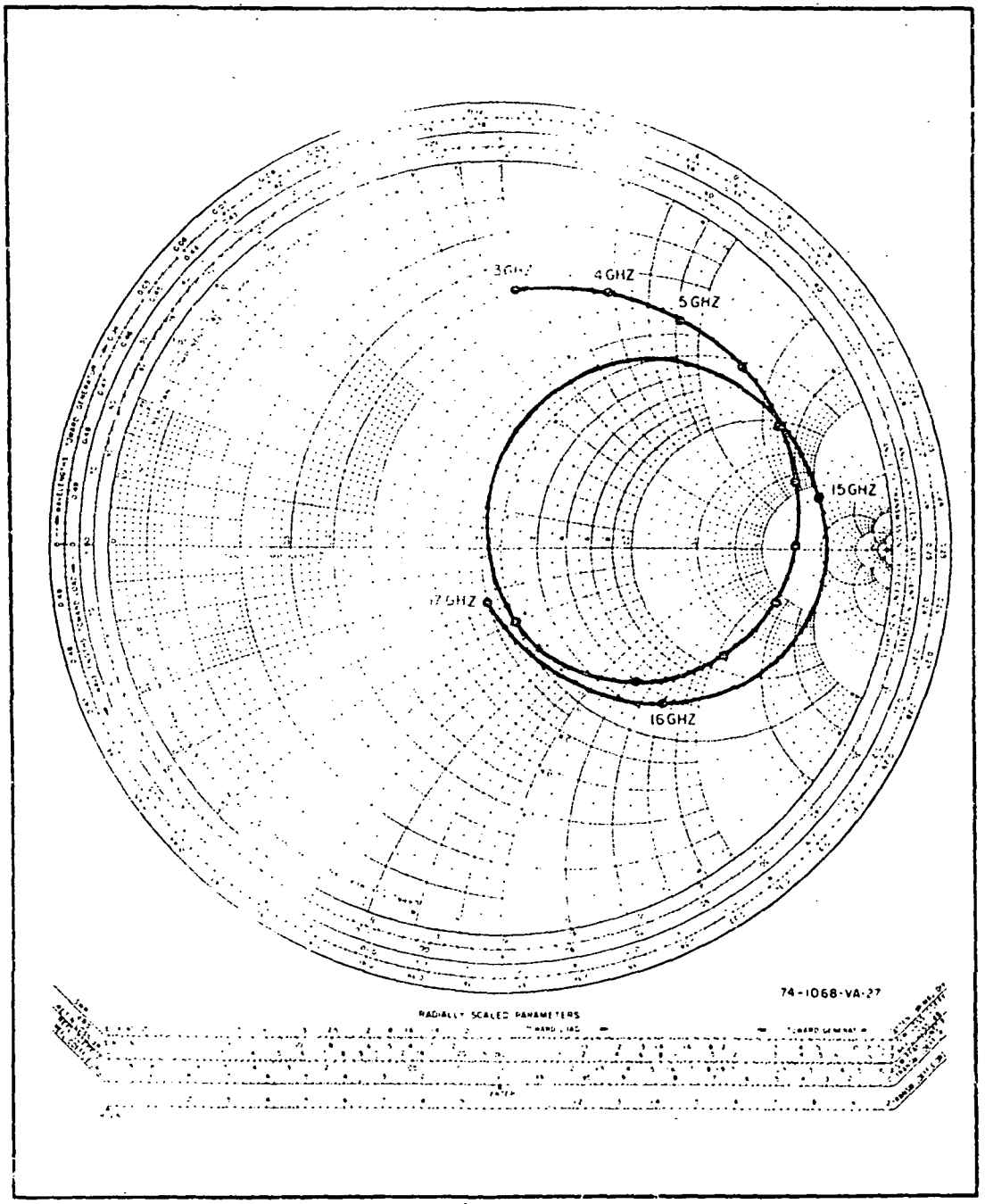

Figure 6-2. Computed Impedance Locus of Circuit of Figure 6-1

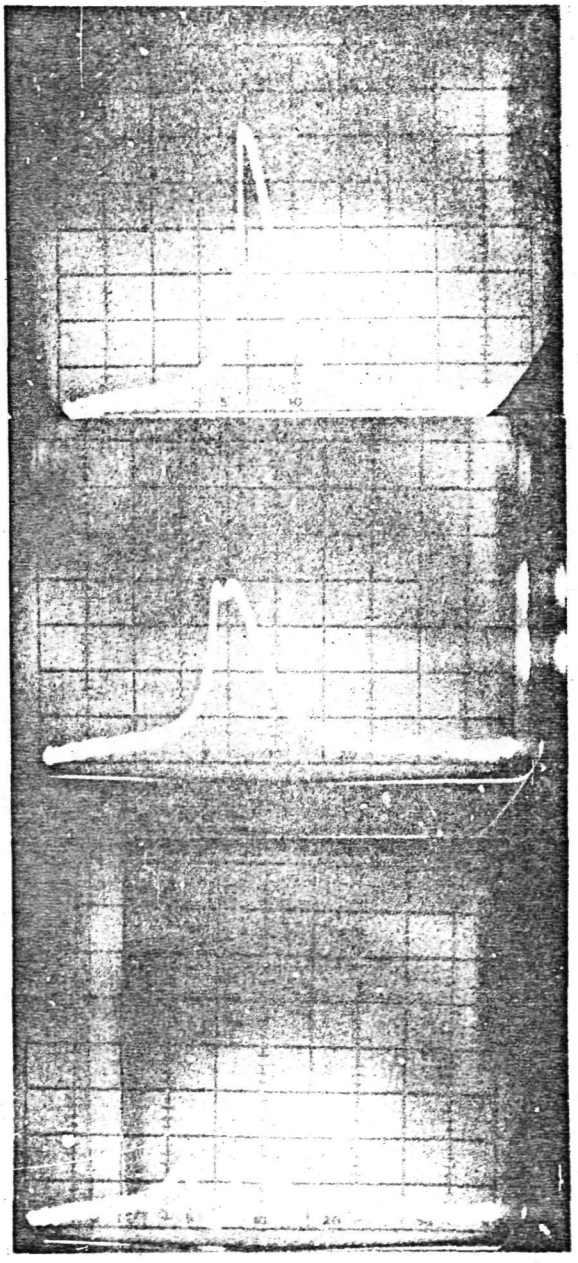

Figure 6-3. Gain Reduction Due to Parametric Oscillation (2 dB/div., 14.5 to 15.5 GHz)

Several techniques were attempted to achieve the desired low impedance at the subharmonic frequency and leave unchanged the impedance at the signal frequency. All these suffered from the same drawback, namely of being narrowband solutions to a broadband problem. One approach is worthy of some discussion.

A coaxial open circuited stub was placed directly across the diode terminals in parallel with the transformer network already there. The length of the stub was adjusted to be $\lambda/2$ wavelengths long at 15 GHz and $\lambda/4$ wavelengths long at 7.5 GHz. The stub impedance would, therefore, be high at the signal frequency and low at the subharmonic frequency. The resulting structure increased the gain at the signal frequency to 4 dB but instead of having a single "degenerate" parametric oscillation there now appeared two oscillation frequencies, at approximately 6 and 9 GHz. It was discovered, in fact, that by mistuning the amplifier even a greater number of frequencies could be made to appear. In order to increase the range of frequencies over which the stub was to present a low impedance, the packaged diode was remounted into a stud which had a machined recess. The purpose of this was to reduce the effective package inductance, which appears in series with the impedance presented across the external package terminals. A recess of 0.040" was tested and resulted in a 50 percent reduction in package inductance. A diode mounted in this stud was placed in a 50 Ω coaxial test fixture having a 1.2:1 VSWR in a 1-GHz band around 15 GHz and 2:1 in the subharmonic frequency range (~ 6 to 9 GHz). A stub which was $\lambda/2$ wavelengths long at 14 GHz was placed across the diode and resulted in,

again, two oscillation frequencies but this time at approximately 4 and 10 GHz, a separation of 6 GHz compared to the 3-GHz separation before the reduction of package inductance.

The fact that the two parametric oscillations were spread apart in frequency indicated that the reduction in package inductance had the beneficial effect of increasing the band over which the stub had effect. The major drawback of using the stub, however, was that the requirements of small reactance slope at both the subharmonic and signal frequencies were incompatible. This may be seen immediately from the expression for the input impedance of an open-circuited transmission line and its derivative with respect to electrical length

$$Z_{in} = jZ_o \cot \theta. \qquad (6\text{-}1)$$

$$\frac{d Z_{in}}{d \theta} = \frac{-j Z_o}{\sin^2 \theta}. \qquad (6\text{-}2)$$

For $\theta = \pi/2$ (subharmonic), the reactance slope is finite and proportion to Z_o. For $\theta = \pi$ (signal frequency), the reactance slope goes to infinity. This can have the effect of severely narrowing the bandwidth of the amplifier.

At this point, the matched transmission line was reconsidered as a technique by which the impedance at the subharmonic could be easily controlled. The disadvantage of this technique, however, was the loss in circuit efficiency which would result from the three-to-one impedance ratio. It was calculated, however, that the circuit efficiency could be increased considerably by increasing the Q_L of the cavity and thereby increasing the coupled cavity impedance. This would have the effect of reducing the bandwidth of the amplifier but for the case which was considered the reduction would be small.

The structure which was considered is illustrated schematically in Figure 6-4. The packaged diode is parallel-resonated by a shunt capacitance of approximately 0.3 pf. A $\lambda/2$ length of 27-ohm transmission line is used to transform the cavity impedance (in series with the stabilization load) to the resonated diode terminals. This structure has the advantage over others that were considered in presenting a very well behaved (and reproducible) admittance locus at the resonated diode terminals. At 15 GHz, the load admittance is purely real and is given by $1/(R_C + R_S)$. The value of R_C is adjusted during operation, through adjustment of the probe penetration, to maintain stability under small signal conditions. At all frequencies sufficiently removed from 15 GHz, the load impedance is uniquely 27 ohm, a value which was considered sufficiently low to suppress parametric oscillations.

The choice of characteristic impedance in this structure is based on three major criteria.

a. Circuit efficiency

b. Suppression of parametric oscillations

c. Low Q_L

For the 27-ohm system, the circuit efficiency is given by

$$\eta_c = \frac{R_C}{R_C+R_S} . \qquad (6-3)$$

and the Q_L of the circuit is given by

$$Q_L = \frac{\pi}{2} \left(\frac{Z_L}{Z_o} - \frac{Z_o}{Z_L}\right) \qquad (6-4)$$

where $Z_L = R_C + R_S$, $Z_o = R_S$. Figure 6-5 is a plot of Q_L vs. Z_L/Z_o. For the present case, $Z_L = 1./.012 = 83$ ohm, $Z_o = 27$ ohm, and therefore $Q_L = 4.3$.

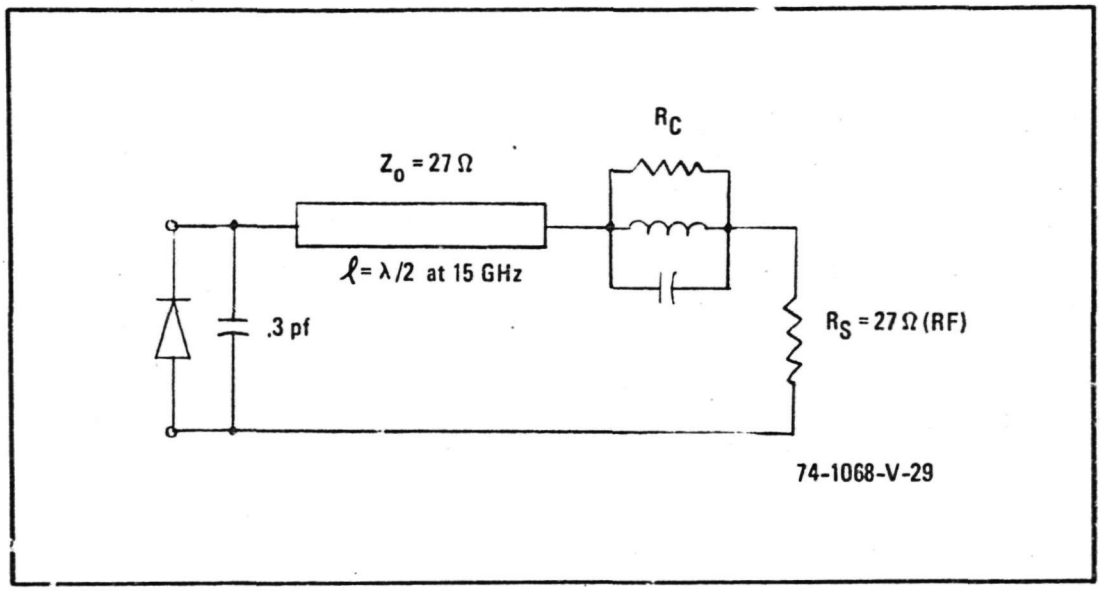

Figure 6-4. Elemental Amplifier Circuit Using Matched Termination

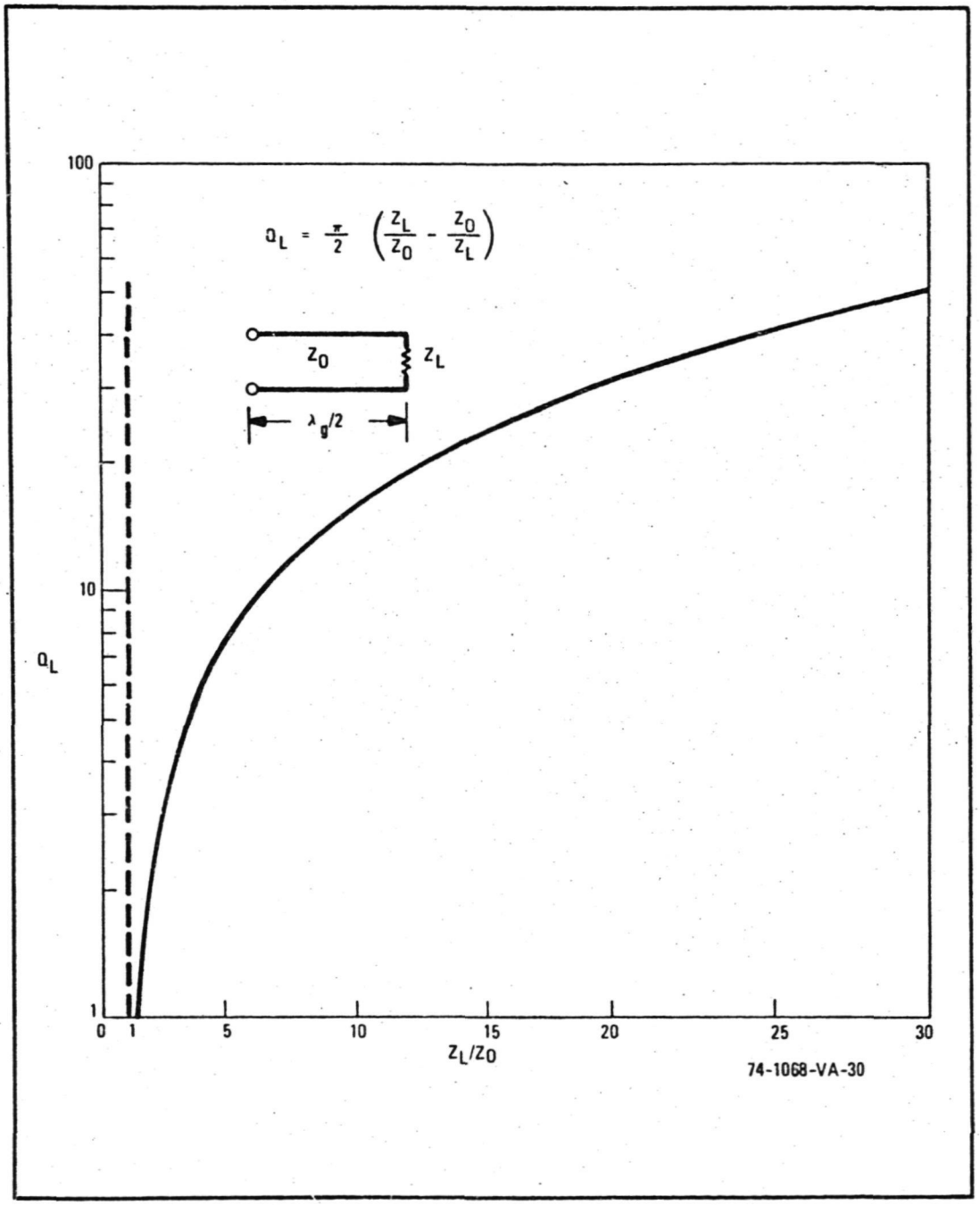

Figure 6-5. Loaded Q for $\lambda/2$ Resonator

Several center conductors were constructed along with several versions of an insert which would act both as the diode contact and a shunt capacitor. Figure 6-6 illustrates the complete center conductor assembly. In order to determine exactly what insert diameter would be required to resonate the diode under large signal conditions, five inserts were constructed, having diameters ranging from 0.150" to 0.130" in steps of 0.005". Each of these inserts was tested by adjusting the input cavity coupling probe to maximize the output power of the diode acting as an oscillator. Table 6-1 presents the results.

TABLE 6-1

Single Diode Oscillator Output Power
at 15 GHz for Various Insert Diameters (Diode # H5)

Insert Diameter (Inches)	Output Power (mW)
0.150	0
0.145	80
0.140	260
0.135	450
0.130	200

Subsequently, four other diodes were similarly tested in the cavity with only the .135 inch diameter insert. Table 6-2 summarizes the results of these tests.

TABLE 6-2

Measured Single Diode Oscillator Output Power

Diode Number	Output Power (mW)
H5	450
H6	480
E3	290
E4	370
G24	310

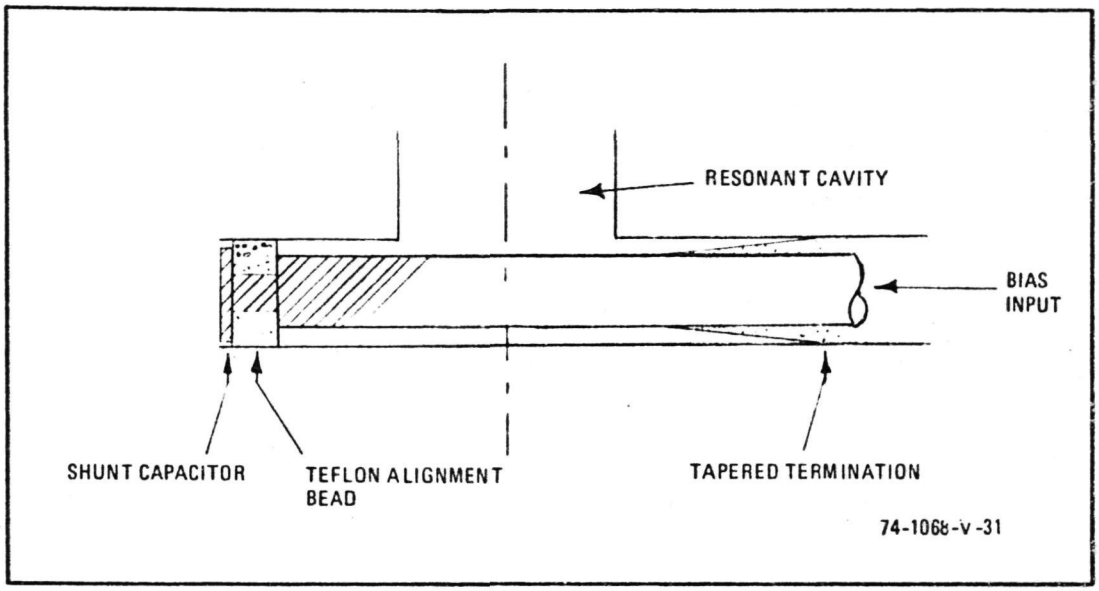

Figure 6-6. Final Center Conductor Assembly

It should be noted that these measured powers are below half the output power claimed by the manufacturer. The low output power as an oscillator is due to the high Q_L to which the cavity must be adjusted in the oscillator case. Using Figure 5-9, the conductance at which the diode would add 0.9 watt is approximately -0.002. Using $G_{CIRC} = 0.012$, therefore, the gain in this case would be 2.9 dB. Using equation 6-4 we find that Q_L would be 64.2 for a 200-MHz, 3-dB bandwidth at 15.00 GHz. For this case R_C would be 56 ohm (1/(56 + 27) = 0.012). In the oscillator case, however, R_C would have to be re-adjusted to present 500 - 27 = 473 ohm, implying an increase of Q_L by a factor of 8.45 to 542.

The transmission efficiency of the cavity is now given by

$$\eta = \left(1 - \frac{Q_L}{Q_U}\right) \qquad (6\text{-}5)$$

and for $Q_L = 542$ and $Q_U = 1000$, $\eta = 0.46$. This low transmission efficiency accounts for the low oscillator output powers of Table 6-2. Diode H5, according to this analysis, was actually generating 450/0.46 = 978 mW, which is very close to its rated output power.

Tests were then carried out on a single diode (#G24), with the input coupling adjusted for operation as a stable amplifier. Figure 6-7 illustrates the response of the amplifier over the frequency range 14.5 GHz to 15.5 GHz for a range of input RF power levels. Note that the sharp gain reduction, characteristic of the presence of a parametric oscillation, is absent.

The first power combining experiment was carried out with two diodes, #H5 and #H6, and the cavity adjusted for operation as an oscillator. Total output power was 910 mW, corresponding to individual powers of 450 mW and 480 mW which were measured earlier. The efficiency of the combiner was, therefore, about 98 percent.

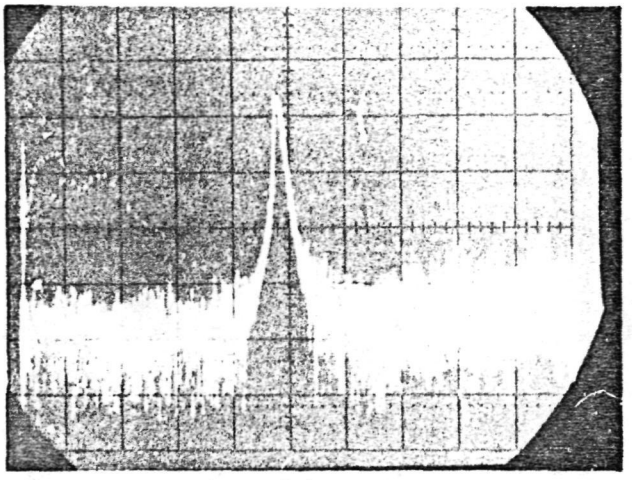

P_{in} = 4mW

(a)

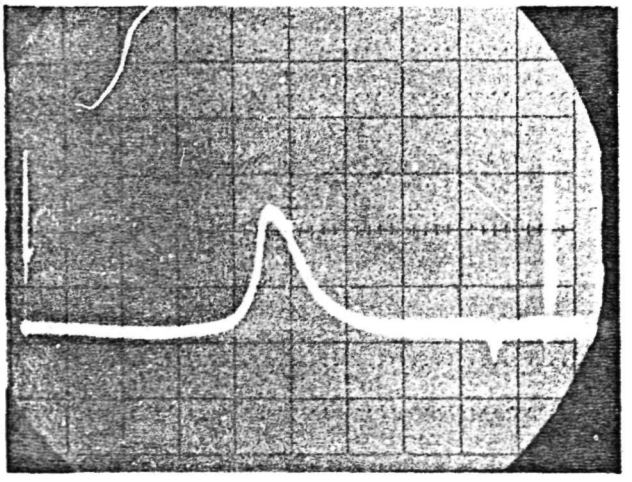

10 mW

(b)

74-1068-BA-32

Figure 6-7. Single-Diode Amplifier in Cavity. Gain vs Frequency as Function of Input Power. Diode # G24. (5 dB/div., 14.5 to 15.5 GHz) (Sheet 1 of 2)

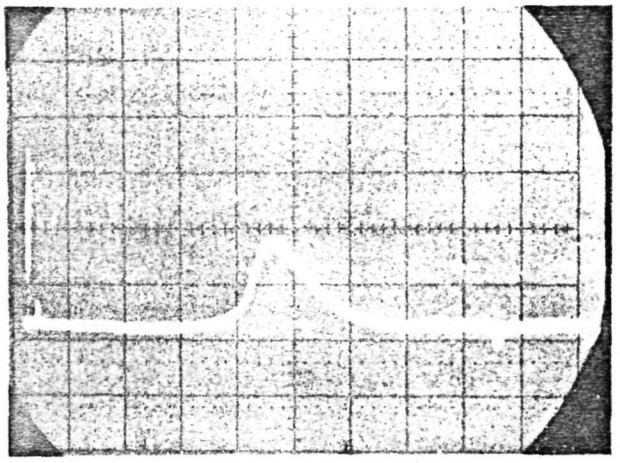

20 mW

(c)

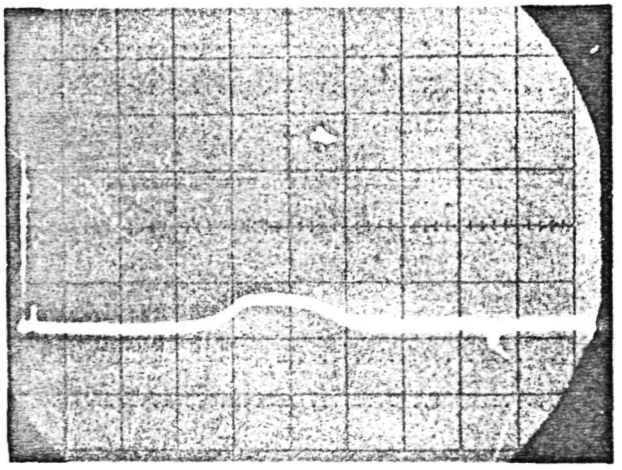

175 mW

(d)

74-1068-PA-33-G

Figure 6-7. Single-Diode Amplifier in Cavity. Gain vs Frequency as Function of Input Power. Diode # G24. (5 dB/div., 14.5 to 15.5 GHz) (Sheet 2 of 2)

The second power combining experiment was carried out with three diodes, #E3, #E4, and #G24, the sum of whose individual output powers was 970 mW. The total measured output power in this case was only 700 mW, corresponding to a combining efficiency of 72 percent. These diodes were somewhat lower in rated output power than the previous two, indicating that their impedances may be sufficiently different to call for a different shunt capacitance than was used in the test. These same three diodes were also tested in the combiner as an amplifier. Figure 6-8 illustrates the response of the amplifier over the 14.5-GHz to 15.5-GHz frequency range and for various input drive levels. Small signal gain was 20 dB and at 0.6-W input was approximately 3 dB. Again, note the absence of the gain reduction encountered earlier.

Each of the 6-diode combiners was tested individually in a reflectometer system (without circulator and "magic tee"). Figure 6-9 illustrates the pass-band characteristics of the amplifiers over the 14.5-to 15.5 GHz range for a range of input powers from 0.4 mW to 2 watts (under normal operation $P_{IN}^{MAX} = 1.0$ watt). The small signal gain was adjusted in both cases to 20 dB. Note the similarity between the two characteristics.

The pass-band characteristic of the complete 12-diode amplifier is illustrated in Figure 6-10. It is worth noting at this point that no individual diode tuning was used and also that neither of the 6-diode combiners required phase adjustments on the hybrid level. Figure 6-11 illustrates the complete amplifier breadboard, including cooling fans.

Figure 6-12 is a plot of power in intermodulation sidebands as a function of input power. Also included is the fundamental P_{OUT}/P_{IN} characteristic at 15.0 GHz. For the intermodulation test, Δf was 12 MHz and the

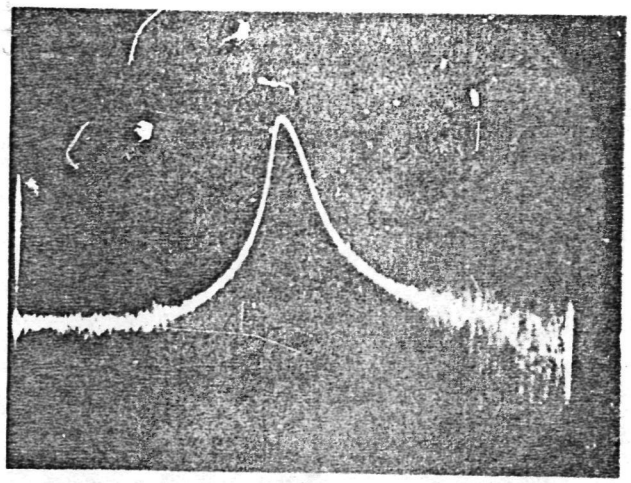

P_{in} = 4 mW

(a)

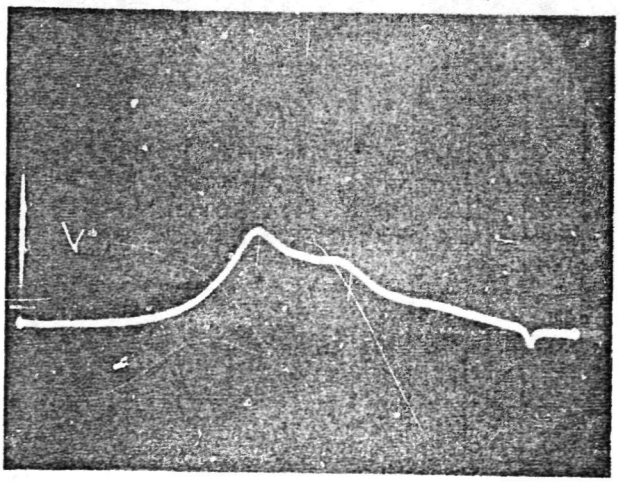

60 mW

(b)

74-1068-BA-34

Figure 6-8. Three-Diode Amplifier in Cavity. Gain vs Frequency as Function of Input Power. Diodes # G24, E3, E4. (5 dB/div., 14.5 to 15.5 GHz) (Sheet 1 of 2)

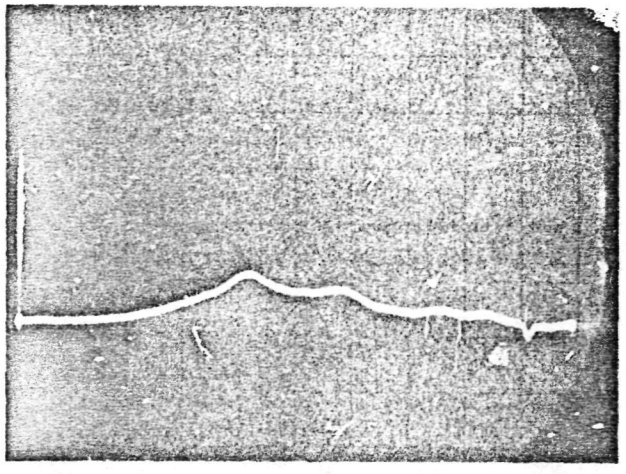

600 mW

(c)

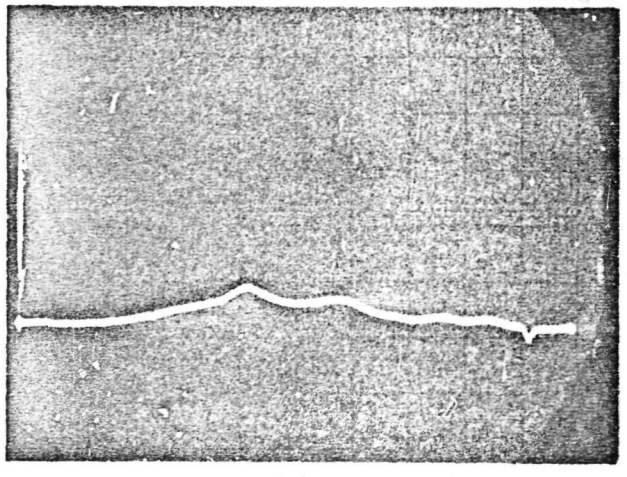

1100 mW

(d)

74-1068-BA-35

Figure 6-8. Three-Diode Amplifier in Cavity. Gain vs Frequency as Function of Input Power. Diodes # G24, E3, E4. (5 dB/div., 14.5 to 15.5 GHz) (Sheet 2 of 2)

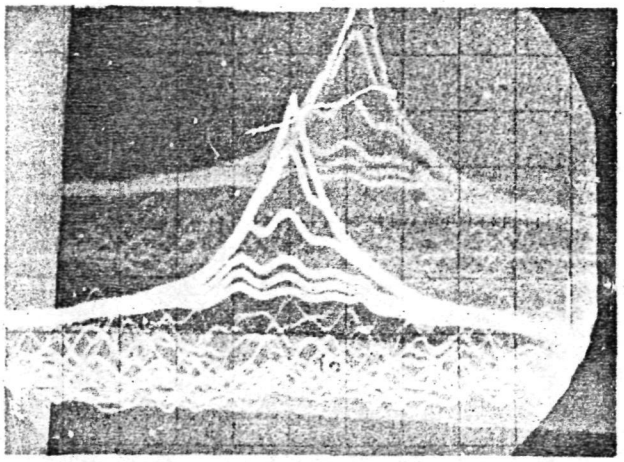

P_{in} = 0.4 mW
2.0 mW
20.0 mW
500.0 mW
1.0 W
2.0 W

(a)

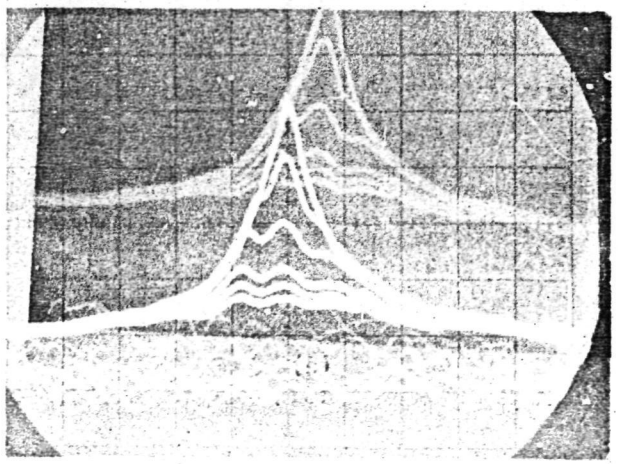

(b)

Figure 6-9. Pass-Band Characteristics of (a) Combiner #1 and (b) Combiner #2. (5 dB/div., 1... ... 1.5 GHz)

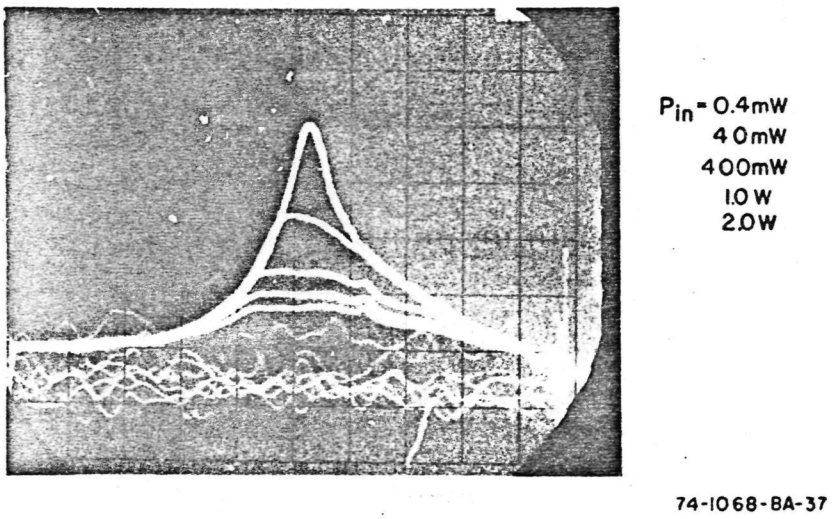

Figure 6-10. Pass-Band Characteristic of 12-Diode Amplifier (5 dB/div., 14.5 to 15.5 GHz)

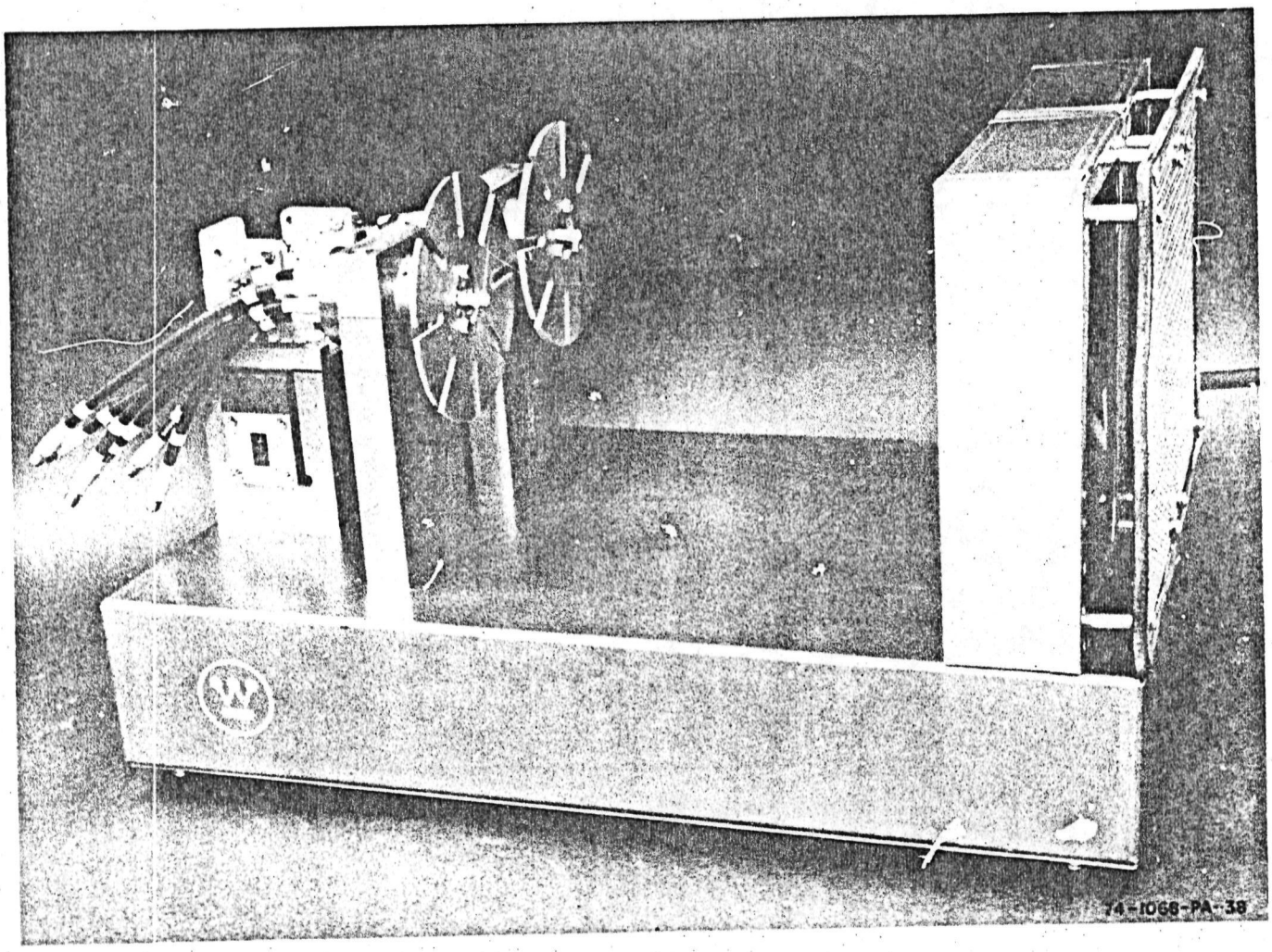

Figure 6-11. Twelve-Diode Amplifier Breadboard, Including Cooling Fans

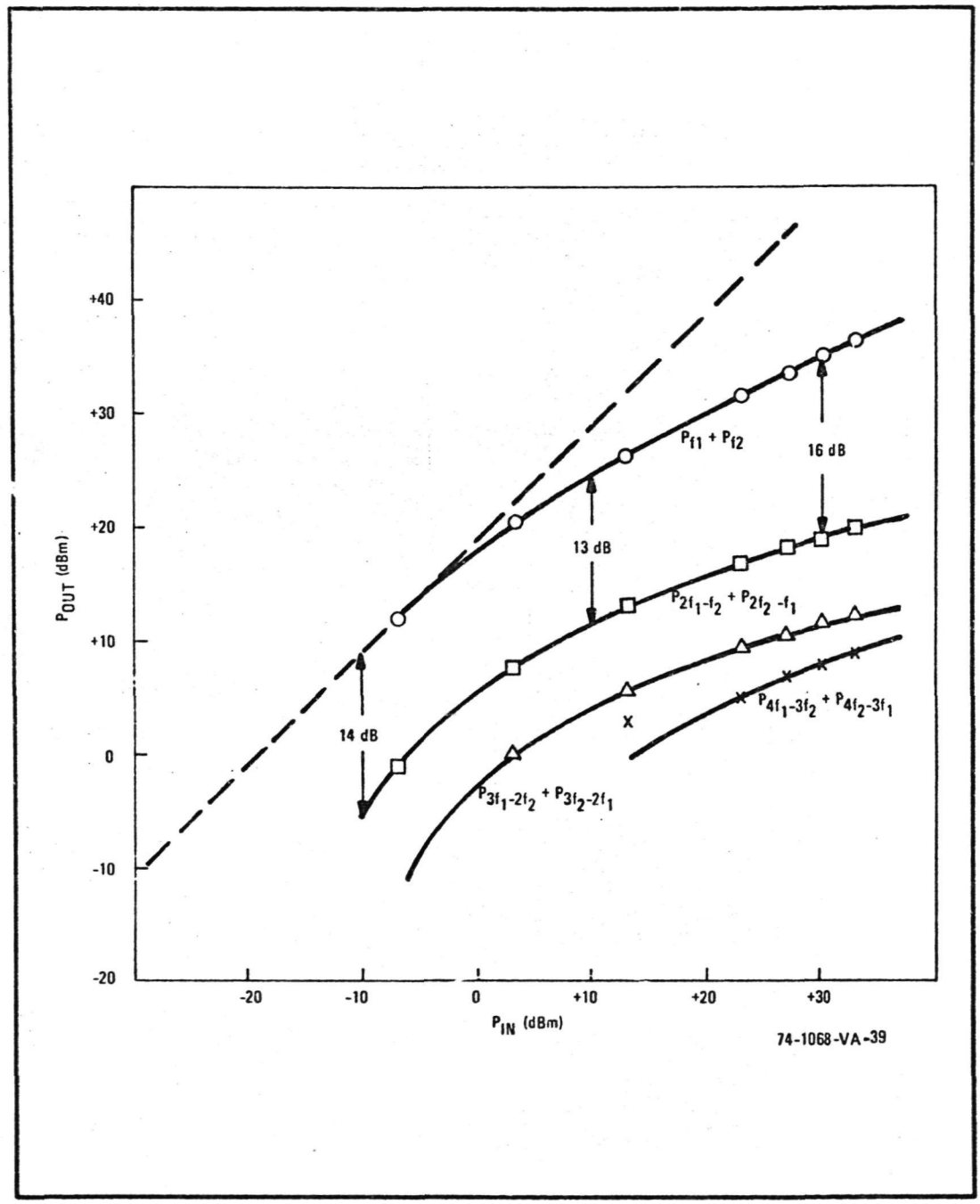

Figure 6-12. Twelve-Diode Amplifier Intermodulation Distortion
(Δf = 12 MHz, f = 15.0 GHz, Driver Third Order IMP's = 24 dB)

measured third order IMP level for the TWTA used as a driver was - 24 dB. The third order IMP's were symmetrical to within approximately 1 dB over the input power range 20 mW to 2 W. At lower input levels the relatively narrow band of the amplifier caused the sidebands to be subjected to possibly different gains, thus producing an asymmetry of approximately 3 dB.

One of the major concerns of any systems designer is the reliability of the various components in the system and their possible failure modes. In the case of the present amplifier, tests were conducted on the effects of individual diode failures on the overall performance of the amplifier under small and large signal conditions. Table 6-3 presents the various failure configurations which were tested. The simulated "failures" were unbiased diodes.

Table 6-3

CONFIGURATION NUMBER	COMBINER # 1 NUMBER OF "FAILED" DIODES	COMBINER #2 NUMBER OF "FAILED" DIODES
1	1	0
2	1	1
3	1	2
4	2	2
5	0	2

Figures 6-13a through 6-13f illustrate the variation of gain with frequency under small and large signal (2-W input) conditions for various failure configurations.

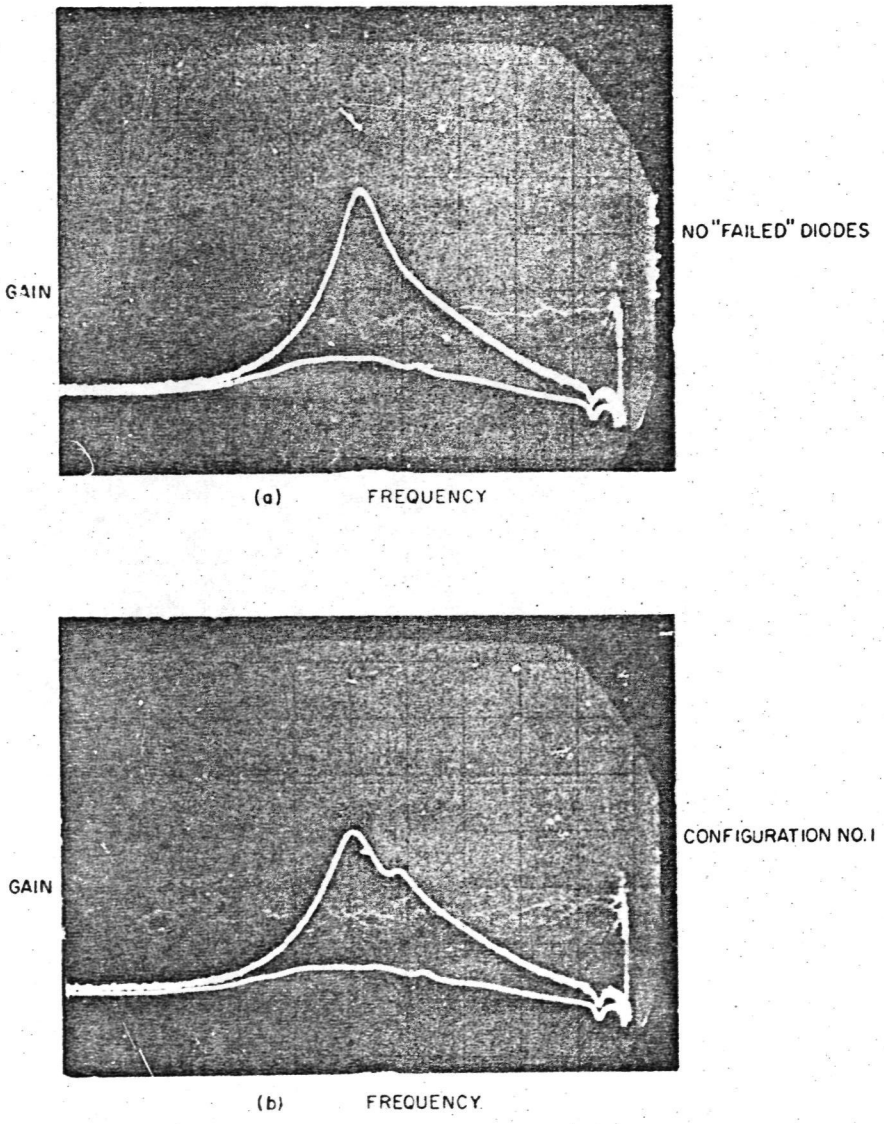

Figure 6-13. Amplifier Characteristics for Various "Failure" Configurations (5 dB/div., 14.5 to 15.5 GHZ) (Sheet 1 of 3)

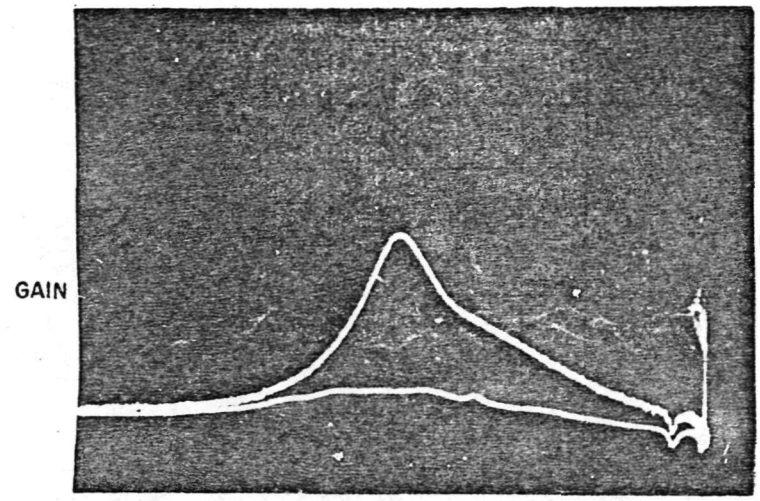

(c) FREQUENCY

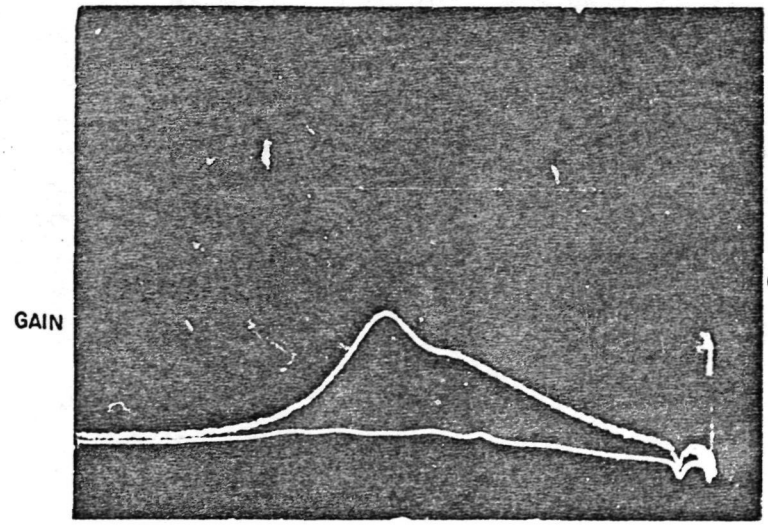

(d) FREQUENCY

74-1068-PA-45

Figure 6-13. Amplifier Characteristics for Various "Failure" Configurations (5 dB/div., 14.5 to 15.5 GHz) (Sheet 2 of 3)

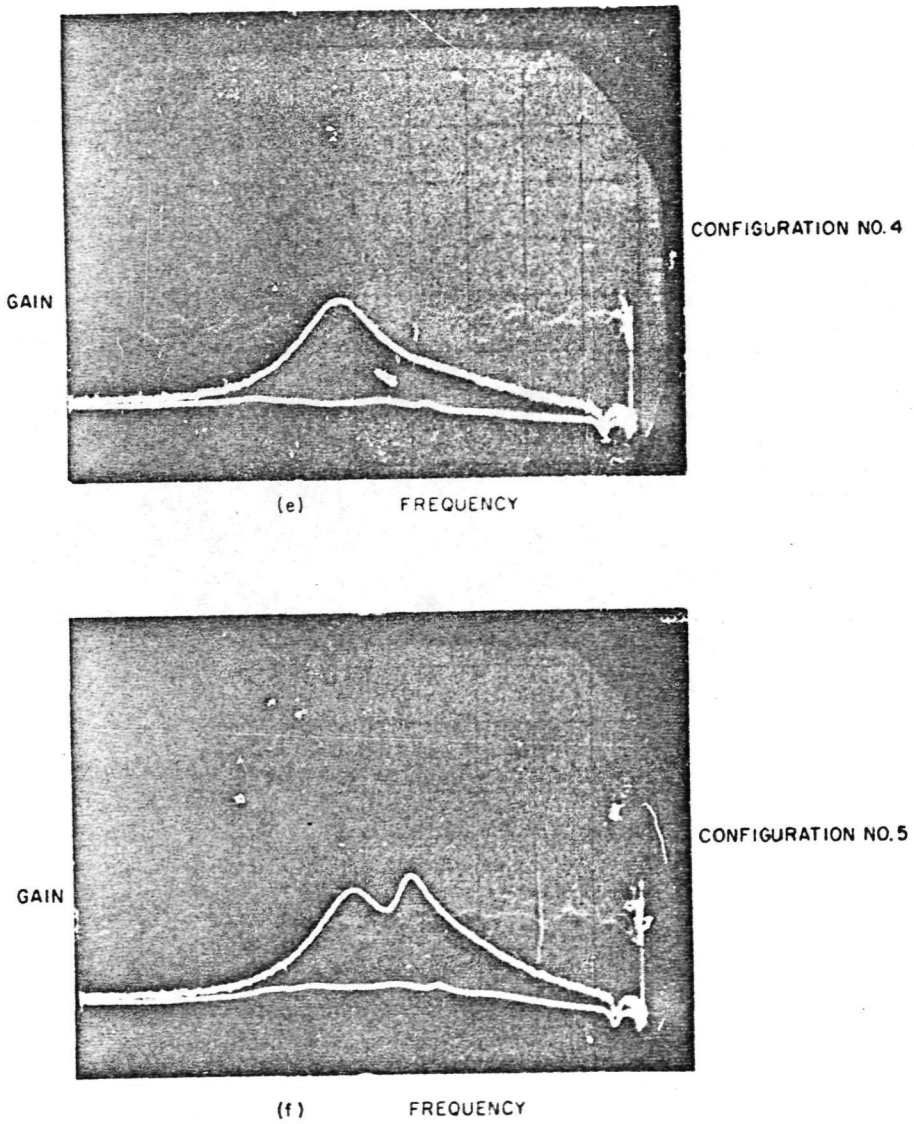

Figure 6-13. Amplifier Characteristics for Various "Failure" Configurations (5 dB/div., 14.5 to 15.5 GHz) (Sheet 3 of 3)

None of the failure configurations caused oscillations or parametric instabilities.

Thermal tests were carried out on the complete amplifier over the range -25° C to $+50^{\circ}$ C. The pass-band characteristic was monitored at a 2-W input power level. Figures 6-14a through 6-14f illustrate the variation of gain with temperature. The overall gain sensitivity was 0.021 dB/$^{\circ}$ C.

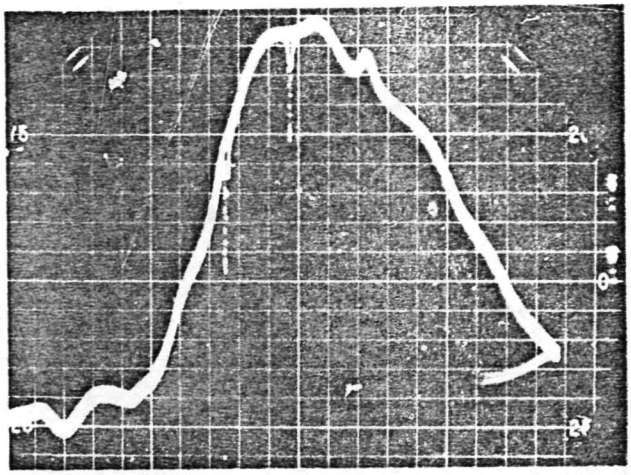

Ambient - -25° C
Heat Sink - -2° C

(a)

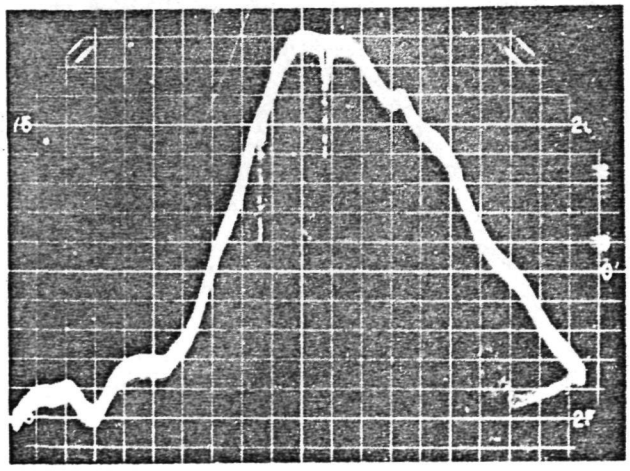

Ambient - -9.2° C
Heat Sink - +13° C

(b)

74-1068-BA-41

Figure 6-14. Amplifier Gain Variation As A Function of Temperature (0.4 dB/div., markers at 14.91 and 15.01 GHz)
(Sheet 1 of 3)

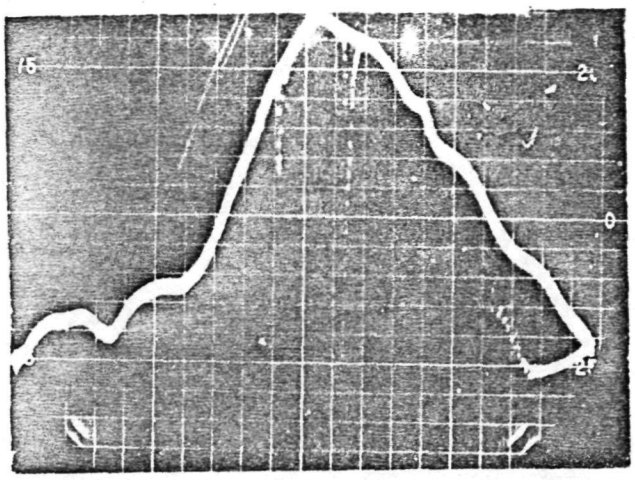

Ambient – +10° C
Heat Sink – +32° C

(c)

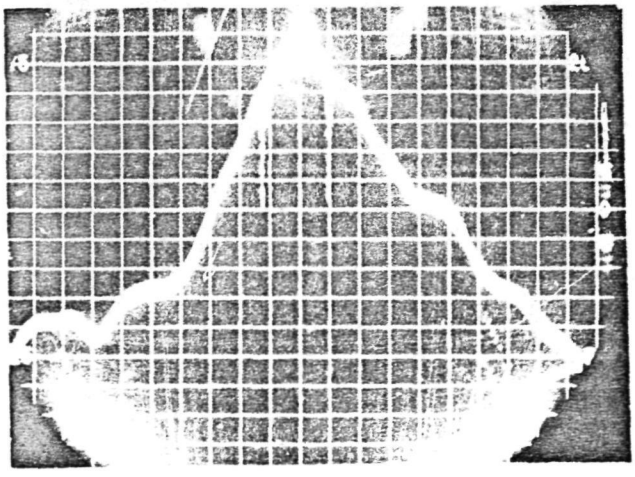

Ambient – +29° C
Heat Sink – +50° C

(d)

74-1068-BA-47

Figure 6-14. Amplifier Gain Variation As A Function of Temperature (0.4 dB/div., markers at 14.91 and 15.01 GHz)
(Sheet 2 of 3)

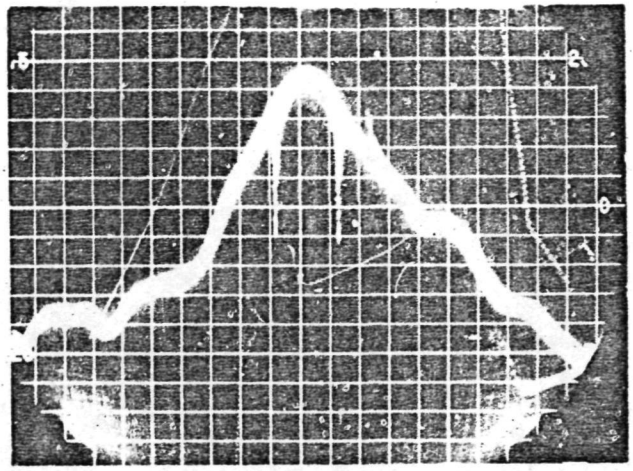

(e)

Ambient – +40.5° C
Heat Sink–+60° C

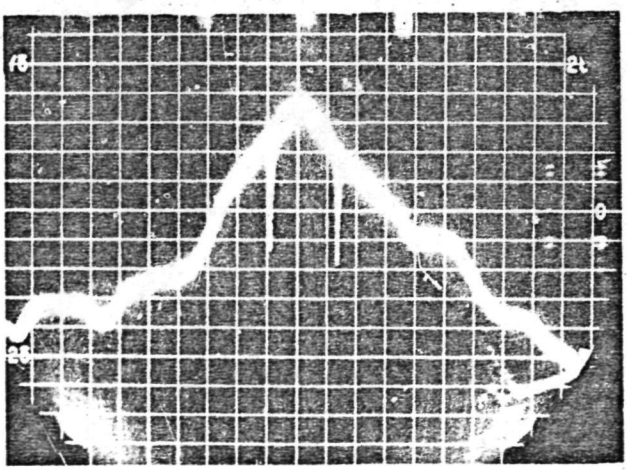

(f)

Ambient – +50.5° C
Heat Sink – +70° C

74-1068-BA-48

Figure 6-14. Amplifier Gain Variation As A Function of Temperature (0.4 dB/div., markers at 14.91 and 15.01 GHz) (Sheet 3 of 3)

7. CONCLUSIONS AND RECOMMENDATIONS

Although the original goals of this program were not achieved, the results of the program have made a substantial contribution to the state-of-the-art of high power IMPATT amplifiers. The amplifier which was delivered is, at this time, the highest power solid-state amplifier above X-band. Aside from the hardware aspects, however, much knowledge was gained about power combining, stabilization techniques, parametric oscillations, and "graceful failure". In addition to these specific areas, much additional information was obtained about IMPATT devices in general and the critical role played by the diode package in the overall design of the amplifier.

As is true in most such programs, many of the things which were learned could not be applied to the immediate program because of the constraints of funds available and the demands of the schedule. The knowledge gained will, therefore, have to wait for application in future programs. Following is a brief discussion of the recommended design procedure to be used in future programs.

Choice of Diode

Assuming that one of the primary goals is maximum dc-to-RF conversion efficiency, the choice of diode must be made on the basis of the maximum available gain of the device at its maximum power added point. This characteristic is different for different semiconductor materials and different doping profiles. In the present case, for example, the large variation between the small signal negative conductance and the negative conductance

at the P_{ADD}^{MAX} point established a maximum gain of approximately 4.5 dB at P_{ADD}^{MAX}. This gain is further reduced by the circuit losses (especially the stabilization load). It was necessary, therefore, to use a large number of diodes, operate at a lower RF voltage level where the gain is higher, and concede a loss in efficiency. If there is a substantial variation of susceptance with RF voltage an additional available technique is to set the circuit admittance to give the required gain at P_{ADD}^{MAX} and rely on the detuning effect of the susceptance variations to ensure stability under small signal conditions. This technique was used in the present amplifier to some extent.

Choice of Package

The diode package is a complex impedance transformation network. It will affect the apparent diode impedance and will increase the loaded Q of the circuit. The ideal situation would be to use the unpackaged chip and thereby regain some control over the parasitics associated with the diode and its mounting configuration. At the operating frequency, the package parasitics will determine what form the resonating network will take to maximize bandwidth. At other frequencies, particularly in the vicinity of the subharmonic, the parasitics (especially inductances) can affect the maximum conductance presented by the circuit to the diode chip. This circuit conductance can have severe effects on the presence (or absence) of parametric oscillations under large signal conditions.

Choice of Elemental Amplifier Circuit

The elemental amplifier circuit must be chosen with the following criteria in mind:

a. Proper impedance locus in the vicinity of the operating frequecy (gain, bandwidth).

b. Proper impedance locus in the vicinity of the subharmonic.

c. High circuit efficiency.

d. Low loaded Q.

e. Proper bias circuit impedance (low frequency).

f. Proper coupling to cavity.

g. Reproducibility.

h. Ease of fabrication.

Choice of Power Combiner

Assuming a cylindrical cavity combiner, the fundamental decision is whether to use a dominant mode cavity or a cavity operating at a higher mode. The decision is based on the number of diodes that are required and in the efficiency of the mode suppressing structure used to eliminate all unwanted modes. In the present case a dominant mode approach was taken. The height of the cavity will affect the unloaded Q. It will, however, also affect the coupling factor between the cavity and the elemental amplifier and will affect the location and character of the cavity equivalent circuit as seen by the diode.

Adjustment of cavity frequency and RF coupling into the cavity must be accomplished by a technique which minimizes losses since these losses will tend to reduce the effective cavity unloaded Q.

APPENDIX A

DERIVATION OF GAIN-BANDWIDTH RELATIONSHIP FOR A NEGATIVE RESISTANCE AMPLIFIER

APPENDIX A

DERIVATION OF GAIN - BANDWIDTH RELATIONSHIP FOR A NEGATIVE RESISTANCE AMPLIFIER

Assume the following microwave circuit:

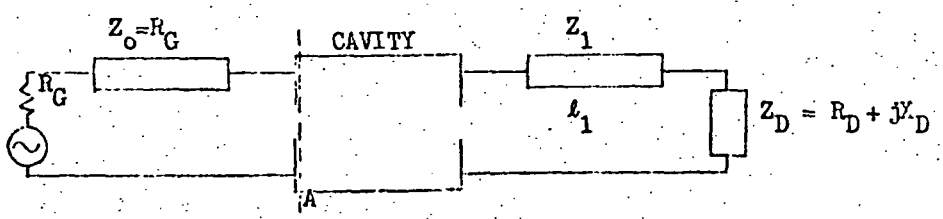

Assume, further, that we can choose Z_1 and ℓ_1 such that the device impedance will appear purely real at the cavity terminals at the resonant frequency of circuit (for a cavity with negligible losses)

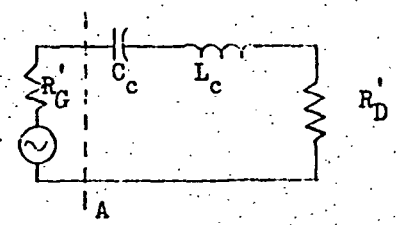

where C_c, L_c are cavity parameters valid in the vicinity of the resonant frequency. The loaded Q of the circuit is given by

$$Q_L = \frac{\omega_o L_c}{R'_G + R'_D} \quad . \qquad \text{(A-1)}$$

Let us now define a new parameter, Q_G, given by

$$Q_G = \frac{\omega_o L_c}{R'_G} \quad . \qquad \text{(A-2)}$$

Combining (A-1) and (A-2), we get

$$Q_L = \frac{R_G' \; Q_G}{R_G' + R_D'} = \frac{Q_G}{1 + R_D'/R_G'} \qquad \text{(A-3)}$$

And since Q_L is a measure of the relative half-power bandwidth of the circuit,

$$\frac{Q_G}{1 + R_D'/R_G'} = \frac{\omega_o}{\Delta \omega} = \frac{1}{b} \qquad \text{(A-4)}$$

Now at reference plane A we may define a voltage reflection coefficient, Γ, given by

$$\Gamma = \frac{R_D' - R_G'}{R_D' + R_G'} \qquad \text{(A-5)}$$

$$= \frac{R_D'/R_G' - 1}{R_D'/R_G' + 1} \qquad \text{(A-6)}$$

Solving for R_D'/R_G' in equation (A-6) and substituting into (A-4), we get

$$Q_G = \frac{1}{b} \left(1 + \frac{1 + \Gamma}{1 - \Gamma}\right)$$

$$Q_G = \frac{1}{b} \left(\frac{2}{1 - \Gamma}\right) . \qquad \text{(A-7)}$$

Up to this point in the derivation no assumption was made as to whether R_D' were a positive or negative resistance. It is apparent however that if R_D' were negative and smaller in magnitude than R_G' (as required for stability), the condition

$$\Gamma \leq -1 \qquad \text{(A-8)}$$

would hold.

In practice, one would of course have to embed the one port negative resistance device in a nonreciprocal network (ferrite circulator at point A) in order to separate incident and reflected waves and obtain useable power from the device. Under these conditions the gain of the amplifier can be defined as the ratio

$$G = \frac{\text{output power}}{\text{maximum available input power}} \qquad \text{(A-9)}$$

or

$$G = |\Gamma|^2 \qquad \text{(A-10)}$$

and

$$\Gamma = -\sqrt{G} \; . \qquad \text{(A-11)}$$

Substituting (A-11) into (A-7) we get

$$Q_G = \frac{2}{(1 + \sqrt{G})\, b} \; . \qquad \text{(A-12)}$$

Equation (A-12) states that for a given gain and bandwidth only the passive parts of the circuit will determine the required Q. This result assumes that the cavity is the only, or at least major, energy storage element in the network.

APPENDIX B

AMPLIFIER TEST PROCEDURE

APPENDIX B

AMPLIFIER TEST PROCEDURE

B.1 INTRODUCTION

Testing of the amplifier was carried out using the circuit illustrated in Figure B-1. It should be noted that the above circuit is one of several possible configurations, all of which will yield accurate data. This particular circuit, however, was found to be flexible enough to accomodate the various required tests with minimal changes, while maintaining accuracy and ease of calibration. The HP 8755M Swept Amplitude Analyzer was included in the circuit due to its flexibility, accuracy, and ease of operation. A ratio meter may be substituted if proper care is taken in calibration.

Operating instructions, including initial set-up procedure and instructions for amplifier adjustments are given in section B2. In operation, the amplifier should be placed securely on a flat surface with consideration given to maintaining enough open space around it not to restrict air flow. The rear of the Auxiliary Power Supply (APS) should, likewise, not be blocked in order to allow cooling. Following is a list of general precautions:

a. Do not exceed rated diode bias current. Note that some diodes are rated at 160 mA and others at 180 mA.

b. Adjust bias current slowly. Be sure meter is switched to Current position.

c. If a diode is to be removed during operation, reduce current to zero before disconnecting.

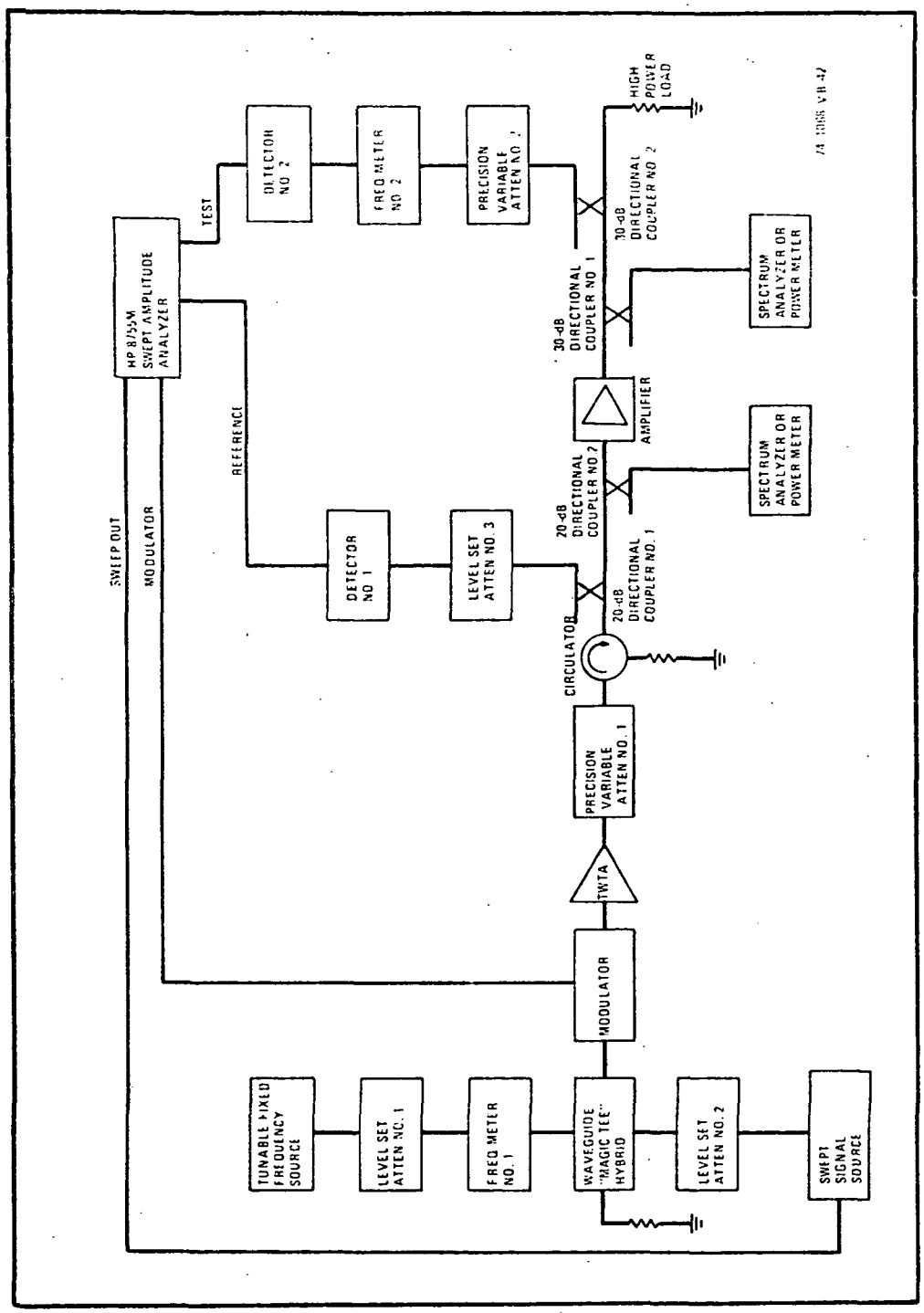

Figure B-1. Solid-State K_u - Band Power Amplifier Test Circuit

ORIGINAL PAGE IS
OF POOR QUALITY

d. Periodically check that all diodes are operating by using Diode rotary switch.

e. Be sure that all bias leads are securely connected.

f. When replacing a diode, be sure that the diode stud is securely tightened.

g. Use a suitable high power waveguide termination.

h. Always reduce input RF level if amplifier is to be removed from test circuit.

B-1.1 CALIBRATION OF TEST CIRCUIT

It is assumed here that all the components included in the Test Circuit are available and have been properly calibrated.

B-1.1.1 Insertion Loss

Using either one or two power meters or detectors measure the insertion loss between the coupled port of 20-dB coupler #2 and the amplifier input port at 15.0 GHz.

Measure insertion loss between the amplifier output port and the coupled port on 30-dB coupler #1.

Measure insertion loss between the amplifier output port and detector #2.

Repeat at other frequencies.

B.1.1.2 Modulation

Using a power meter on the coupled port of 20-dB coupler #2, adjust input power using precision attenuation #1 to read 1.0 mW. Record attenuator setting. Remove modulator. Increase attenuator setting to return power reading to 1.0 mW. Difference in settings is the correction which must be applied to all power meter readings if signal is modulated.

B-1.1.3 Gain (Swept)

Set zero gain reference line on HP 8755M by removing amplifier and replacing it with a short section of waveguide. Adjust level set attenuator #3 and precision attenuator #2 to obtain reference line which does not vary in position as a function of RF drive level up to the maximum anticipated power level. Record setting of precision attenuator #2.

At several power levels, check that the reference line tracks settings on precision attenuator #2. Reset attenuator to zero gain reference.

B-1.1.4 TWTA Intermodulation Products

Using fixed frequency source and swept signal source set to single frequency operation, adjust frequencies and desired Δf. Place termination on output port of 20-dB coupler #2 and remove modulator. Connect power meter to coupled arm of 20-dB coupler #1 and spectrum analyzer to coupled arm of 20-dB coupler #2. With precision attenuator #1 set to 3 dB, adjust powers to give a total of 1.0 watt cw and equal powers in the two main lines. Record power in each main line and power in each third order intermodulation line ($2f_1 - f_2$ and $2f_2 - f_1$). Repeat at other power levels and other frequencies.

B-1.2 MEASUREMENT OF AMPLIFIER CHARACTERISTICS

The following table outlines the specifications to which the test procedure was to be directed.

PARAMETER	SPECIFICATION
1. Center Frequency	15.0 GHz
2. 1-dB Bandwidth	100 MHz
3. Ripple within Pass-Band	± 0.2 dB
4. Power Output at Full Gain	5 watts
5. dc Power Input Maximum	150 watts
6. Gain at Maximum Output Power Level	4 dB
7. Maximum Noise Figure at Full Gain	30 dB(1)
8. Maximum Volume	0.25 ft^3
9. Maximum Weight	2.8 lb
10. Maximum Input/Output VSWR	1.2:1
11. Input and Output Connectors	UG-419/U
12. Intermodulation Products	2 tone test, $\Delta f = 10$ MHz: 10 dB down from each of 2 tones at output, design goal.
13. dc Power Input	Supply as accessary
14. Operating Temperature Range	-25° C/$+50^{\circ}$ C

B-1.2.1 Center Frequency, Bandwidth, Ripple, Power Output, and Gain

The measurement of these parameters is facilitated if a leveled swept frequency source is used. If a leveled sweeper is not available, a point by point (in frequency) measurement can be made.

---

(1) The measurement of this parameter was replaced by an alternate measurement.

The measurement of these parameters is carried out on swept basis with the modulator in the circuit. Set the peak input power to 2.0 watts into the amplifier, applying corrections for coupling and modulation.

The measurement of the above parameters is carried out in a straightforward manner, with consideration being given to the following:

a. Correct measured gain and P_{out} values for insertion loss between the amplifier output port and the measurement port.

b. It was suggested that the swept measurements be verified by single frequency measurements, using a power meter, at several frequencies in the band. The modulator was removed from the circuit for these measurements.

c. If any amplifier adjustments are required refer to section B-2.

B-1.2.2 Amplifier Spurious Output

The measurement of amplifier noise figure was replaced by a measurement of the spurious RF output relative to the signal amplitude under various drive conditions. The measurement was relatively straightforward.

a. If the amplifier has been off, allow approximately 20 minutes for warm-up (a low-level oscillation may be present on initial turn-on).

b. Connect a power-calibrated spectrum analyzer to the coupled port of 30-dB coupler #1.

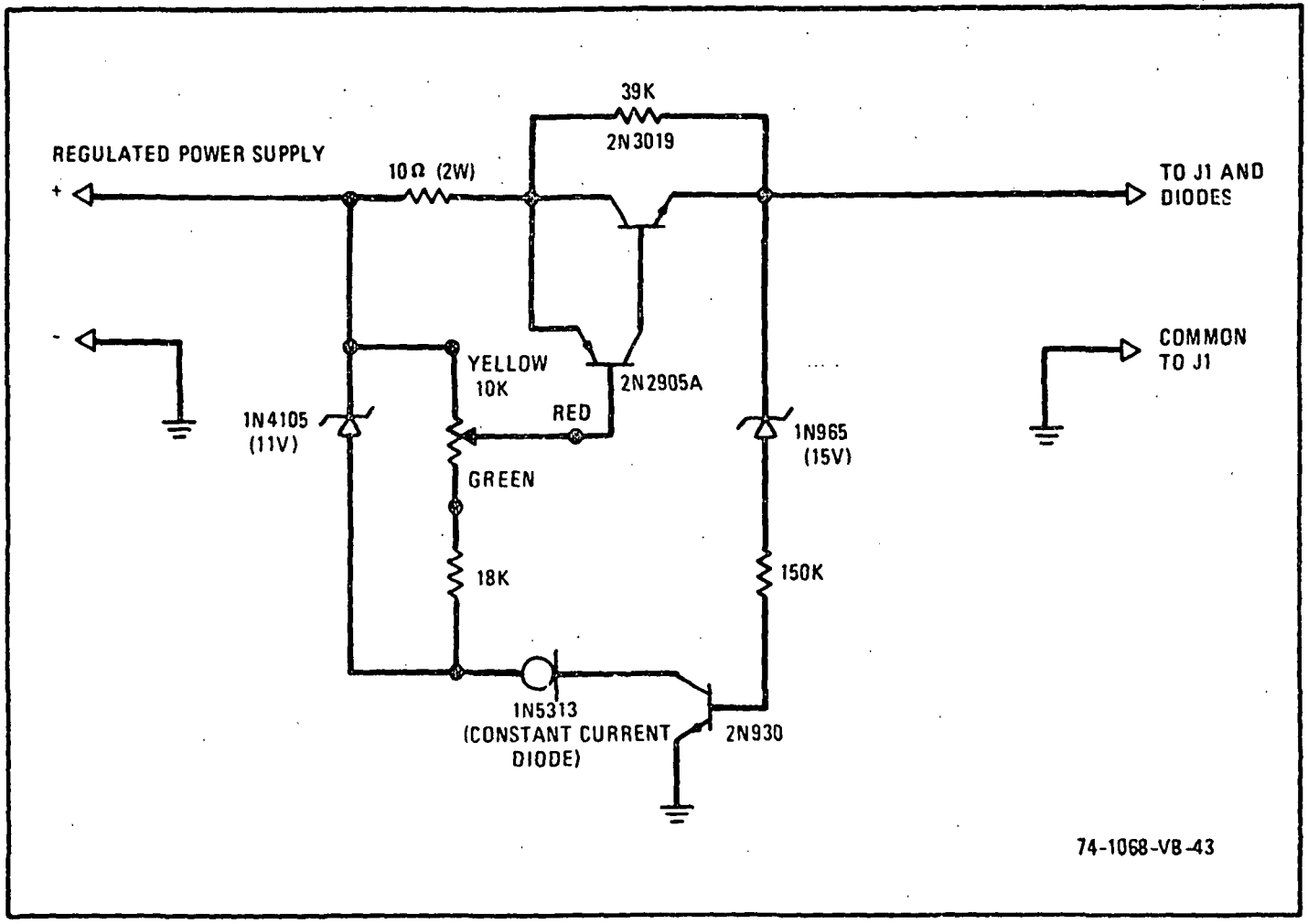

Figure B-2. Constant Current Regulator

c. Vary the input power (using a single frequency source) using precision attenuator #1.

d. Record the relative magnitude and frequency of any observed spurious signal at each drive level.

B-1.2.3 Input/Output VSWR

Input VSWR was measured either under full or low drive by reversing 20-dB coupler #2 so that a reflectometer system was set up at the amplifier input. For this test, detector #2 was moved to the coupled arm of the coupler and a reference short used to establish a return loss reference.

The measurement of output VSWR was made under zero input drive conditions since that situation would present a "worst case" (greatest amplifier reflection gain). Using the reflectometer system in the previous measurement, the amplifier was reversed such that the output port was connected to the output port of 20-dB coupler #2. Terminated the amplifier input port in a matched load.

B-1.2.4 Intermodulation Distortion

The measurement of third order intermodulation distortion was carried out using the technique described in paragraph B-1.1.4. The major difference was that the spectrum analyzer was moved to the coupled arm of 30-dB coupler #1. The measured intermodulation products now consisted of components generated by the amplifier as well as those generated by the TWTA. It was essential, therefore, that the characteristics of the TWTA be known at the output drive level required for the amplifier. Minimum TWTA distortion would

obviously occur at the lowest possible drive level which would produce 2.0 W input power into the amplifier, requiring minimum attenuation in precision attenuator #1.

Once the amplitudes of the third order products were obtained for the cascaded amplifier system, it was necessary to separate the effects of the two. This could be done subject to the following assumptions:

a. Intermodulation between the carriers and the TWTA IMP's in the amplifier is negligible.

b. In-phase addition of AM phasors will occur.

By making the above simplifying assumptions one can convert the measured distortion sidebands into equivalent voltages, subtract, and reconvert back to power.

B-1.2.5 Operating Temperature Range

The performance of the amplifier over the -25° C to $+50^{\circ}$ C temperature range was measured by placing the entire amplifier (excluding power supply) into an oven of suitable size. The cooling fans included in the amplifier assembly were used.

B-1.2.6 Miscellaneous Measurements

It was assumed that measurements of parameters not covered in the preceeding (i.e., dc Power Input, Volume, etc.) did not require discussion.

B-2 OPERATING INSTRUCTIONS

Initial set-up:

a. Connect bias harness to receptacle in rear of Auxiliary Power Supply (APS).

b. Connect fan power cord to receptacle in rear of APS.

c. Connect each APS bias lead to the corresponding numbered flexible cable (black) on amplifier chassis. Hand tighten each black cable at its mating point with amplifier body.

d. Plug APS power cord into 110-V, 60-Hz outlet.

e. Turn on APS using toggle switch on front panel. Red light on APS panel will light and fans on amplifier chassis will operate.

f. Switch meter to "Current".

g. Adjust bias current on each diode by successively switching rotary diode selector switch and adjusting corresponding potentiometer using small screwdriver. Initial current setting should be approximately 5 mA <u>below</u> I_{max} shown on diode list.(2)

Amplifier adjustment:

a. Using a swept-frequency test set-up (network analyzer, reflectometer, etc.) covering 14.5 GHz to 15.5 GHz, adjust input power to amplifier to < 1 mW at 15 GHz.

b. Using a screwdriver, detune cavity #1 approximately 500 MHz <u>downward</u> in frequency using nylon tuning screw at center of cavity.

c. Loosen four clamping bolts using suitable Allen wrench.

---

(2) A schematic of the constant current regulator is given in Figure B-2.1.

d. On cavity #2 adjust cavity coupling by gently exerting pressure on cavity body (either towards circulator or away from circulator) while rotating it through as small an angle as possible. Adjust center frequency using nylon screw. Adjust for 13-dB gain at 15.05 GHz. Retighten two clamping bolts.

e. Detune cavity #2 upward in frequency approximately 500 MHz.

f. Following same procedure as in step 4, adjust cavity #1 for 13-dB gain at 15.05 GHz.

g. Retighten clamping bolts.

h. Tune cavity #2 downward in frequency to overlap gain characteristic of cavity #1.

i. Small signal gain peak of tuned amplifier will be approximately 19 dB.

APPENDIX C

SPURIOUS OSCILLATIONS IN IMPATT DEVICES

(G.I. HADDAD)

APPENDIX C

SPURIOUS OSCILLATIONS IN IMPATT DEVICES (G. I. Haddad)

Spurious oscillations in IMPATT amplifiers and oscillators fall into three main categories as follows:

a. Bias-circuit oscillations, which have a great effect on the noise and power output. These have been described by Brackett.[13]

b. Parametric-type oscillations in which the sum of the frequencies of the two signals equal the main strong signal.

c. Oscillations at a subharmonic frequency. This is a special case of the second and may be considered as a degenerate parametric oscillation.

Hines[12] recently presented a theory for parametric interactions in IMPATT diodes and gave expressions for the stability criteria of an IMPATT-diode microwave circuits.

Some of the main results of Hines' theory are reviewed next.

He assumes the presence of a strong pump signal at ω_p.

$\omega_o \triangleq$ the lowest perturbing frequency

$$\omega_1 \triangleq \omega_p + \omega_o$$

$$\omega_{-1} \triangleq \omega_p - \omega_o$$

The equivalent circuit shown in Figure C-1 is applicable to small-signal parametric interactions when the diode is being pumped by some large signal at ω_p.

The pump frequency of the diode does not appear directly in the equivalent circuit but the pump state is introduced through the admittance $Y_{m,n}$

Hines[12] derived the following characteristic equation which governs the stability of the diode-circuit system:

$$D \triangleq 1 - M_1 M_{-1} S_o (S^*_{-1} + S_1) - M_2 M_{-2} S_1 S^*_{-1} + (M_1^2 M_{-2} + M_{-1}^2 M_2) S_o S_1 S^*_{-1} = 0 \qquad (C\text{-}1)$$

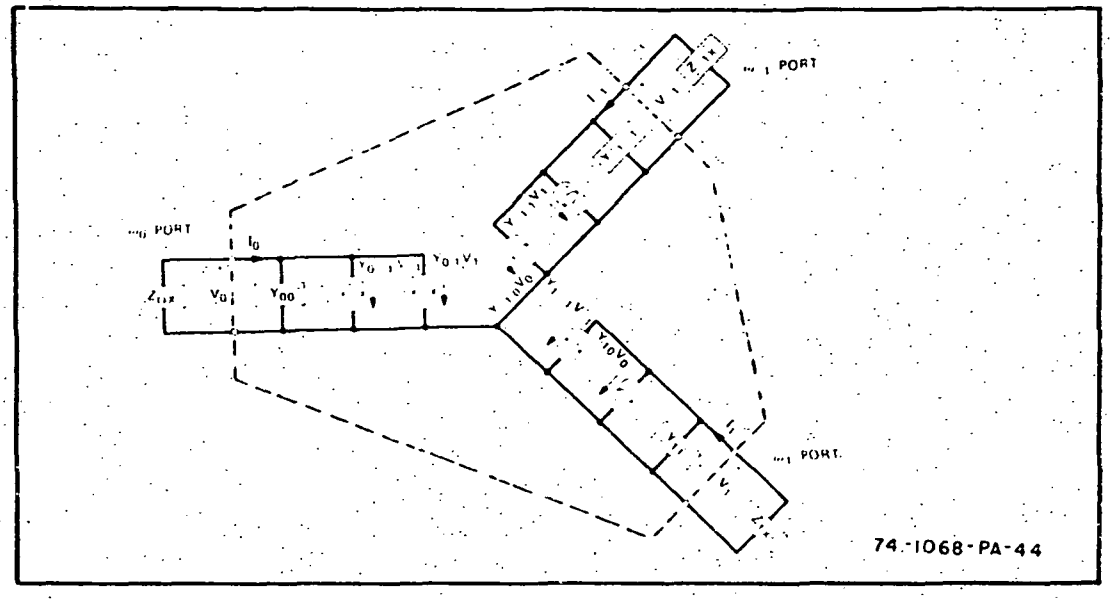

Figure C-1. Equivalent Circuit for Parametric Interaction

$M_n \triangleq$ the avalanche current at the n^{th} pump harmonic divided by the d.c. current.

The subscript n in M refers to $n\,\omega_p$, whereas the subscripts of the S quantities refer to the parametric frequencies ω_m. Also:

$$M_n = M_{-n}^*$$

$$|M_n| \leq 1$$

The complex quantities S_m may be thought of as stability factors. They are defined as[12]:

$$S_m = S(\omega_m) = 1 + r\,\frac{Z_x(\omega_m) + \frac{1}{j\omega_m C_T}}{Z_x(\omega_m) + Z_d(\omega_m)} \qquad \text{(C-2)}$$

where $r = \dfrac{\omega_m^2}{(\omega_a^2 - \omega_m^2)}$

ω_a = avalanche resonance frequency of the diode

$$\omega_a^2 = \frac{2\alpha(E_c)\,J_o\,v_s}{\epsilon}$$

C_T = total capacitance of the diode

α = the ionization rate

$$\alpha' = \left.\frac{d\alpha}{dE}\right|_{E_c}$$

$Z_d(\omega)$ = the small-signal diode impedance[15]

$$= \frac{\bar{x}_d - \bar{x}_d\,\frac{\sin\theta_d}{\theta_d} - \frac{\omega^2}{\omega_a^2} + j\bar{x}_d\left(\frac{1-\cos\theta_d}{\theta_d}\right)}{j\omega C_T\left(1 - \frac{\omega^2}{\omega_a^2}\right)} \qquad \text{(C-3)}$$

$\bar{x}_d$ = ratio of drift-region length to the total length of the diode

$\theta_d = \omega T_d$ = Transit angle of the drift region.

The stability of the diode-circuit system may be studied by examining the roots of equation C-1 for complex frequency. It can be seen that the effect of the large-signal pump upon stability is completely described by the two factors M_1 and M_2 since the stability factors S depend only upon the small-signal diode impedance and the circuit impedance. This is a very important result of the theory. If, for a given circuit and diode, the stability factors are such that there are no unstable roots for $0 < |M_1| < 1$ and $0 < |M_2| < 1$, then the system is stable for any pump level.

Under certain conditions, there are simplified forms of the characteristic equation which are valid and useful. If $|M_2| << |M_1|$, then equation C-1 reduces to

$$1 - |M_1|^2 S_o (S_{-1}^* + S_1) \cong 0 \qquad (C-4)$$

Also, if $|S_1| << |S_o|$ and $|S_{-1}|$, then equation C-1 simplifies to:

$$1 - |M_1|^2 S_o S_{-1}^* \cong 0 \qquad (C-5)$$

This is the one suggested by Hines for the degenerate case.
The justification of equation C-5 is as follows.

For $\omega << \omega_a$, the term $\frac{\omega^2}{\omega_a^2 - \omega^2}$ is

much smaller than 1 and $S(\omega)$ approaches unity. For ω in the vicinity of ω_a, $Z_d(\omega)$ is quite different from $\frac{1}{j\omega\tau_T}$ and of course $\frac{\omega^2}{\omega_a^2 - \omega^2}$ is large. Therefore, $S(\omega)$ is not negligible in general. However, there is no pole for S at $\omega = \omega_a$ since the pole in Z_d cancels that of $\omega^2/(\omega_a^2 - \omega^2)$. Since it is usually desirable to pump the diode where the negative conductance is large, $\omega_p^2 \geq 2\omega_a^2$. Therefore

for $\omega > \omega_p$

$$\frac{\omega^2}{\omega_a^2 - \omega^2} \longrightarrow -1 \qquad (C-6)$$

and also $Z_d \longrightarrow \frac{1}{j\omega C_T}$

and $S(\omega)$ tends to zero. Therefore, equation C-5 is reasonable especially for $\omega_o \approx \omega_p/2$.

Equation C-5 can be successfully employed to determine the stability criteria, if the diode impedance and circuit impedance are known.

It is obvious that in order for equation C-5 to be satisfied, $S_o S^*_{-1}$ must be real and greater than one. Therefore, a plot of the real and imaginary parts of $S_o S^*_{-1}$ as a function of frequency will show whether such a plot will intersect the real axis or not and at what frequencies it will intersect. If $S_o S^*_{-1}$ intersects the real axis, and its magnitude at that point is greater than 1, then the possibility of a spurious oscillation exists. If $S_o S^*_{-1}$ is real at some frequency, then the magnitude of $|M_1|$ at which the spurious oscillation is initiated is given by

$$|M_1| = \left(\frac{1}{S_o S^*_{-1}}\right)^{\frac{1}{2}} . \qquad \text{(C-7)}$$

If $\omega_o = \omega_p/2$, then $\omega_{-1} = \omega_p/2$ and $S_o = S_{-1}$ and $S_o S^*_{-1} = |S_o|^2$.

Thus the phase condition for instability is always satisfied at the subharmonic and thus it suggests that spurious oscillation most likely occurs at the subharmonic; note however that for this case $|S_o|^2$ must be larger than 1. Parametric-type instabilities are also predicted from this equation.

If the small-signal admittance of the diode is known (by either calculation or measurement) and if the circuit impedance is known (either by calculation or measurement), then equation C-5 can be readily employed to determine whether spurious oscillations are possible or not.

On the other hand it is important to be able to derive some general criteria in order to be able to make some general statements concerning the circuits required for stability.

In order to obtain unconditional stability, it is necessary to have an $S_o S_{-1}^*$ function which does not intersect the real axis beyond unity for $0 \leq \omega_o \leq \omega_p/2$.

This is the most general stability criteria which applies to both parametric and subharmonic oscillations.

One way to simplify the problem is to make $|S_o S_{-1}^*| < 1$ or to lie inside the unit circle. Although this is restrictive (since actually this only applies to the subharmonic), it is sufficient to guarantee stability and makes the problem more tractable to deal with analytically. Using this criterion, one can concentrate on the magnitude of $S_o S_{-1}^*$ and neglect the phase. We can also make an additional requirement that $|S_o|$ and $|S_{-1}|$ be less than unity and therefore use as a criterion for stability that

$$|S(\omega)| \leq 1 \text{ for } 0 < \omega < \omega_p \qquad \text{(C-8)}$$

Note that it is necessary to consider frequencies up to ω_p, because no matter how small S_o may be S_{-1} could be such that it would yield an unstable product. Equation C-8 is <u>sufficient</u> for stability but not <u>necessary</u> and may be too restrictive in certain situations. One then has to resort to the more general stability criteria.

From equation C-2 we have

$$[Z_x(\omega) + Z_d(\omega)]\,[S - 1] = r\,[Z_x(\omega) + \frac{1}{j\omega C_T}]$$

and therefore,

$$Z_x = -Z_d + \left(\frac{r}{1 + r - S}\right)\left(Z_d - \frac{1}{j\omega C_T}\right), \qquad \text{(C-9)}$$

where $r = \dfrac{\omega^2}{\omega_a^2 - \omega^2}$

For any set of Z_d, r, ω and C_T equation C-9 is a bilinear transformation between Z_x and S.

A bilinear transformation always maps circles into circles; a straight line is regarded as a circle with infinite radius. Thus circles of constant $|S|$ map into circles in the external impedance plane. We can construct the circles as follows:

Let us write $S = |S|e^{j\theta} = be^{j\theta}$,

$$1 + r = a,$$

$$r\left(Z_d - \frac{1}{j\omega C_T}\right) = c$$

$$X = Z_x + Z_d$$

Substituting into equation C-9, we find

$$X = \frac{c}{a - be^{j\theta}} \qquad \text{(C-10)}$$

This is the equation of a circle and is shown below:

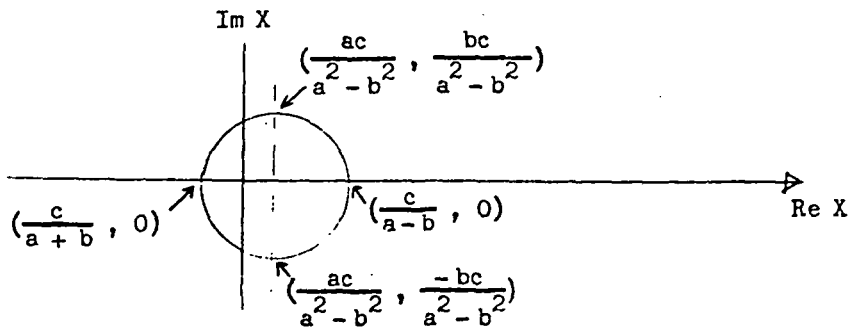

The radius of the X-circle is $= \frac{1}{2}\left[\left|\frac{c}{a+b} - \frac{c}{a-b}\right|\right]$

$$= \frac{1}{2}\left|\frac{bc}{a^2-b^2}\right| = \left|\frac{|S|\, r\left(Z_d - \frac{1}{j\omega C_T}\right)}{(1+r)^2 - |S|^2}\right| \qquad \text{(C-11)}$$

and is equal to the radius of the Z_x circle.

The center of the X - circle $\left(\frac{ac}{a^2 - b^2}, 0\right)$, is given by

$$\frac{(1 + r)\, r\, (Z_d - 1/j\omega C_T)}{(1 + r)^2 - |S|^2} \qquad \text{(C-12)}$$

The center of the Z_x circle is

$$Z_{x_{center}} = \frac{ac}{a^2 - b^2} - Z_d = -Z_d + \frac{(1+r)\, r\left(Z_d - \frac{1}{j\omega C_T}\right)}{(1 + r)^2 - |S|^2} \qquad \text{(C-13)}$$

Therefore there is a region in the Z_x plane (even though it may be quite limited) such that for any Z_x within this region $|S| \leq 1$. The region is bounded by a circle and in some cases, it may be the entire Z_x plane "outside" of a circle. Thus if we know the properties of the diode, we can determine the Z_x values as a function of frequencies where instabilities will not occur.

It is relatively straightforward to program the pertinent equations on a computer and thus be able to make these computations relatively quickly.

As a summary, the procedure for determining whether instabilities will occur is as follows:

a. After a particular diode is chosen, one can measure the small-signal impedance $Z_d(\omega)$ of the diode from a very low frequency up to the operating frequency as well as the total capacitance of the diode. If the diode doping profile and area are known, Z_d can be computed.

b. If a particular circuit is chosen one can measure the impedance of the circuit as a function of frequency or it may be calculated.

c. $S(\omega_o)$ is computed using equation C-2 for $0 \leq \omega_o \leq \omega_p/2$. ω_p is the operating frequency. Then S^*_{-1} [which is $S(\omega_p - \omega_o)$] is computed from equation C-2 for $0 \leq \omega_o \leq \omega_p/2$. The product $S_o S^*_{-1}$ is plotted in the complex plane for $0 \leq \omega_o \leq \omega_p/2$. If $S_o S^*_{-1}$ does not intersect the real axis beyond unity, then the diode-circuit system is unconditionally stable. If it does

intersect the real axis beyond unity, then the magnitude of M_1 at which spurious signals are initiated is given by,

$$|M_1| = \left(\frac{1}{S_o S_{-1}^*}\right)^{\frac{1}{2}} \quad . \tag{C-14}$$

If one needs to obtain an approximate idea as to the value of Z_x which is required to prevent instability, then equation C-13 can be employed to determine this; it should be noted, however, that the values of Z_x computed in this manner may be too restrictive but will provide a good start. The way to proceed here is to use equation C-11 and C-13 as follows:

a. Here again, the small-signal impedance and C_T for the device have to be measured or calculated. From these ω_a can also be determined.

b. Using equation C-11 and C-13, we can determine the center of the Z_x circle and its radius for $|S| = 1$; this circle provides the boundary for allowable values of Z_x at each frequency. In order to determine whether the allowable values of Z_x are inside or outside the circle, we can then determine whether at each frequency Z_x lies inside or outside the circle for $|S| > 1$. If Z_x lies outside the $|S| = 1$ circle for $|S| > 1$, then the region inside the circle is the allowable region and vice-versa. This procedure has to be carried out for $0 \leq \omega \leq \omega_p$.

c. If one can then design an external circuit whose impedance meets the restrictions obtained in (2), then one is assured of no spurious oscillations. However, if one has a circuit which does not meet those conditions, it is not <u>necessarily unstable</u> and one should resort to the previous procedure for determining instability.

It is worth noting here, that the Z_x employed here also includes the package parasitics.

Appendix D

BIBLIOGRAPHY

BIBLIOGRAPHY

1. C.T. Rucker, "A Multi-Diode High Average Power Avalanche Diode Oscillator," IEEE Trans. on MTT, Vol. MTT-17, pp. 1156-1158 December 1969

2. K. Kurokawa, "An X-Band 10-Watt Multiple-IMPATT Oscillator," Proc. IEEE, Vol. 59, pp. 102-103, January 1971

3. R.S. Harp and H.L. Stover, "Power Combining of X-Band IMPATT Circuit Modules,: ISSCC Digest of Technical Papers, pp. 118-;;9, February 1973.

4. R.S. Harp and K.J. Russel, "Improvements in Bandwidth and Frequency capability of Microwave Power Combinatorial Techniques, "ISSCC Digest of Technical Papers, pp. 94-95, February 1974.

5. N.D. Kenyon, "A Circuit Design For MM-Wave IMPATT Oscillators," MTT Symposium Digest, pp. 300-303; 1970.

6. W.S. Shockley, "Negative Resistance Arising from Transit Time in Semiconductor Diodes," Bell System Technical Journal, Vol. 33, No. 4, pp. 799-826, July 1954.

7. W.G. Read, Jr., "A Proposed High Frequency-Negative Resistance Diode," Bell System Technical Journal, Vol. 37, No. 2, pp. 401-466, March 1958.

8. T. Misawa,"Negative Resistance in P-N Junctions Under Avalanche Breakdown Conditions, - Parts I and II," IEEE Trans. Elec. Dev., Vol. ED-13, No. 1, pp. 137-151, January 1966.

9. M.S. Gupta, "Large Signal Equivalent Circuit for IMPATT-Diode Characterization and Its Application to Amplifiers, " IEEE Trans. on MTT, Vol. MTT-21, No. 11, pp. 689-694, November 1973.

10. E.F. Scherer, "Large Signal Operation of Avalanche Diode Amplifiers," IEEE Trans. on MTT, Vol. MTT-;8, No. 11, pp. 922-932, November 1970

11. R.W. Laton and G.I. Haddad, "Characteristics of IMPATT-Diode Reflection Amplifiers," IEEE Trans. on MTT, Vol. MTT-21, No. 11, pp. 668-680, November 1973.

12. M.E. Hines, "Large Signal Noise, Frequency Conversion, and Parametric Instabilities in IMPATT Diode Networks," Proceedings of IEEE, Vol. 60, No. 12, pp. 1534-1548, December 1972.

13. C.A. Brackett, "The Elimination of Tuning-Induced Bias Circuit Oscillations in IMPATT Oscillators," Bell System Technical Journal, Vol. 52, No. 3, pp. 271-306, March 1973.

14. Ramo, Whinnery and Van Duzer, Fields and Waves in Communication Electronics, Wiley, pp. 549-550, 1965

15. W.E. Schroeder, "Spurious Parametric Oscillations in IMPATT Diode Circuits," Bell System Technical Jouunal, Vol. 53, No. 7 pp. 1187-1210, September 1974

16. E. Jones and J. Bolljahn, "Coupled-Strip-Transmission-Line Filters and Directional Couplers," IRE Trans. on MTT, Vol. MTT-4, pp. 75-81, April 1956.

17. W.J. Getsinger, "Coupled Rectangular Bars Between Parallel Plates," IRE Trans. on MTT-10, No. 1, pp. 65-72, January 1962.

18. W.J. Getsinger, "The Packaged and Mounted Diode as a Microwave Circuit," IEEE Trans. on MTT, Vol. MTT -14, No. 2, pp. 58-69, February 1966.

19. J.W. Monroe, "The Effects of Package Parasitics on the Stability of Microwave Negative Resistance Devices," IEEE Trans. on MTT, Vol. MTT-21, No. 11, pp. 731-735, November 1973.

20. D.F. Peterson, "A Device Characterization and Circuit Design Procedure for Realizing High-Power Millimeter-Wave IMPATT-Diode Amplifiers," IEEE Trans. on MTT, Vol. MTT-21, No. 11, PP. 681-689, November 1973.

21. M. Gilden and M.E. Hines, "Electronic Tuning Effects in the Read Microwave Avalanche Diode," IEEE Trans. on Electron Devices, Vol. ED-13, No. 1, pp. 169-175, January 1966.